

# UC Irvine

## UC Irvine Electronic Theses and Dissertations

### Title

Understanding The Interaction Mechanism Of Nogo-66 With (i) NgR1 And (ii) Membrane Phosphocholine And The Structure Determination JSRV Envelope Protein Cytoplasmic Tail And Transmembrane Domain

### Permalink

<https://escholarship.org/uc/item/7qd2n8tt>

### Author

Alhoshani, Ali Rashed

### Publication Date

2014

Peer reviewed|Thesis/dissertation

UNIVERSITY OF CALIFORNIA,  
IRVINE

UNDERSTANDING THE INTERACTION MECHANISM OF NOGO-66 WITH (I) NGR1 AND (II)  
MEMBRANE PHOSPHOCHOLINE  
AND  
THE STRUCTURE DETERMINATION JSRV ENVELOPE PROTEIN CYTOPLASMIC TAIL AND  
TRANSMEMBRANE DOMAIN

DISSERTATION

submitted in partial satisfaction of the requirements  
for the degree of

DOCTOR OF PHILOSOPHY

in Pharmacological Science

by

Ali Rashed Alhoshani

Dissertation Committee:

Associated Professor Melanie J. Cocco, Chair  
Professor Thomas Poulos  
Associated Professor Andrej Lupták

2014

Chapter 3 © 2014 BBA: Biomembranes vol 1838, p 2350-6  
Portion of Chapter 1 © 2014 BBA: Biomembranes vol 1838, p 2350-6  
Portion of Chapter 5 © 2014 BBA: Biomembranes vol 1838, p 2350-6  
All other materials © 2014 Ali Rashed Alhoshani

## **DEDICATION**

To

my parents, family and friends

for their support and encouragement



## TABLE OF CONTENTS

	Page
LIST OF FIGURES	iv
LIST OF TABLES	vii
ACKNOWLEDGMENTS	viii
CURRICULUM VITAE	ix
CHAPTER 1: INTRODUCTION	1
CHAPTER 2: THE MODEL OF NOGO	11
CHAPTER 3: GLUTAMATE PROVIDES A KEY STRUCTURAL CONTACT BETWEEN RETICULON-4 (NOGO-66) AND PHOSPHOCHOLINE	47
CHAPTER 4: JSRV ENVELOPE PROTEIN CYTOPLASMIC TAIL AND TRANSMEMBRANE DOMAIN STRUCTURE DETERMINATION	66
CHAPTER 5: MATERIAL AND METHODS	81
REFERENCES	94
APPENDIX A: REVEALING P53 RESCUE MUTANT MECHANISMS	110
APPENDIX B: SUPPLEMENTAL INFORMATION FOR NOGO-66, NOGO- $\Delta$ 20, JSRV	135

## LIST OF FIGURES

	Page
Figure 1.1: Membrane protein classes	3
Figure 1.2: Micelles and Bicelles formation	6
Figure 1.3: RTN domain organization	9
Figure 2.1 A: Schematic representation of i-normal, ii-injured adult CNS	14
Figure 2.1 B: The MAI's proteins	15
Figure 2.2: Nogo proteins isoforms –A –B –C. Ex=Exon	16
Figure 2.3: Nogo-66 Receptor PDB ID1OZN ( NgR)	18
Figure 2.4. Nogo-A and its Receptors	19
Figure 2.5. Nogo-A topologies	20
Figure 2.6: Circular Dichroism (CD) of Nogo-Δ20	23
Figure 2.7: Nogo-66 NMR Structure	23
Figure 2.8: Mutagenesis studies test relative binding affinities	28
Figure 9: Nogo-66 and NgR binding interface	29
Figure 2.10: Active residues Arg 53 and Arg 54 interaction	30
Figure 2.11: Active residues Lys50 Asn46 and Asn 39	31
Figure 2.12: HADDOCK score vs i-RMSD and I-RMSD	32
Figure 2.13: SELEX steps	36
Figure 2.14: 2%Agrose gel	37
Figure 2.15: Out put fasta file format from FASTAptamer-Count script	38

Figure 2.16: (A) Mfold for N66-59; Ali3	42
Figure 2.16: (B) Mfold for N66-1; Ali4 and Ali7	43
Figure 2.17: (A) Ali3 (B) Ali3 and Nogo-66	44
Figure 2.18: <sup>15</sup> N HSQC NMR of Nogo66 with Ali3	46
Figure 3.1: Structure and homology of Nogo-66	51
Figure 3.2: Model of a single DPC molecule	52
Figure 3.3: Secondary structure and lipid partitioning	55
Figure 3.4: Tertiary structure of WT and E26A Nogo-66 in DPC	57
Figure 3.5: Apparent Binding Affinity of Nogo-66 WT and E26A	60
Figure 3.6: Compare Nogo-66 E26A and WT binding affinity	61
Figure 3.7: Summary of the effect of E26 mutation in Nogo-66	65
Figure 4.1: JSRV Genome contain and Env Structure	69
Figure 4.2: Downstream effect of JSRV	69
Figure 4.3: portion of CT-JSRV Helical Wheel Plot	70
Figure 4.4: Model of JSRV Env protein	71
Figure 4.5: Mutagenesis studies test in CT-JSRV	72
Figure 4.6: CT-JSRV <sup>15</sup> N HSQC	72
Figure 4.7: CT-JSRV Circular Dichroism	73
Figure 4.8: CT-JSRV sequences	74
Figure 4.9: CT-JSRV <sup>15</sup> N HSQC and <sup>15</sup> N NOESY-HSQC:	74
Figure 4.10 A: NOESY backbone walk	76

Figure 4.10 B: Part of the NOESY and TOCSY spectra of CT-JSRV	76
Figure 4.11: preliminary structure of JSRV cytoplasmic tail	76
Figure 4.12: Optimized JSRV in pET15b vector	77
Figure 4.13 A: 15N CT-JSRV (A) Mass spectrometry for CT-JSRV	79
Figure 4.13 B: UV-spectrophotometry scan for CT-JSRV	79
Figure 4.14: CT UV-spectrophotometry scan (i and ii)	80
Figure 5.1: HADDOCK protocol	82
Figure 5.2: Method of SELEX	93
Figure A.1: p53 pathway and downstream effect	111
Figure A.2: p53 structural domains	113
Figure A.3: Hydrogen-Deuterium Exchange mechanism	115
Figure A.4: HSQC after different time period of exchange in D2O	117
Figure A.5 (i): Protection factor comparison wild type and N235K	118
Figure A.5 (ii): Protection factor comparing wild type and N239Y	118
Figure A.6: highly protected residues	119
Figure A.7: Average of protection factors for WT, N235K, N239Y	119
Figure A.8: H-bonds involved in D259 and N268	122
Figure A.9: Wild Type HSQC	131
Figure A.10: N235K HSQC	132
Figure A.11: N239Y HSQC	133

## LIST OF TABLES

	Pages
Table 1.1: Common lipid and detergents	5
Table 2.1 : Critical Assessment of CAPRI docking experiment	26
Table 2.2. Aptamers and antibodies side by side	35
Table 2.3: Representative sequences from SELEX after round 14	39
Table 2.4: QGRS mapper for N66-59 and N66-1	44
Table 4.1 : Dialysis conditions for CT-JSRV	78
Table A.1: Krc values for all Amino acid	126
Table A.2: Ka, Kb, and Kw reference values	126
Table A.3: Protection Factor for Stable residues	127
Table A.4: Exchange rate for stable residues (experimental 'Kex' and random coil 'Krc')	128
Table A.5: Chemical shifts for WT Assignments residues	129

## **ACKNOWLEDGMENTS**

I would like to thank my advisor Dr.Cocco for her countless help and support. Without her guidance and help this dissertation would not have been achievable. I would like to thank my committee members, Dr. Poulos and Dr. Lupták for their advice and suggestions. In addition, a thank to my friends Ahmed, Milad, Sanaz, Amien, Tuan and my lab members Sean and Verna for their encouragement and help. I would like to thank the National Institutes of Health, Roman Reed Research Fund, the Saudi ministry of higher education, and King Saud University for the financial support.

## CURRICULUM VITAE

**Ali Alhoshani**

- 2005 King Saud University, College of Pharmacy, Riyadh, Saudi Arabia
- 2007 Research Assistant, King Saudi University, Riyadh, Saudi Arabia
- 2013-14 Teaching Assistant, Graduate School of  
Biological Science, University of California, Irvine

### FIELD OF STUDY

Pharmacological Science

### PUBLICATIONS

*Glutamate provides a key structural contact between reticulon-4 (Nogo-66) and phosphocholine.*  
Biochim Biophys Acta. 2014 May 24.

# Chapter 1

## Membrane protein

Part of this chapter published in BBA: Biomembranes (2014) vol 1838, p 2350-6

Ali Alhoshani<sup>a</sup>, Rosemarie Vithayathil<sup>b</sup>, Jonathan Bandong<sup>b</sup>, Katherine M. Chrnyk<sup>b</sup>,  
Gabriel O. Moreno<sup>b</sup>, Gregory A. Weiss<sup>b,c</sup> and Melanie J. Cocco<sup>a,b\*</sup>

<sup>a</sup>Department of Pharmaceutical Sciences; <sup>b</sup>Department of Molecular Biology and Biochemistry; <sup>c</sup>Department of Chemistry University of California, Irvine, CA 92697



## Introduction

Membrane proteins play a part in various biochemical and regulatory processes including cellular communications and division, macromolecule transportation, and shaping up the plasma membrane structure. They form around 20-30% of eukaryotic proteome (Wallin and von Heijne 1998). Such high percentage of membrane protein indicates the importance of this class to maintain proper biological functions. Thus, any misfolding or mutations will lead to many diseases such as neurodegenerative disease, heart diseases, cancer and others. The membrane proteins are classified into two different classes based on the interaction with the membrane: (i) integral membrane proteins; (ii) membrane-associated proteins. Integral membrane proteins have segments that embed in the lipid bilayer of the membrane and have domains on one or both side(s) of the membrane. They span the membrane as  $\beta$ -sheets or  $\alpha$  helices. These transmembrane proteins are often amphipathic, with hydrophobic and hydrophilic residues. The hydrophobic side faces the membrane lipid, and hydrophilic side faces the aqueous phase (Bowie 1997, Tamm, Hong et al. 2004). The membrane-associated proteins are attached directly (hydrophobic or charge interaction with lipid polar head group) or indirectly (through integral membrane proteins) to the membrane. They are monotopic membrane proteins, i.e. do not span the membrane. (Binda, Hubalek et al. 2004).

Only until today, more than 60% of drugs target membrane proteins, yet we know relatively little about their structures. For years, researchers have been targeting membrane proteins and studied their functions using different methods such as high-throughput screening (HTS), and functional assays. These methods are great; yet miss the detailed structural

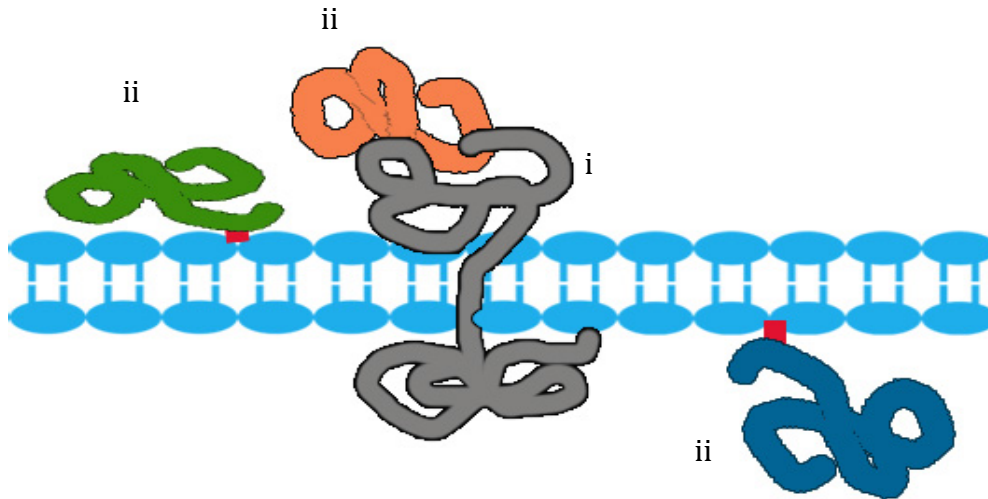


Figure 1.1: Membrane protein classes (i) Gray, Integral membrane protein (ii) blue and green, membrane-associated proteins directly attached to the cellular membrane. Orange, membrane-associated protein attached to integral membrane protein.

information, which is crucial for understanding the function, or to develop more selective drugs. X-ray crystallography and nuclear magnetic resonance (NMR) are the only powerful tools of elucidating comprehensive information about the structure.

The membrane protein structure field has various challenges. They range from overexpression of recombinant membrane proteins to developing new ways to improve solubility. A biological membrane is a complex lipid bilayer in which membrane proteins interact closely with the lipids and surrounding proteins. Membrane protein structural determination and characterization studies, mainly via NMR, X-ray crystallography, and circular dichroism (CD), need an environment that mimics the membrane lipid bilayer. Thus, artificial detergents and lipid, to mimic the native biological membrane lipid bilayer environment, are necessary for such studies. Micelles and bicelles are feasible membrane mimetic solutions to prevent aggregation and insolubility (Figure 1.2A-B). Micelles are formed when the polar groups

(head) of the phospholipid form hydrogen bonds with water molecules in an aqueous solution, while the hydrophobic groups (tail) clusters due to hydrophobic interactions (Figure 1.2A). The properties, shape, and size of micelles depend on the type of detergents used (Table 1.1). Another membrane mimetic is the bicelles (binary bilayered mixed micelles). They are a combination of a long-chain phospholipid, lipid, short-chain phospholipid, and detergents. The most commonly used formula is a mixture of 1,2-dimyristoyl-sn-glycero-3-phosphocholine (DMPC), long-chain, and 1,2-Dihexanoyl-sn-Glycero-3-Phosphocholine (DHPC), short chain, at certain ratio (q). The bicelles bilayer is formed by the long-chain phospholipid surrounded by a rim around the edge of short-chain phospholipid. (Figure 1.2B) (Durr, Gildenberg et al. 2012).

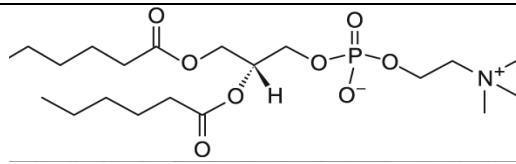
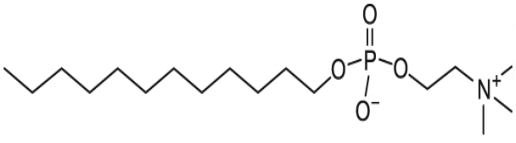
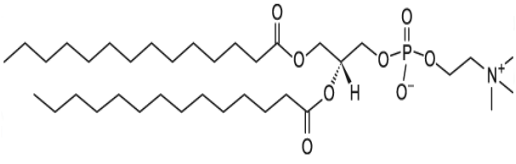
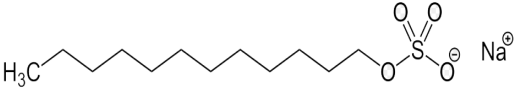
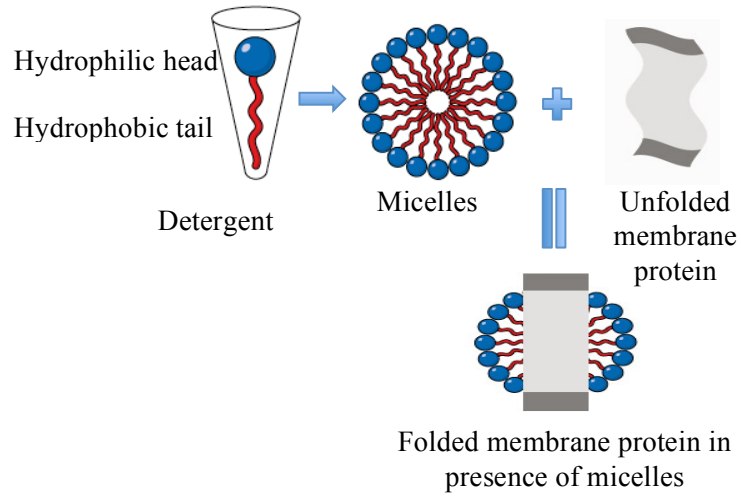
Detergents/lipid	MW	CMC	Structure
DHPC	453.507	15mM	
DPC	351.462	1.1 mM	
DMPC	677.933	6 nM	
SDS	288.372	8.2 mM	

Table 1.1: Common lipid and detergents. CMC: is the critical minimal concentration to form micelle and bicelles. MW: Molecular weight. Source Avanti lipid Inc, Fisher Inc,

A



B

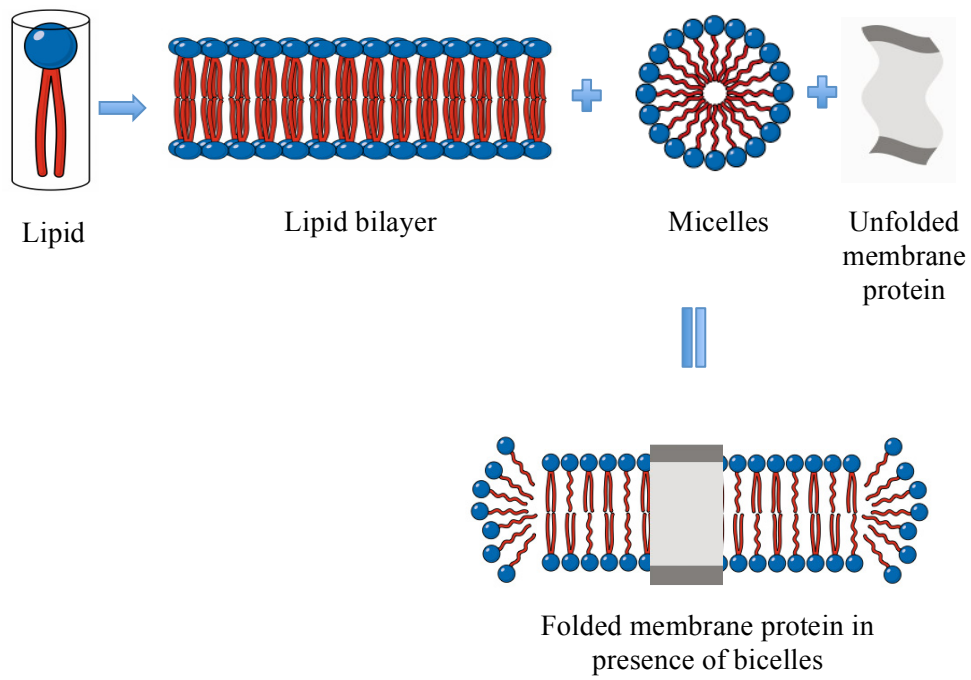


Figure 1.2: (A) Micelles formation (B) Bicelles formation, disk-like shape (Adapted (Anatrace)).

In the following chapters, I will discuss two different membrane proteins: (i) membrane-associated protein Reticulon-4/Neurite out growth (RTN-4/Nogo); and (ii) integral membrane protein Jaagsiekete Sheep Retrovirus (JSRV). Both have been associated with disease development.

Reticulons (RTNs) are found in the endoplasmic reticulum (ER) of most eukaryotes. It has been proposed that RTNs evolved when the endomembrane system developed ~ 1.7 billion years ago (Oertle, Klinger et al. 2003). RTNs function to establish curvature of the ER membrane (Voeltz, Prinz et al. 2006) and have been implicated in assembly of the nuclear envelope (Kiseleva, Morozova et al. 2007), ER-Golgi trafficking, and vesicle formation (Yang and Strittmatter 2007). Some viruses exploit the ability of host RTNs to drive lipid bilayers into membrane compartments, enabling the virus to sequester viral replication behind a host membrane (Diaz and Ahlquist 2012). In addition to defining the architecture and topology of a lipid membrane, RTNs have been adapted for other cellular functions including: the regulation of apoptosis (Tagami, Eguchi et al. 2000, Zhu, Xiang et al. 2007); the inhibition of  $\beta$ -amyloid-converting enzyme 1 (BACE1) to block amyloid formation (He, Lu et al. 2004, He, Shi et al. 2007); vascular remodeling (Acevedo, Yu et al. 2004); the inhibition of angiogenesis in the CNS (Walchli, Pernet et al. 2013); the inhibition of myelination (Chong, Rosenberg et al. 2011); and as an axonal growth inhibitor, RTN-4 limits plasticity in the brain (Pernet and Schwab 2012, Schmandke, Schmandke et al. 2014). RTNs have also been implicated in a range of neurodegenerative diseases (Di Sano, Bernardoni et al. 2012). The C-terminal 150-200 amino acids are common among all RTNs and are referred to as the reticulon homology domain (RHD). RHDs have two hydrophobic membrane-embedded regions (Figure 1.3); between these helices is a span of 66

amino acids (RHD-66) that extends beyond the membrane into the aqueous phase. The N-terminal regions of RTNs can vary dramatically in length and sequence, according to their distinct function.

RTN-4 is also known as the neurite outgrowth inhibitor (Nogo). Nogo-A is an isoform with two active domains Nogo-66 in common C-terminal RHD and Nogo- $\Delta$ 20 in N-terminal (Kempf and Schwab 2013). In CNS, It has been well studied that these are involved in axonal regrowth inhibition and mediates their inhibitory activity by binding to the Nogo receptor (NgR) and sphingosine 1-phosphate receptor 2 (S1PR2), respectively (Kempf and Schwab 2013) (Kempf, Tews et al. 2014). In chapter 2, I characterize the Nogo- $\Delta$ 20 structure in lipid and aqueous environment using CD. In addition, I use High Ambiguity Driven protein-protein DOCKing server HADDOCK) (de Vries, van Dijk et al. 2010) to identify the key residues and nature of interaction with between Nogo-66 and NgR. Then, I use single stranded DNA (ssDNA) aptamer library to disrupt the interaction, remove the negative effect of Nogo-66, and promote axonal growth. In ER, RHDs share a common function. Specific contacts between the RHD and lipid and the dominant forces that enable the RHD to establish membrane curvature are currently unknown.



Figure 1.3: RTN domain organization; the N-terminus varies in length, sequence and function; M=membrane embedded

Recently, we determined the NMR structure of Nogo-66 embedded in a native-like environment (Vasudevan, Schulz et al. 2010). Nogo-66 is disordered in an aqueous environment, but folds into a five-helix bundle in dodecylphosphocholine (DPC). We used accessibility to paramagnetic reagents and nuclear Overhauser effects (NOEs) between the protein and DPC to define the regions of Nogo-66 that are either in contact with DPC or exposed to the aqueous phase, which enabled us to orient the protein. In early functional assays, the peptide corresponding to residues 31-55 of Nogo-66 was found to have the most activity in blocking neuronal growth (GrandPre, Nakamura et al. 2000). The residues that are the most solvent and exposed amino acids in our model of Nogo-66 at the cell surface are also most active in binding NgR. In Nogo-66, we found several positions conserved in higher vertebrates that are in contact with lipid including aromatic and hydrophobic side chains. The position, E/D26 in the 66-amino acid domain, was identified as hyperconserved in RTNs of all eukaryotes in 2003 (Oertle, Klinger et al. 2003). Furthermore, the structure surrounding Glu-26 is interesting because the side chain is positioned at the base of a cavity that could easily accommodate a phosphocholine (PC) with no positively charged protein groups in proximity to



neutralize the Glu carboxylate. The distance between Glu26 and the Lys or Arg side chains of helix 1 and 5 make it impossible for direct interaction, but collectively or individually these groups could form salt bridges to bind the choline and phosphate of a PC molecule. We propose a model for the interaction of a single PC with Nogo-66. Here we explore the structural role of Glu26 and find that interactions between Glu26 and the PC surface of a micelle or lipid vesicle influence the Nogo-66 structure. Moreover, mutation of Glu26 to Ala has structural consequences resulting in increased helical content in aqueous solutions, consistent with Glu26 destabilizing the fold when unpaired with choline. Conversely, E26A shows significantly decreased order and helical content in a membrane-like environment, revealing the role that this Glu plays in defining the Nogo-66 structure at the membrane surface. In Chapter 3, I use Nogo-66 to identify the structural mechanisms by which RTNs establish membrane curvature.

In chapter 4, I showed the NMR spectra assignment of Jaagsiekete sheep retrovirus (JSRV) C-terminal cytoplasmic tail (CT) and got the preliminary structure. JSRV is the causative agent of lung cancer in sheep. It is called ovine pulmonary adenocarcinoma (OPA). OPA resembles bronchiole-alveolar carcinoma in humans and it is an excellent animal model for this disease. Chapter 5, describes the experiments for all conducted studies in all chapters. Finally, in Appendix A, I describe how the rescue mutants of p53 restore the function of wild type.

## **Chapter 2**

### **The Model of Nogo**

## Abstract

Several myelin-associated proteins, the neurite outgrowth inhibitor (Nogo), myelin-associated glycoprotein (MAG), and oligodendrocyte myelin glycoprotein (OMgp) contribute to inhibiting central nerve system (CNS) regeneration after injuries, mainly by blocking axonal regrowth. The neurite outgrowth inhibitor (Nogo A) is a multi-domain transmembrane (TM) protein. The loop domain, connecting the two hydrophobic C-terminal TM helices, is referred to as Nogo66. The inhibitory effect of Nogo is established when Nogo66 binds to its receptor (NgR) on the axon. Based on mutagenesis studies performed in our lab, residues Ser 38, Asn 39, Ser 40, Leu 42, Arg 53 and Arg 54 affected the binding of Nogo66 to NgR. Arg 53 and Arg 54 are among the most affected residues. On the other hand, combinatorial studies on NgR, Asp 111, Asp 114, Asp 163 are the most residues contributing to the interaction of NgR with Nogo66 (1). To confirm this observation, High Ambiguity Driven Docking (HADDOCK) expert interface server was used (2). As starting structures for docking studies, I used the crystal structure of NgR (PDB id 1OZN) and the NMR solution structure of Nogo66 (PDB id 2KO2). The complex structures that resulted from the HADDOCK studies were in agreement with our mutagenesis studies and provided insight into the mechanism of inhibition. Following the docking analysis, I used an aptamer to inhibit its function and help promote the axonal regeneration after injuries. One of the identified sequences (Ali 3) showed some specificity and affinity.

## **Introduction**

The mammalian nervous system is divided into two parts: central nervous system (CNS) and peripheral nervous system (PNS). The CNS (mainly represented by brain and spinal cord) has a restricted ability to naturally regenerate after injuries/diseases, whereas the PNS has a self-repair mechanism that allows axonal regrowth. CNS injuries/diseases are complicated and usually lead to a loss/impaired function. They result from several causes including infections (meningitis); alteration in blood flow (CNS stroke); immune system (Multiple Sclerosis); or trauma, as in spinal cord injuries (SCI).

SCI, as an example, results from two mechanisms: (1) primary, physical damages, and (2) secondary, complex processes as the result of the primary injury. In the United State alone, the annual report of spinal cord injuries is approximately 12,000 new cases per year. Each year, there are over 700 cases per 1 million people that have resulted in permanent disability, which decreases the quality of life. A quarter of a million Americans are currently living with spinal cord injuries, and the cost of managing the care of spinal cord injury patients approaches \$4 billion each year. So far there is no treatment available to restore the spinal cord to its original state after injury. The current treatment is more on prevention of further complication rather than a cure. Life expectancies of individuals suffering from spinal cord injury are significantly lower and mortality rates are quite high. Therefore, there is a high demand for the development of new drugs for proper treatment of spinal cord injuries (Varma, Das et al. 2013).

Axons are normally enclosed with myelin to protect them from the surrounding environment. After injury, these axons are unsheathed and exposed to myelin-associated inhibitors (MAI's) (Mosyak, Wood et al. 2006, Pernet and Schwab 2012) and reactive astrocytes (Yiu and He 2006) (Figure 2.1A). At least three proteins are expressed on myelin membranes in the adult CNS; Neurite outgrowth protein (Nogo) (Chen, Huber et al. 2000), Myelin Associated

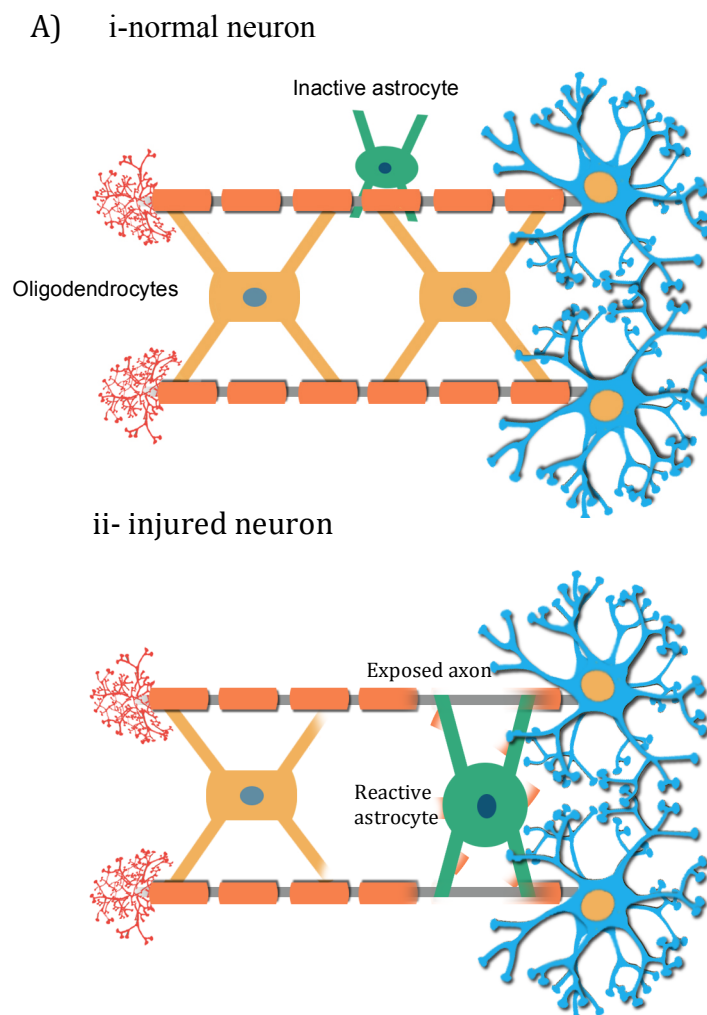


Figure 2.1: Schematic representation of (A) i-normal and ii- injured adult CNS. After injuries MAIs are released and astrocytes are activated, leading to collapsed growth cones

Glycoprotein (MAG) (McKerracher, David et al. 1994) and Oligodendrocytes Myelin Glycoprotein (OMgp)( Figure 2.1B) (Wang, Koprivica et al. 2002). Among these, Nogo was found to exert the greatest inhibitory effect on axonal growth in the adult mammalian CNS.

B)

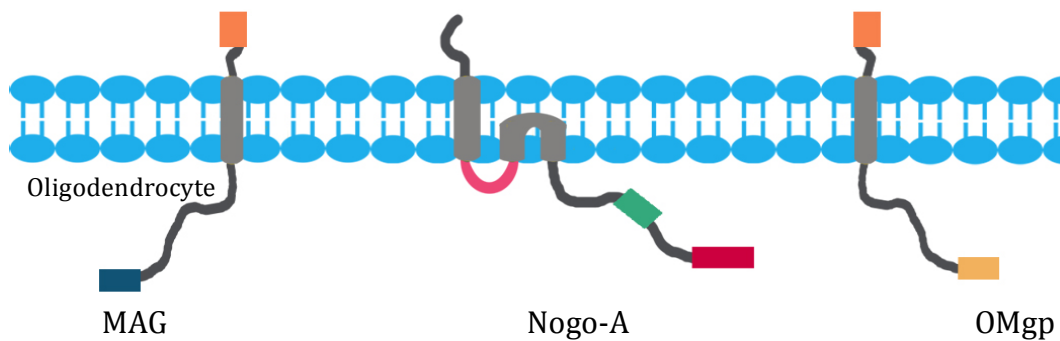


Figure 2.1 B: The MAIs proteins are mainly expressed in oligodendrocytes. They form a secondary barrier axonal regeneration.

Nogo has three different isoforms Nogo-A, Nogo-B, and Nogo-C (Chen, Huber et al. 2000, GrandPre, Nakamura et al. 2000, Oertle, van der Haar et al. 2003). The three isoforms of Nogo differ in their size and protein sequence. Nogo-A is the largest of the Nogo isoforms with 1163 amino acid long polypeptide chain and is highly expressed in CNS, mainly in oligodendrocytes. The 172 amino acid long amino terminal of Nogo-A and -B are similarly encoded by the same exon (exon 1) followed by another short exon 2. Exon 1 and 2 are followed by a very long exon 3, which adds 800 amino acid long sequence to Nogo A but is absent in Nogo-B and -C. The N terminal of Nogo-A and -B and the 800 amino acid long stretch of Nogo-A are rich in proline content and share no homology with any other known protein (CNS) (Figure 2.2).

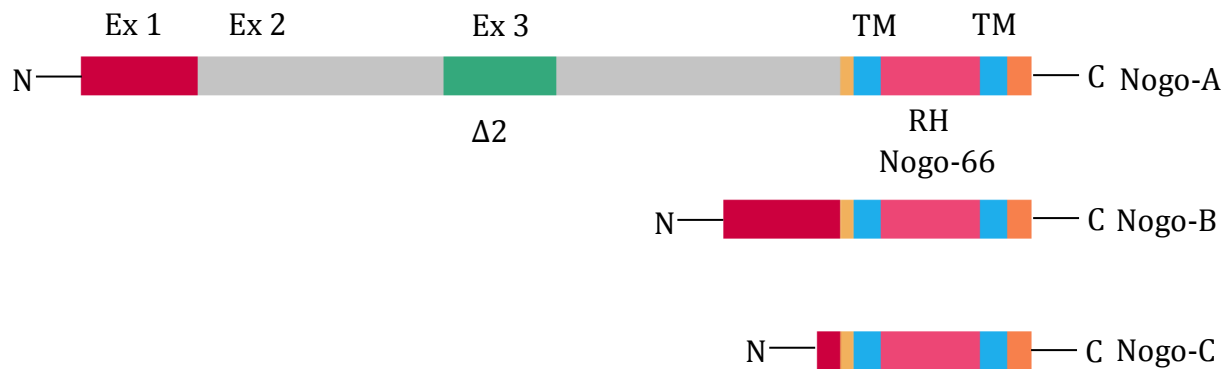


Figure 2.2: Nogo proteins isoforms –A –B –C. Ex=Exon. C-terminals ( 150-200 amino acids ) are the same in all isoform and contain the highly conserved reticulon homology domain (RHD) .

The RHD of Nogo protein consists of two long hydrophobic chains, which forms the two transmembrane domains. The transmembrane domain of Nogo RHD is separated by a 66 amino acid long stretch called Nogo-66. These 66 amino acids are there to execute the function. Another important domain is Nogo- $\Delta 20$ , which presents in the amino terminal extra cellular domain, has been shown to be critical for Nogo functions. Nogo-C represents the smallest isoform and consists of a small amino terminal region followed by RHD domain. The N terminal of Nogo-C is produced by transcript made through different promoter activity to the Nogo-A and -B promoter (Schwab 2010). The RTNs isoforms N-terminal heterogeneity implying that they interact with diverse proteins and thus perform different functions (Kempf and Schwab 2013).

### ***Nogo-66 and Nogo-Δ20 receptors and downstream effect:***

Nogo-66 binds to Glycosylphosphatidylinositol (GPI)-linked surface protein called the Nogo receptor 1 (NgR1; also known as Nogo-66 receptor and reticulon 4 receptor (Fournier, GrandPre et al. 2001). NgR1 consists of 473 amino acids with N- and C- terminals. It has two surfaces;(i)concave surface ;(ii) convex surface. The convex surface has 8.5 repeats of Leucine Rich Region (LRR) (Figure 2.3)(He, Bazan et al. 2003). The N-terminal is responsible for signaling while the C-terminal is responsible for hosting both NgR1 partners' p75 neurotrophin receptor p75<sup>NTR</sup> (Wang, Kim et al. 2002) and LINGO1(Mi, Lee et al. 2004), and consequently forms a trimeric complex. TROY, tumor necrosis factor-α receptor, is another identified transmembrane receptor that has ability to replace p75<sup>NTR</sup> and form trimeric complex (NgR1/TROY or p75<sup>NTR</sup>/LINGO-1) (Park, Yiu et al. 2005). The LRR region is involved in binding to Nogo-66 via its conserved acidic vicinity (Kempf and Schwab 2013). In addition, Nogo-66 binds to another receptor, immunoglobulin-like receptor B (PriB).; however, the mechanism of interaction is still to be discovered.

As for Nogo-Δ20, the binding receptor was unknown until Anissa Kempf from the Martin Schwab group in Zurich published their new finding about Nogo-Δ20 receptor. They showed that it binds to a G protein-coupled receptor (GPCR) sphingosine 1-phosphate receptor 2 (S1PR2). The binding site of S1PR2 is different from S1P (previous proposed by binding site) (Kempf, Tews et al. 2014). Although the exact mechanism is still unknown, Nogo -Δ20 is believed to play a major role in increment in level of intracellular calcium and reduction in levels of phosphorylated cAMP response element- binding (pCREB) (Joset, Dodd et al. 2010).



Both Nogo-A functional domains, Nogo-66 and Nogo- $\Delta$ 20, bind to their respective receptors and execute similar downstream inhibitory effect via the small GTPase RhoA/ Rho-associated coiled-coil-containing protein kinase (ROCK) signaling pathway (Schmandke, Schmandke et al. 2007) (Figure 2.4). Furthermore, blocking RhoA or ROCK activation has been shown to neutralize the negative effects on neurite growth, and helps in regeneration and sprouting after brain and spinal cord injury in mice and rats.

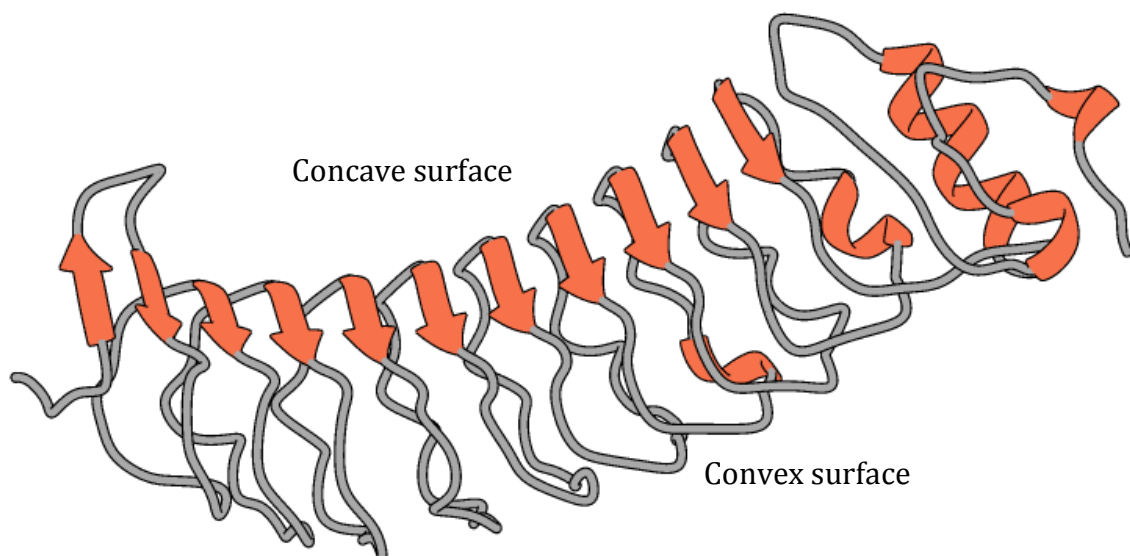


Figure 2.3: Nogo-66 Receptor PDB ID1OZN ( NgR)(He, Bazan et al. 2003)

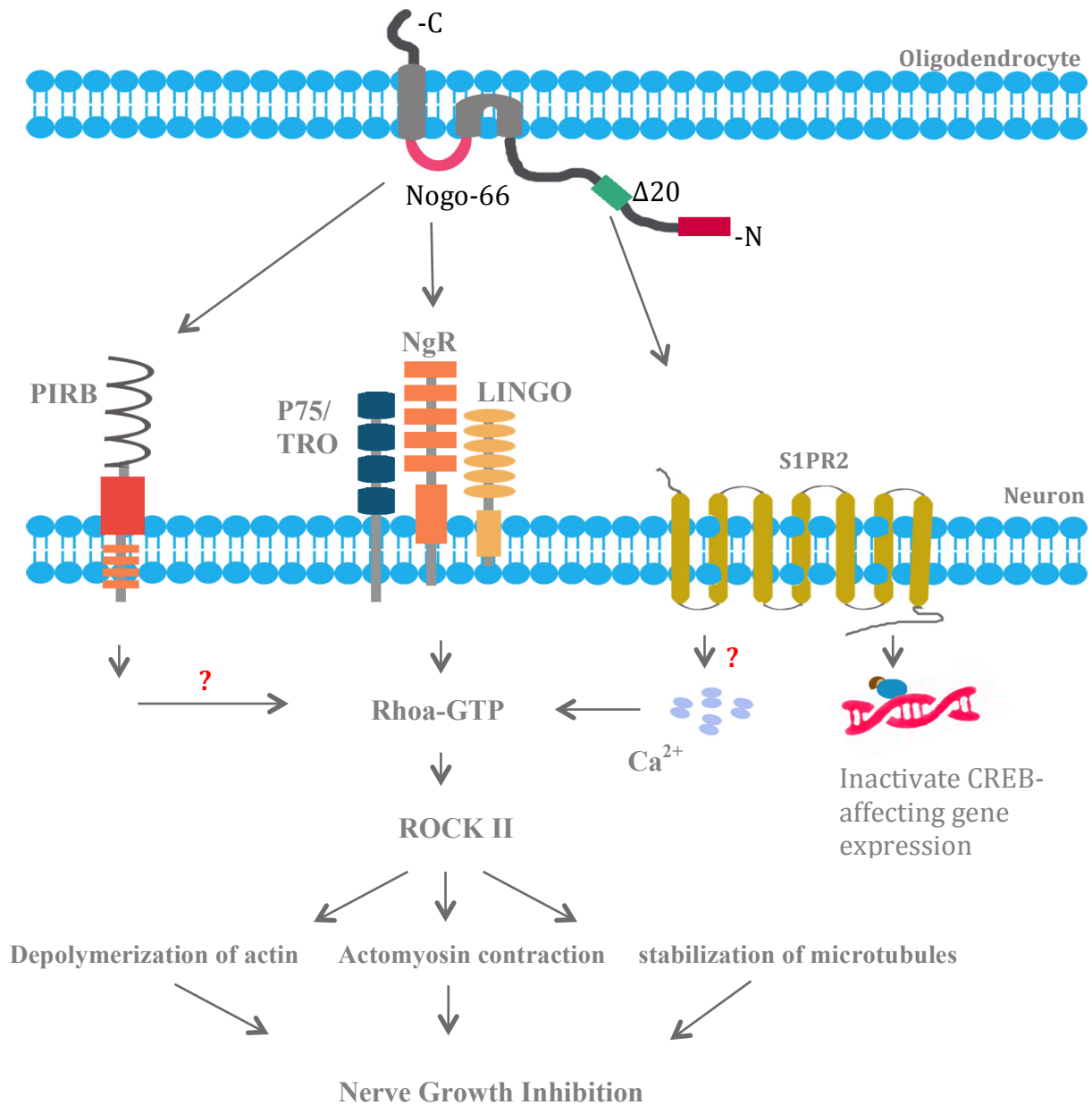


Figure 2.4. Nogo-A and its Receptors: This scheme summarizes the main signaling pathways targeted by Nogo-A and its corresponding receptors. Remyelination inhibition is achieved when (i) Nogo-66 binds to NgR1 and form the complex (LINGO-1/p75) or PirB and (ii) Nogo-A-Δ20 binds to S1PR2. This binding leads to activation of RhoA/ROCK pathway, and then, depolymerization actin cytoskeleton, increased actomyosin contraction, and reduced stabilization of microtubules. In addition, Nogo-A-Δ20 was demonstrated to inactivate CREB and affect gene expression.

***Nogo-A topology and functional domains structures:***

Nogo-A adapts a topology different from the typical transmembrane protein because it has long hydrophobic transmembrane region. In the ER, only Nogo-66 can be detected in the cytoplasm while in cellular membrane both can be detected on the extracellular space (Figure 2.5). This suggests that RTNs are involved in various functions (Schwab 2010).

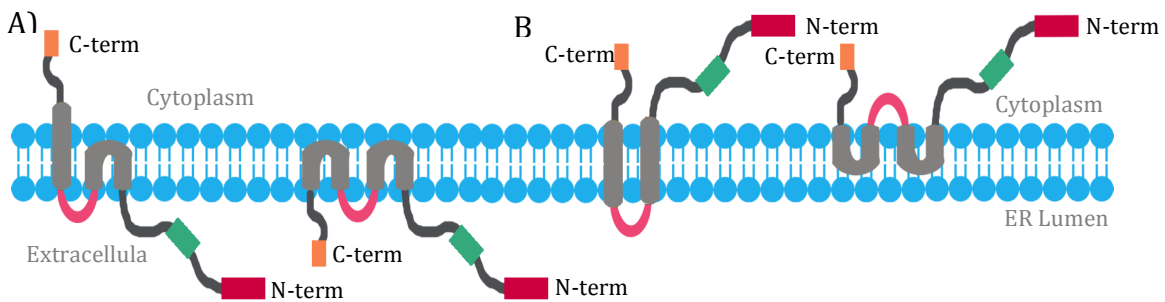


Figure 2.5. Nogo-A topologies: (A) in the plasma membrane, The C-terminal transmembrane (i) span the whole membrane or (ii) fold into a hairpin. (B) in ER, the C-terminal are found in the cytoplasm, along with N-terminal. Nogo-66 can be in the (i) ER lumen or (ii) in the cytoplasm

### ***Nogo-Δ20 secondary structure:***

Li and Sang have analyzed the ~800-long amino acids at the N-terminal, a domain specific for Nogo-A, by Circular Dichroism (CD) and Nuclear Magnetic Resonance (NMR). Circular dichroism spectroscopy is an effective tool for structural biologists. It is a quick technique to characterize unknown proteins. Mainly, it allows one to estimate the secondary structure of polypeptides or proteins. When measuring the CD for polypeptides/proteins, the light (circularly polarized) passes through the sample. The difference in the absorbance (spectral shapes) of the left and right polarized light in the far-UV range is unique for the different types of secondary structure ( $\alpha$ -helix, negative bands at ~222 and 208 nm and positive bands at ~192 nm;  $\beta$ -sheet, negative bands at ~215 and 180 nm, and positive bands at ~196 nm). This 800-long amino acids segment includes Nogo-Δ20. They did two different studies. In the first study, they divided the long domain (from 201-1016) into 200 amino acids overlapped fragments. In the second study, they included amino acids from 334-966 as one fragment. Unfortunately, all fragments from both studies were intrinsically disordered (Li, Shi et al. 2004, Li and Song 2007).

In contrast, I examined Nogo-Δ20 alone (in a phosphate buffer) and in a native-like environment (dodecylphosphocholine, DPC) to mimic the cell membrane. I found slightly different results. First, I expressed and purified the Nogo-Δ20 fragment, then eluted with 8M urea. To exchange the urea, the protein was dialyzed against 5 mM sodium phosphate ( $\text{Na}_2\text{PO}_4$ ) buffer, pH7. Subsequently, I collected CD spectra for Nogo-Δ20 (1mg/ml) in the phosphate buffer and in the presence of 10 mM DPC micelles (Figure 2.6). The spectra showed that the

Nogo- $\Delta$ 20 is disordered in Na-phosphate. This is in agreement with previously published data (Li, Shi et al. 2004, Li and Song 2007). However, the CD spectrum is shifted upon addition of DPC micelles (Figure 2.6). The difference in the Nogo- $\Delta$ 20 CD spectra indicates partial changes in the structure. More studies are needed to further characterize the Nogo- $\Delta$ 20 fragment.

In our laboratory, the structure of the Nogo-66 NMR was determined for the very first time in DPC micelles. The determination of the structure was done in 2 phases: (i) based on a partial list of short-range NOEs, the first definition of a low resolution structure was formed; (ii) long-range paramagnetic relaxation enhancements or PREs were measured by probes which used nitroxide spin labels whose attachment points were designed using the previously defined structure. In order to better understand the function as an inhibitor, it is necessary to orient the protein at the phosphocholine surface. Residues 31-55 of Nogo-66 were discovered to have the greatest activity as neuronal growth inhibition (GrandPre, Nakamura et al. 2000, Vasudevan, Schulz et al. 2010).

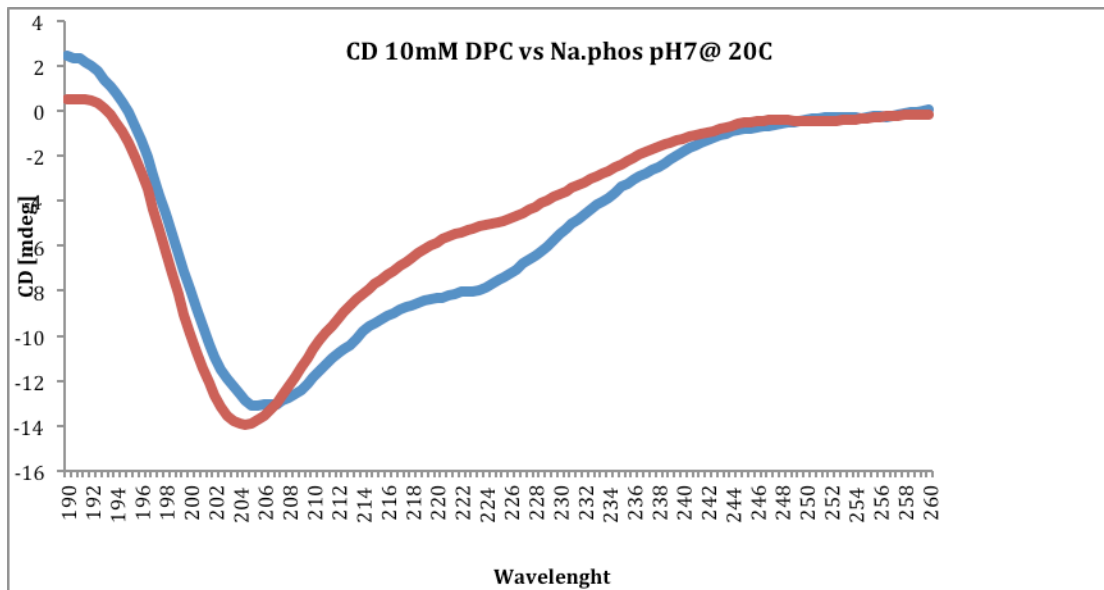


Figure 2.6: Circular Dichroism (CD) of Nogo-Δ20 : (Red) Nogo-Δ20 in Na<sub>2</sub>PO<sub>4</sub> buffer and (blue) in DPC micelles. Changing in spectrum shape indicates some changing in secondary structural formation.

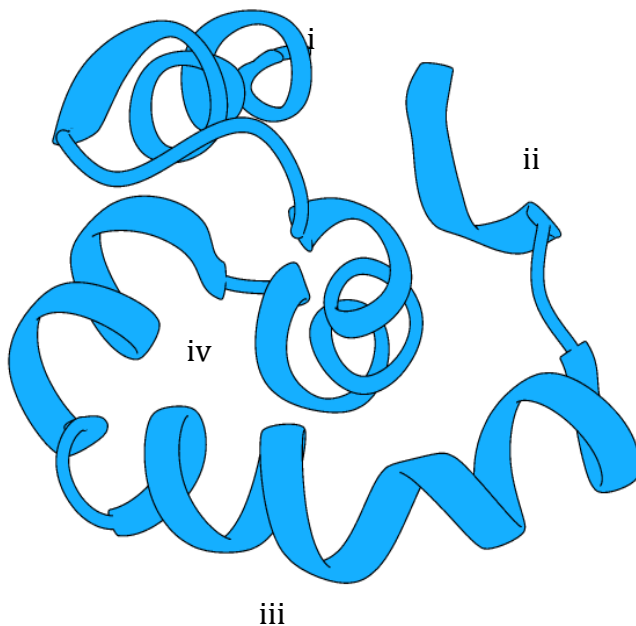


Figure 2.7 : Nogo-66 NMR Structure ( i ) N-terminal ( ii ) C-terminal (iii) binding interface residues (iv) stability residues (Vasudevan, Schulz et al. 2010) (PDB ID 2KO2)

### ***Model of the Nogo: Nogo receptor complex:***

It has been well established that down-regulation of Nogo-A or Nogo receptor increase the regenerative potential of neurons after spinal cord injury. In order to inhibit Nogo, I first used High Ambiguity Driven protein-protein DOCKing (HADDOCK) to gain insight into the nature of the interaction. HADDOCK is a server created for the more experienced modeling user. One of the foremost differences between the HADDOCK web server as compared to less advanced options is that HADDOCK can handle a major class of modeling issues such as protein-protein, protein-nucleic acid, and protein-ligand compounds. The HADDOCK web server also provides a path for the user to upload a hydrogen bond, create and identify a custom distance, and lastly recognize dihedral angle restraint files. Utilizing this type of docking system permits the user to perform a variety of tasks. The user is able to choose the number of structures/complexes to be calculated, while also allowing the user to define and delineate the flexible segments and protonation states within the various histidine containing proteins. The HADDOCK web server supports the established guidelines set forth by the HADDOCK program thus allowing for the same docking mechanisms to be completed with improved efficiency and ease as compared to using HADDOCK on a local machine. (de Vries, van Dijk et al. 2010).

One of the advantages of using HADDOCK for docking studies is using real experimental data that drive the docking process. In addition, HADDOCK uses flexible and semi-flexible backbone and side-chains at the interface (Dominguez, Boelens et al. 2003)(orange website). Therefore, this SA features allow changes to happen in the structure during the binding process.

Nogo-66 mutagenesis studies showed some residues have great impact on the binding to NgR (Figure 2.8). This result suggests these residues are strongly interacting with NgR. To

confirm this observation, I performed binding studies using the HADDOCK server (de Vries, van Dijk et al. 2010). Interestingly, the side chains of the residues show widespread binding between the two molecules at various sites, which remains consistent with our mutagenesis studies. The residues located on the helix nearest to the C-terminal of the Nogo-66 create the binding edge within the complex. This is further exemplified in Figure 2.9 in which one can see that the complex NgR protects the C-terminal of Nogo-66 (Figure 2.9). The HADDOCK docking system takes 162 structures and organizes them into 7 clusters. These clusters represent approximately eighty-one percent of the water-refined models generated by HADDOCK. Based on root-mean-square deviation from lowest energy (i-RMSD) vs. HADDOCK score, and Critical Assessment of Predicted Interactions (CAPRI) docking experiment (Table 2.1), cluster 3 came on the top (Figure 2.12 A B C D). Ideally, the HADDOCK score should only be used to compare the diverse range of solutions for a specific complex. The HADDOCK interface cannot forecast certain binding affinities nor can it differentiate between different complexes.

Cluster 3 contains 17 complexes. The i-RMSD and intermolecular interaction energy ranged between 0 to 2.94 Å and -558.94 to -27.72 Kcal/mol, respectively (Figure 2.12).

The key in this study is to understand how the active residues in Nogo-66 interact with the active residues in NgR and thus suppress re-myelination of spinal cord. I presented the complex that in agreement with our mutagenesis studies and yet satisfied CAPRI.



	RMSD criterion	
	i-RMSD	l-RMSD
Acceptable (*)	i-RMSD <= 4	l-RMSD <= 10
Good (**)	i-RMSD <= 2	l-RMSD <= 5
High (***)	i-RMSD <= 1	l-RMSD <= 1

Table 2.1 : Critical Assessment of Predicted Interactions (CAPRI) docking experiment

The complex is mainly stabilized by elaborate hydrogen bonds/salt bridge networks formed by residues in NgR (Asp111, Asp114, Asp163, Gln162, Gln211, Asp138) and residues in Nogo-66 (Arg53, Arg54, Lys50, Asn46). In 2005, Schimmele *et al* showed that the chief contribution to the binding activity was primarily as a result of a group of four aspartate residues. Reduced binding was found when Asp 111, Asp 114 and Asp 163 were mutated. Asp 138 showed no appreciable effect. A reduction in binding capability was also noted when a mutation was induced at the Gln 162 and Gln 211 residue sites (Schimmele and Pluckthun 2005).

Arg 54 has two binding states. The first is when Arg 53 fully binds to Asp 163. This state has two cases (conformations) where Arg 53 fully binds to Asp 163 (Arg 53 HH21: Asp 163 OD1, Arg 53 HH22: Asp 163 OD2): (i) the side chains of Gln 162 and Gln 211 rotate toward Arg 54 (inward) and form hydrogen bonds with the Arg 54 side chain NH2 group (Arg54 HH21: Gln 162 OE1, Arg 54 HH22: Gln162 OE1)(Figure 2.10); (ii) the side chains of Gln 162 and Gln 211 are

rotated in the opposite direction (outward) (Figure 2.10). The second state is when Arg53 partially binds to Asp 163 (Asp 163 OD1: Arg 53 HH22), Arg 54 side chain NH2 group (HH2) is closer to Asp 163 OD2 than Gln162 (Asp 163 OD2: Arg 54 HH2). This explains why Arg 53 has greater impact in stabilizing the complex, and consequently, executing function. In addition, Li et, showed that Lys50 in Nogo-66 is a major player in the complex. This positively charged residue is located in the center above two negatively charged residues in NgR, Asp 114 and Asp 138. From our docking studies, it is clearly forming strong charge-charge interaction with both Asp 114 and Asp 138 (Figure 2.11). However, Bernhard(.et) showed that mutation of Asp 138 didn't affect the binding to Nogo-66. That's because in the absence of Asp 138, Lys50 side chain rotates and engages itself to another charge-charge interaction with Asp 114 (Ap 114 OD2: Lys50 HZ3, Ap 114 OD1: Lys50 HZ2)(Figure 2.11). This further stabilizes the complex and eliminates the effect of lacking Asp 138. Asp 111 forms hydrogen bonds with Asn 46 (Asp 111 OD1: Asn 46 HD21, Asp 111 OD2: Asn 46 HD22) Ap 114 OD2: Lys50 HZ3, Ap 114 OD1: Lys50 HZ2. Thr 134 is an additional residue bordering the acidic opening. This residue is shown to be an enhancer of the effect (Schimmele and Pluckthun 2005). It forms a salt bridge with Asn 39 in Nogo-66 (Thr 134 OG1: Asn 39 HD22) (Figure2.11).

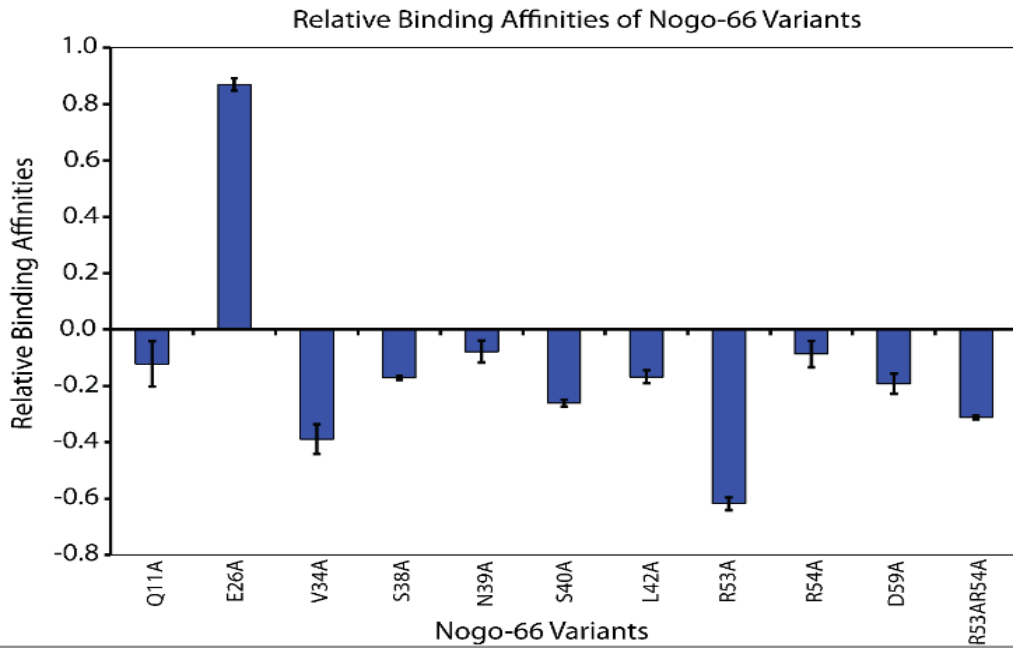


Figure 2.8 : Mutagenesis studies test relative binding affinities. Alanine mutations at each of the active residues in Nogo-66(Vithayathil 2012).

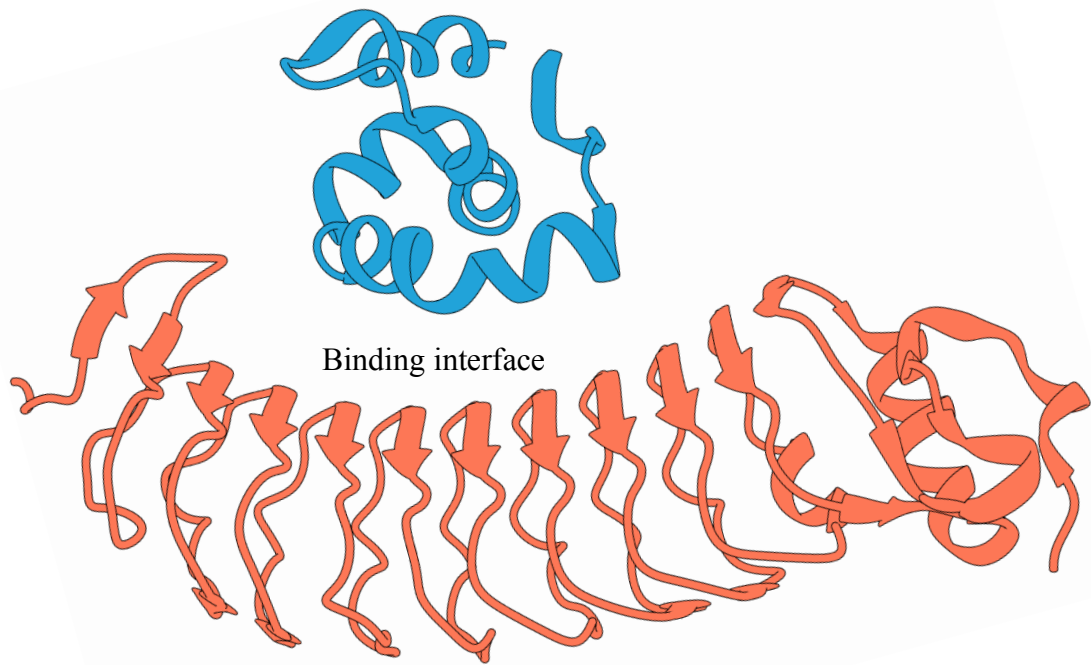


Figure 2.9: Nogo-66 (Blue) and NgR (Orange) binding interface in the complex is formed by concave surface of the receptor and residues of the helix.

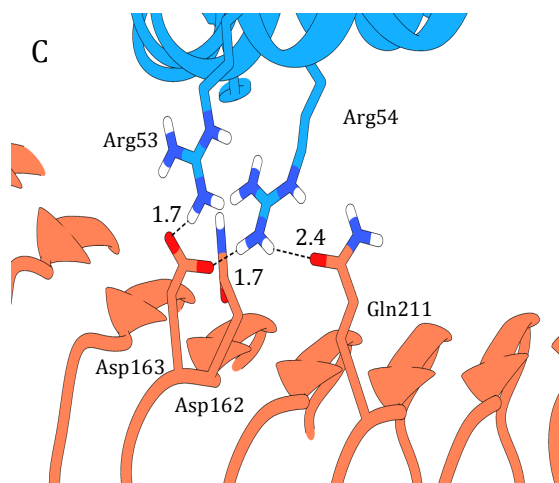
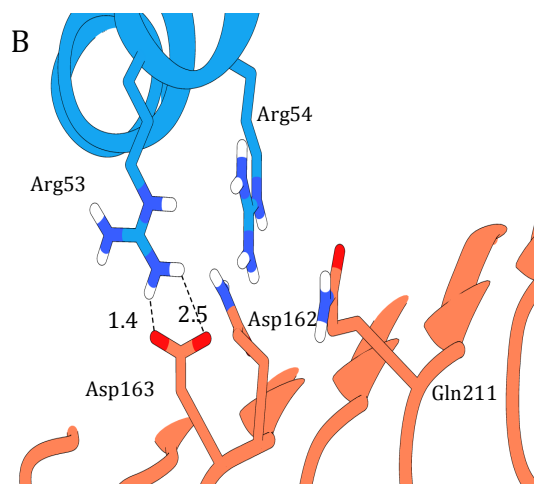
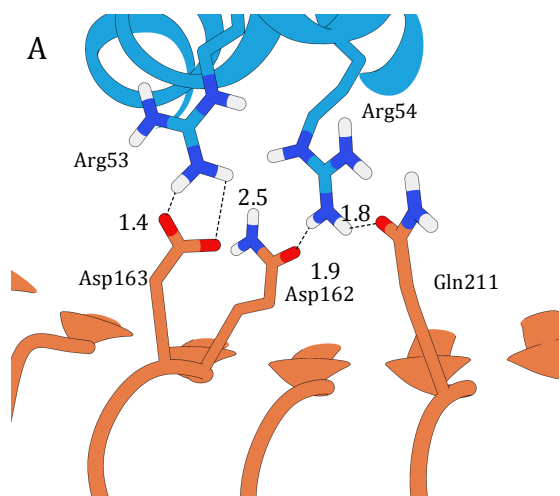


Figure 2.10: Active residues Arg 53 and Arg 54 interaction A) Arg 53-Asp 163 when Arg 54 binds to Q211/Q162. B) Arg 53-Asp 163 when Arg 54 doesn't bind to Q211/Q162. C) Arg 53/54-Asp163 and Arg 54-Q211.

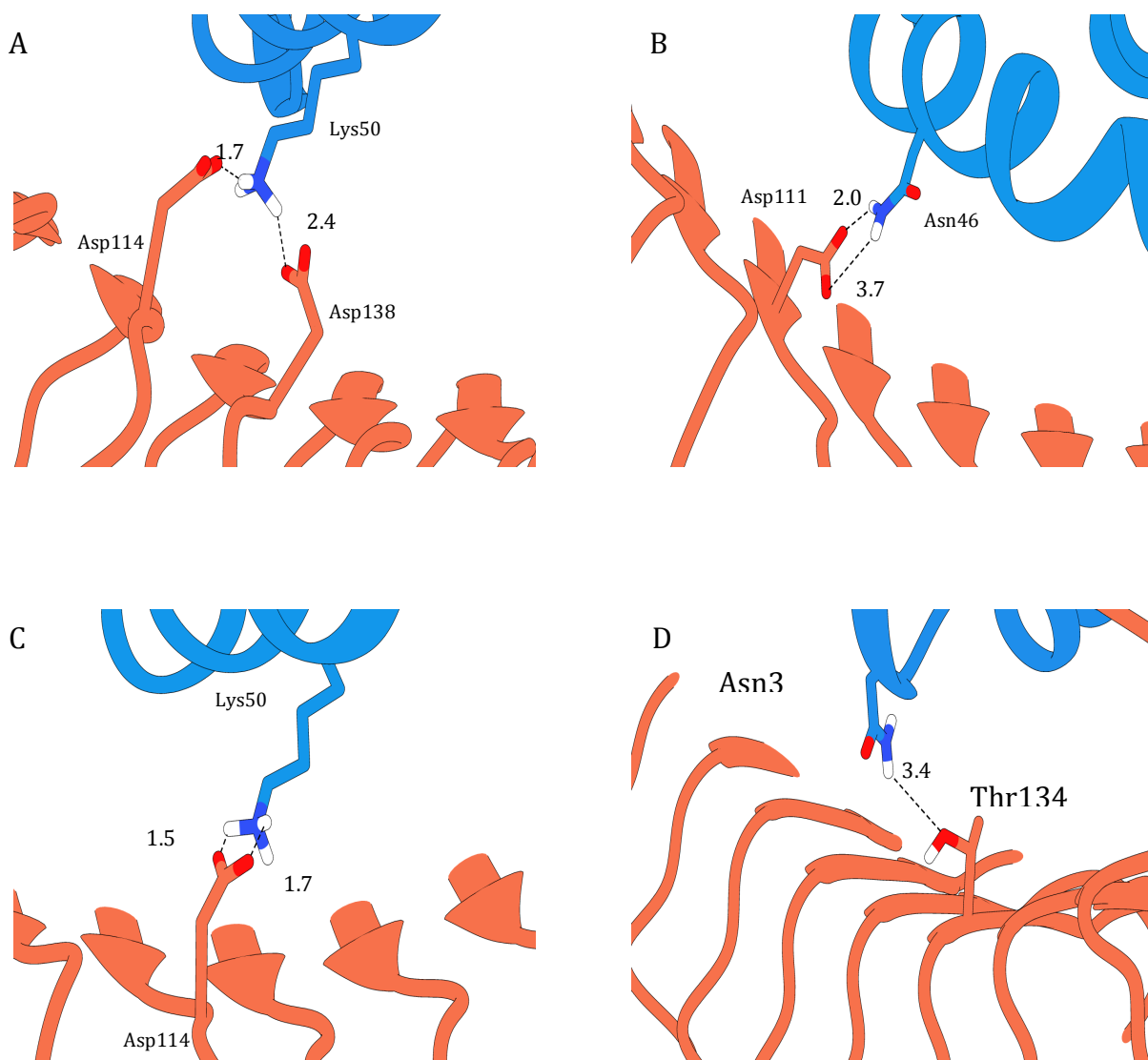


Figure 2.11 : Active residues Lys 50 Asn 46 and Asn 39 A) Lys50-Asp 114/Asp 138 B) Lys 50-Asp 114 in the absence of Asp 138 C) Asn46-Asp11 D) Asn 39-Thr 134.

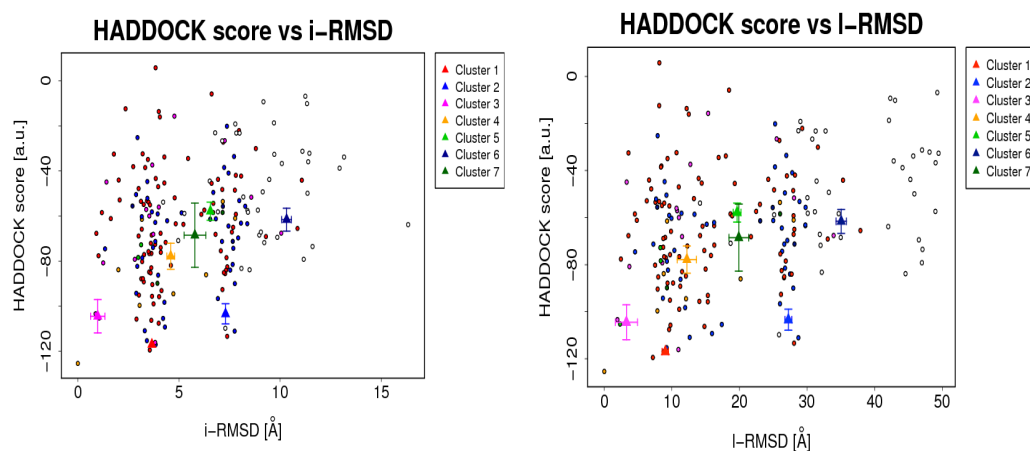


Figure 2.12: (A) Interface root mean square deviation (i-RMSD), Backbone of all residues atoms in the binding site are fitted and then RMSD is calculated over the same atoms (the distance between receptor and protein should be less than 10Å). (B) RMSD -> ligand-RMSD Calculated by first, N=1 molecule backbone atoms (CA,C,N,O) fitting. Then, the backbone atoms of other molecules N>1.

### **Targeting Nogo-A:**

Nogo-66 and Nogo- $\Delta$ 20 proteins and their receptors are good therapeutic candidates. I used aptamers to block the function and help the nervous system recovers after injury.

The term 'aptamer' is derived from the Latin word 'aptus' (to fit) and the Greek word 'meros' (part). Aptamers are short single stranded nucleotides DNA or RNA molecules (20-80 bases ~6-26 kDa) that bind to macromolecule targets (i.e. protein) or small molecules (i.e. organic compounds) with specific binding characteristics and high affinity (Keefe, Pai et al. 2010). The specificity and affinity is based on the ability of the short nucleotides (aptamers) to adapt a unique three-dimensional structure that fits the target. Ellington & Szostak, first described this in 1990 (Ellington and Szostak 1990) (Tuerk and Gold 1990). The interaction between aptamer and a macromolecule target ensues through combination of hydrogen bonding, van der Waals, electrostatic, and stacking interactions.

There are different applications for aptamers. They can be used to understand the interaction between protein and nucleic acid to show original sequences of RNA or DNA recognized by the protein. Aptamers also can be used for diagnostic purposes in human diseases. One example is to use aptamer to detect the existence of Glioblastoma multiform by detecting the presence of Epidermal Growth Factor Receptor (EGFR) (Wan, Kim et al. 2010). The advantages of aptamers over antibodies are summarized in (Table 2.2). Aptamers could surpass antibodies in, for example, ELISA, Western blotting, fluorescent hybridization in situ (Jayasena 1999). In addition, aptamers have been successfully used as therapeutic to treat different diseases. Macugen®, for the treatment of macular degeneration, was the first FDA approved



aptamer based drug. Currently, there are several aptamer-based drugs under clinical trials for treating cancer, immune system, and neurological diseases(Zhou, Bobbin et al. 2012).

Aptamers provide a possible option for CNS disorders: the small size relative to antibodies allows them to penetrate deeper into tissue and potentially cross the blood brain barrier. The likelihood of side effects is reduced due to high affinity, which reduces the amount of aptamers that treatment requires; and easy mechanisms for regulation that provides the treatment with no harm, in case of failure (Zhou, Bobbin et al. 2012)

Neurological disorders like Alzheimer's(Ylera, Lurz et al. 2002, Rentmeister, Bill et al. 2006), multiple sclerosis (Burmeister, Wang et al. 2006, Pendergrast PS 2006), and myasthenia gravis (Lee and Sullenger 1997, Seo 2000) have been investigated using aptamers. We can take the example of an aptamer that was taken in selection against the 40 amino-acid  $\beta$ -amyloid peptide and results showed that it binds fibrils consisting of the peptide. There has been no report regarding fibril dissociation or reduction that has any functional data. Another example for a disorder that has been targeted by aptamers is the neuromuscular disorder Myasthenia gravis. It is an antibody-mediated autoimmune response to the nicotinic acetylcholine receptor or AChR. Against Mab198, a monoclonal antibody that can recognize the major immunogenic epitope on human AChR, modified 29-amino aptamer has been identified. This unique aptamer protected AChR from anti-antibodies, which were found in patients who were afflicted with myasthenia gravis. An even greater protection was offered by 29-fluoropyrimidine- modified aptamer. However, in the instances that have been discussed, the primary application of

aptamers has been the treatment of disorders rather than the modulation of normal neuronal function. Thus, Wang *et al* isolated an aptamer specific for NgR (Wang, Khaing et al. 2010).

Properties	Aptamers	Antibodies
Affinity	Down to pM	Down to pM
Specificity	Very high	High
Stability <i>in vivo</i>	Stable	Stable
Stability <i>in vitro</i>	Sensitive to nucleases without chemical modification	Stable
Selection method	<i>in vitro</i>	<i>in vivo</i>
Reproducibility	Synthesized chemically	Batch to batch variation
Size	Small, <25 kDa	Large, >150 kDa
Thermal stability	Autoclavable, reversible folding	Non reversible thermal unfolding
Chemical modifications	Easy	More difficult
Immunogenicity	None found yet	Present

Table 2.2. Aptamers and antibodies side by side  
Source: <http://rina-gmbh.eu/www/support/technology-aptamer/>

As I previously mentioned, Nogo-A inhibits remyelination of neuronal axons via Nogo-66 and Nogo-Δ20. Recent studies show that Nogo-66 binds not only to NgR but also to PriB. Therefore, targeting NgR alone wouldn't be as effective as targeting Nogo-66 and Nogo-Δ20. Here, I selected DNA aptamers specific for Nogo-66 in different environments (Table 2.3) and another one for Nogo-Δ20.

Typically, the therapeutic strategies to identify selective/specific aptamers are to bind the aptamer directly to the target to regulate downstream effects. The basic process of identifying aptamer starts through *in vitro* selection know as **S**ystematic **E**volution of **L**igands by **EX**ponential enrichment (SELEX) (Ellington and Szostak 1990, Tuerk and Gold 1990), from a large and diverse random sequence DNA/RNA library of typically  $1 \times 10^{13}$  -  $1 \times 10^{16}$  different

members. The final length of each oligonucleotide, including primers, is between 20-100 nucleotides. In SELEX, several rounds of selection are performed. Each round consists of (1) incubation (2) complication (3) amplification (Figure 2.13). First, nucleic acids are incubated with the target molecule. Then, the excess unbound nucleic acid sequences are washed away leaving only the molecules that form a complex with the target molecule. Finally, the bound nucleic acid sequences are amplified by Polymerase Chain Reaction (PCR). Repeating this cycle (6-14 times) will gradually enrich the specificity and the affinity. Treatment of SCI would be done using an aptamer with high specificity and high affinity to inhibit Nogo-66 and Nogo- $\Delta$ 20. To obtain an aptamer with a high affinity for Nogo-A, I focused on Nogo-66 and Nogo- $\Delta$ 20 as the target epitopes.

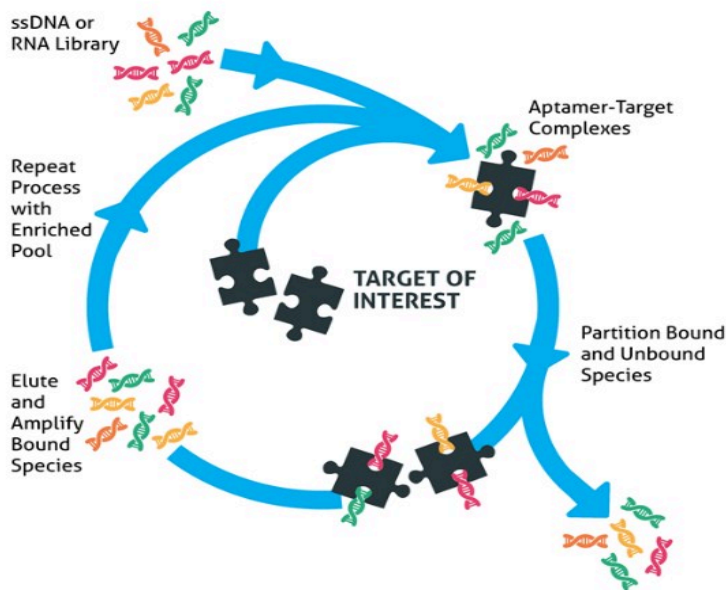


Figure 2.13: SELEX steps

Source: <http://www.aptamergroup.co.uk/Aptamer->

### ***Screening for Aptamer***

To obtain specific aptamer for Nogo-66 and Nogo- $\Delta$ 20, I performed SELEX with an aptamer library (ssDNA) based on 44 nucleotides (nt) flanked by two constant sequences. The target proteins were fused with hexahistidine at the N-terminal (6xHis) and then immobilized individually on separate Ni-NTA (Nickel- Nitrilotriacetic acid) tubes. In each round of selection, the strongly bound DNA species were removed from weak or non-binding species by washing the mixture three times with washing buffer. Retained species were amplified (PCR) and then confirmed of the ssDNA presence by 2% agarose gel (Figure 2.14). I used JSRV protein for negative selections. This step is to remove aptamers that bound species other than the target, including Ni-NTA. After round 14, the recovered library was sequenced by using an Illumina deep sequencing platform, Next Generation Sequencing, NGS (UCI, facility).

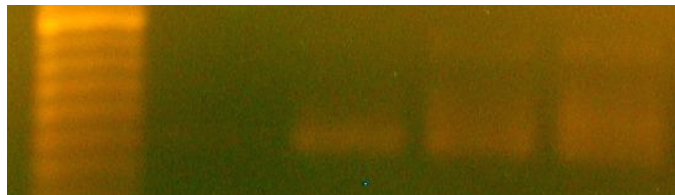


Figure 2.14: 2% agarose gel

### Selecting the best candidate

FASTAptamer v 1.0 tool was used for processing the data and identified potential aptamers for characterization and subsequent analysis (Khalid K. Alam 2014). FASTAptamer toolkit is an open source tool. It comes with five different scripts to perform multiple tasks. These tasks range from simple count, rank, delete the duplicate, sort by decreasing the multiplicity (abundance) to compare the distribution of sequences in two different pools, combined sequences into several cluster by their homology, compute fold-enrichment ratio and searches for specific motifs in multiple pool. I executed the script FASTAptamer-Count to identify the most abundant sequence (Figure 2.15). Then in the next section, I started looking for conserved motifs with a potential to form secondary structure.

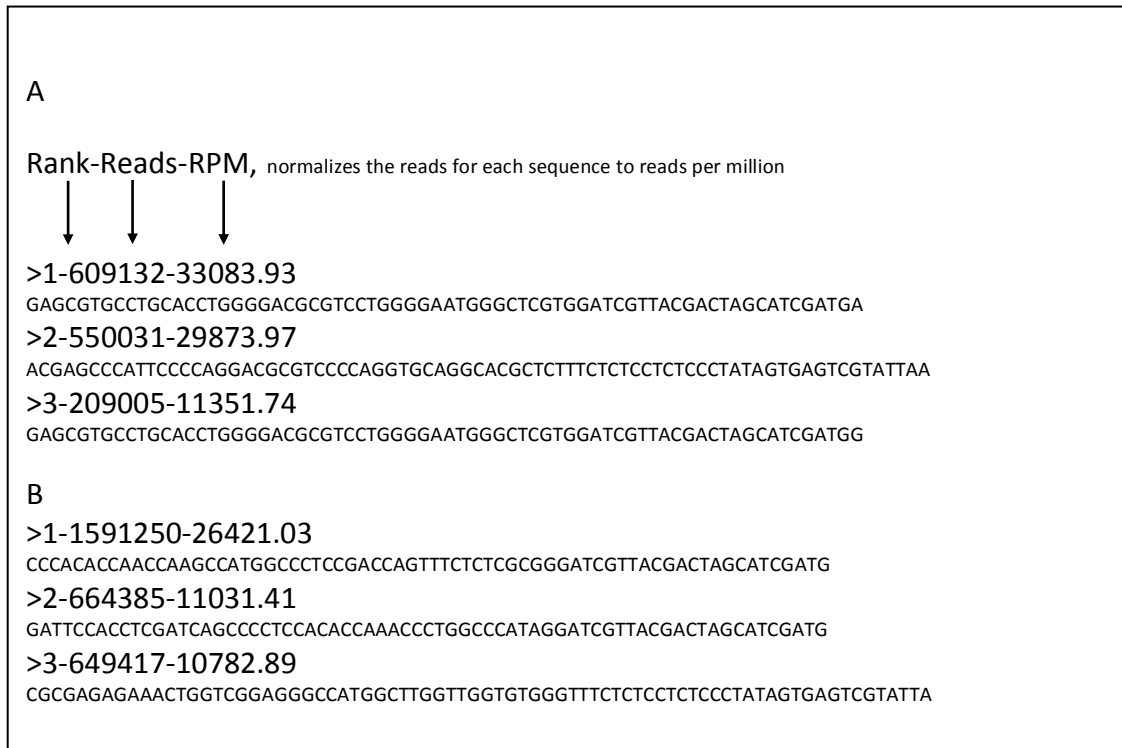


Figure 2.15: Output fasta file format from FASTAptamer-Count script (top three) (A) Nogo-66 aptamers with and with out lipid in presence of traces of urea and (B) Nogo-66 aptamers without lipid and urea.

In Nogo-66, N66-59 and N66-1 are the most abundant in their respective pool. Therefore, they were selected for further investigation.

Nogo-66 without Lipid and with lipid-Traces of Urea		
Name	Frequency	Total sequences (3252581) unique sequences (1154583)
N66-59	68288	GGGAGGGGGCACCAGGGGGCCAGTCC
N66-85	46006	CCGAACCCTCCCCACAGG
N66-33	6792	GCACACCCTATCCGCAAC
Nogo-66 Without Lipid –No Urea		
Name	Frequency	Total sequences (18411717) unique sequences (4120826)
N66-1	609132	GAGCGTGCCTGCACCTGGGGACGCGTCCTGGGGAATGGGCTCGTGGATCGTT ACGACTAGCATCGATGA
N66-2	550031	ACGAGCCCATTCCCCAGGACGCGTCCCCAGGTGCAGGCACGCTCTTTCTCTC CTCTCCCTATAGTGAGTCGTATTA
Rev-Comp		TTAATACGACTCACTATAGGGAGAGGAGAGAAAAGAGCGTGCCTGCACCTGG GGACGCGTCCTGGGGAATGGGCTCGT
N66-3	209005	GAGCGTGCCTGCACCTGGGGACGCGTCCTGGGGAATGGGCTCGTGGATCGTT ACGACTAGCATCGATGG
Nogo-66 With Lipid-No Urea		
Name	Frequency	Total sequences (60226636) unique sequences (23651652).
N66L-1	1591250	CCCACACCAACCAAGCCATGGCCCTCCGACCAGTTTCTCTCGCGGGATCGTT ACGACTAGCATCGATG
N66L-2	664385	GATTCCACCTCGATCAGCCCCTCCACACCAAACCCTGGCCCATAGGATCGTT ACGACTAGCATCGATG
N66L-3	649417	CGCGAGAGAAACTGGTCCGAGGGCCATGGCTTGGTTGGTGTGGGTTTCTCTC CTCTCCCTATAGTGAGTCGTATTA
Nogo $\Delta$ 20 without Lipid-No Urea		
Name	Frequency	Total sequences (120169601) unique sequences (4222587)
N $\Delta$ 20-910	73080	GTACGGGGAAGGACGTCAATAGTCACACAGTCCTTGACGGTATAATAACCA
N $\Delta$ 20-271	70369	GAAACCAATCCGCGGCATTTAGTAGCGGTAAAGTTAGACCAAACCATGAAA
N $\Delta$ 20-49	64440	GGGGAAGGACGTCAATAGTCACACAGTCCTTGACGGTATAATAACCACCAT

Table 2.3: Representative sequences from SELEX after round 14. Top three sequences for Nogo-66 and Nogo $\Delta$ 20.

### ***Structure prediction and Docking:***

I used two different DNA secondary structure prediction servers: i- Mfold and ii-G-Rich Sequences (QGRS) Mapper. Mfold predicts the secondary structure of RNA and DNA using thermodynamic methods while QGRS mapper is based on algorithms that recognize the QGRS in the context of alternatively spliced isoforms of your sequence (Zuker 2003, Kikin, D'Antonio et al. 2006). Mfold predicted that N66-59 should have four secondary structures and three secondary structures for N66-1 (Figure 2.16 A , B). These predicted secondary structures contain a stem-loop motif (hairpin). In DNA and RNA aptamers, hairpin motifs are one of the most common secondary structures. In addition, QGRS Mapper also showed that N66-59 and N66-1 could fold into G-quadruplex (Table 2.4). G-quadruplex is four-guanine bases each forming a hydrogen bond with two neighboring bases (Kulbachinskiy 2007). Interestingly, conserved sequence motifs were observed in both hairpin and G-quadruplex. One structured motif was observed in all predicted secondary structures in N66-59, that I will call Ali3 and another one in N66-1, that I will call Ali4. All conserved motifs (Ali3, Ali4) sequences were synthesized by eurofins, San Diego for docking studies and functional assays.

Ali3 (CCGGGAGGGGGCACCAGGGGGGCC) is GC rich region, 87.5%, which indicates that this region is very stable due to stacking interaction and hydrogen bonds. In order to perform our docking studies, I used the Rosetta server to generate a 3D de novo structure model for Ali3 (Figure 2.17 A). The server generated 1000 structures and ranked (scored) them according to their energy. The selected structure was the second best model in terms of energy (Das, Karanicolas et al. 2010, Lyskov, Chou et al. 2013). Then, I used UCSF Chimera to fit Nogo-66 into

Ali3 (Figure 2.17 B) (Pettersen, Goddard et al. 2004). From the fitted-model, it is clear that Ali3 is interacting with Nogo-66 active binding site. Ali4 (GAGCGTGCCTGCACCTGGGGACGCGTC) generated 3D structures could not fit the Nogo-66 binding site. This may indicate that this motif binds to a different site in Nogo-66.



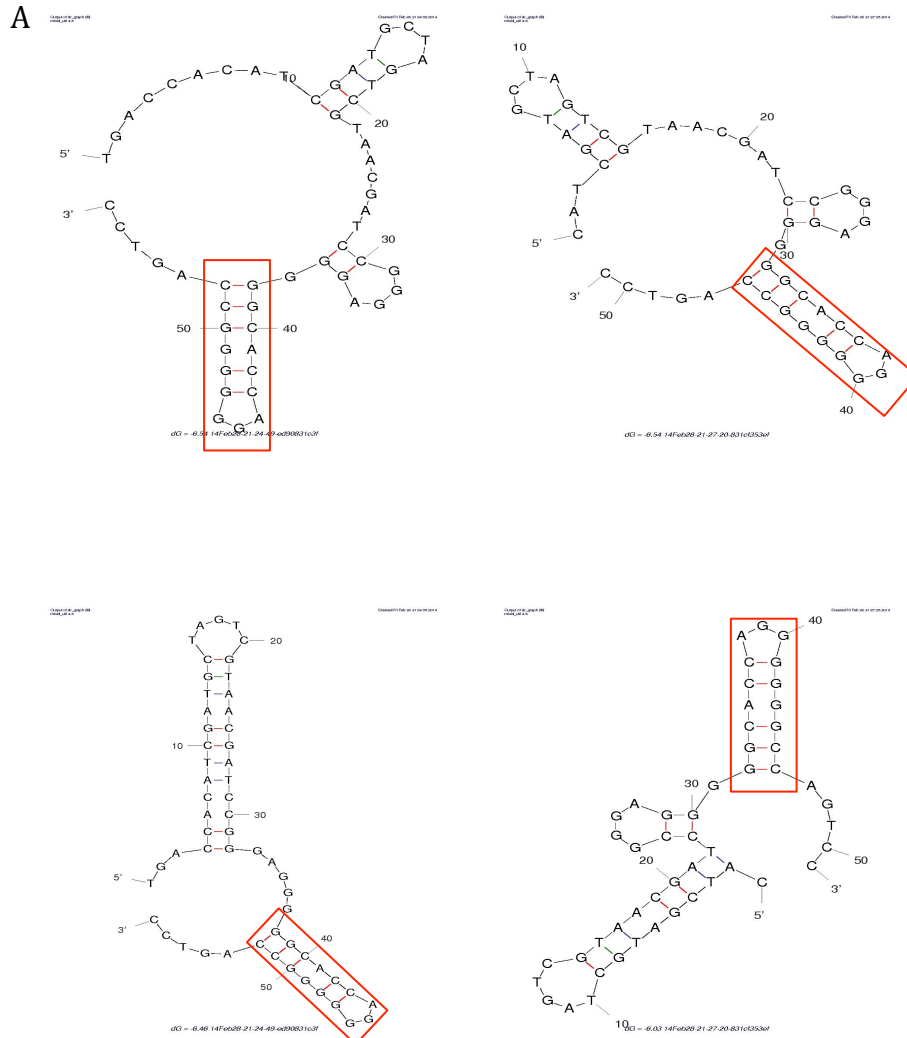


Figure 2.16: (A) Mfold for N66-59; Ali3 (red)

B

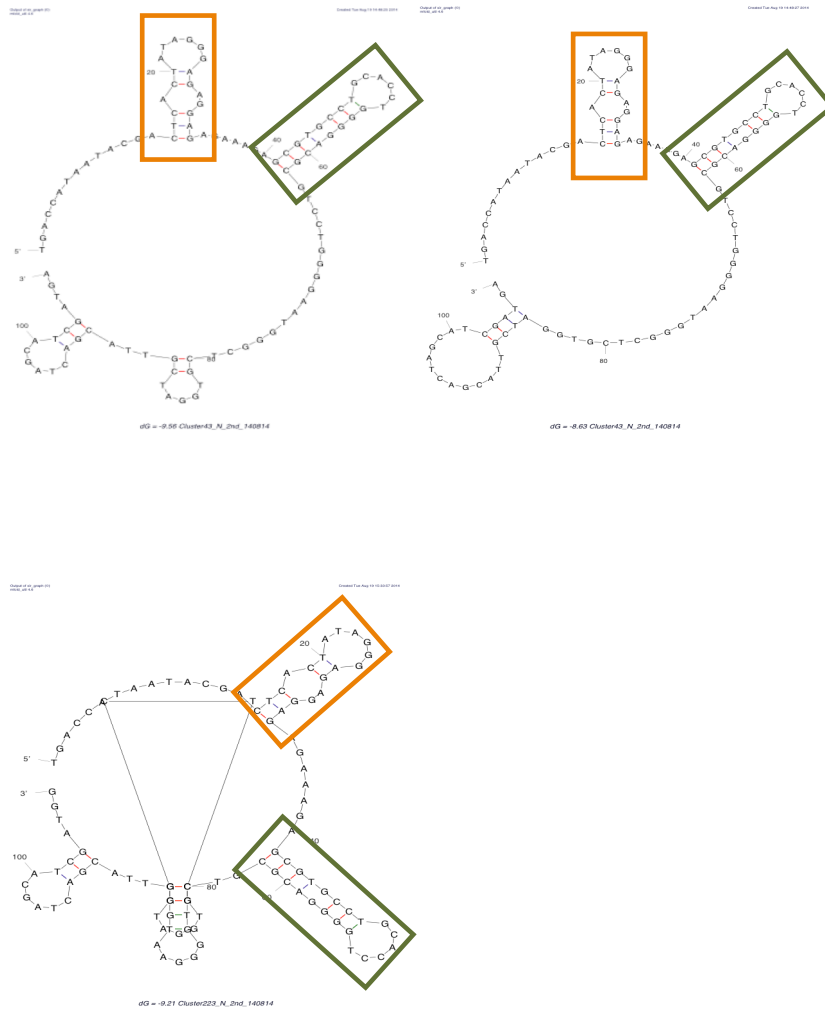


Figure 2.16: (B) Mfold For N66-1 ; Ali4 (Green) Primer binding site (Orange)

N66-59	CATCGATGCT AGTCGTAACG ATCC <u>GGG</u> AGG <u>GGG</u> CACCAGG <u>GGGG</u> CCAGTC
N66-1	CTGCACCTGG <u>GG</u> ACGCGTCC <u>TGGG</u> GAAT <u>GG</u> GCTCGT <u>GG</u> AT CGTTACGACT
Table 2.4: QGRS mapper, predicted secondary structures for N66-59 and N66-1	

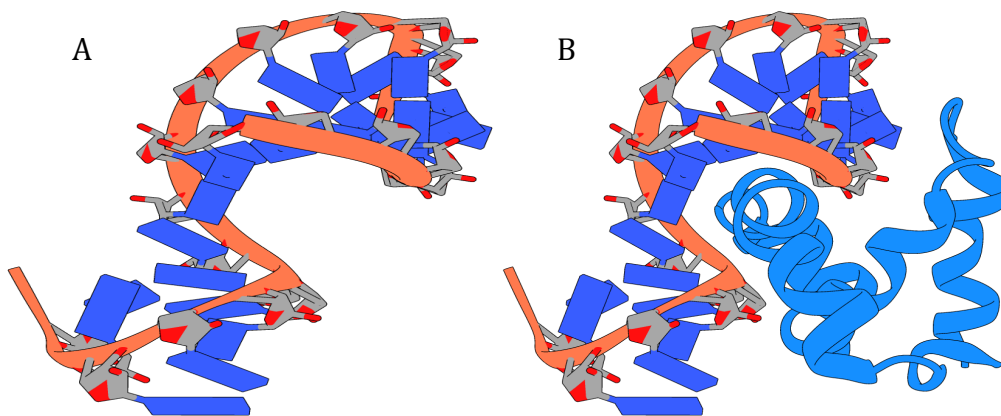


Figure 2.17: (A) Ali3 (B) Ali3 and Nogo-66

### ***Confirmation of Ali3 binding to Nogo-66 by NMR***

I used NMR target resonance-based approach chemical shift perturbation, to detect the intermolecular interaction between Ali3 and Nogo-66 (Hajduk, Meadows et al. 1999). A chemical shift is very sensitive to ligand binding to a target. It can detect molecules with a wide range of affinities, (nM up to mM). In this approach, the difference in chemical shift of the magnetic nuclei between bound and unbound protein indicates the binding site. Thus, the chemical shift perturbation approach analysis can be a useful experiment to identify the binding site of the ligand on the target protein.

<sup>15</sup>N Nogo-66 was prepared to reduce the complexity of the NMR spectrum and increase the sensitivity and resolution. Then, a two-dimensional <sup>1</sup>H-<sup>15</sup>N heteronuclear single quantum coherence (HSQC) NMR spectrum was recorded on Varian Inova 800 MHz for both <sup>15</sup>N Nogo-66 alone and in the presences of Ali3 (CCGGGAGGGGGCACCAGGGGGGCC). HSQC is a fingerprint of a protein backbone; each peak in the spectrum represents one amino acid. Comparing both spectra, it appears that Ali3 has affected some residues, mainly in the binding interface with NgR, by significantly changing the positions of corresponding peaks (Figure 2.18). This observation reveals that Ali3 did bind at the binding interface between Nogo-66 and NgR.

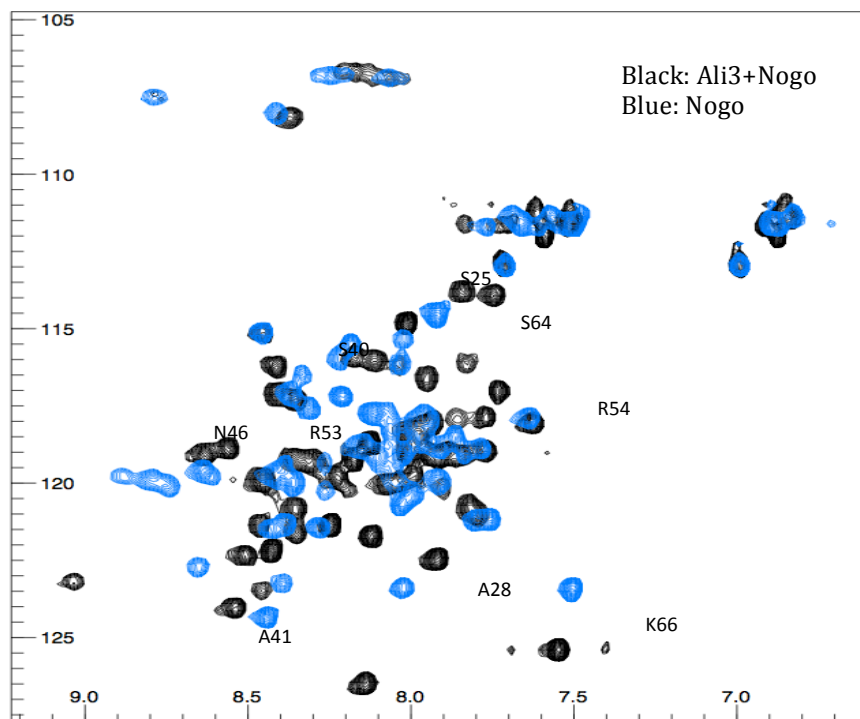


Figure 2.18:  $^{15}\text{N}$  HSQC NMR of Nogo66 with Ali3. The reference Nogo-66 alone (blue) is overlaid with data from a sample of Nogo-66 mixed with Ali3 (Black) 1:1 ratio. These are contoured differently for visualization. Complete fingerprint spectrum of backbone amide signals; most of the peaks are shifted, indicating that Ali3 did bind to the Nogo66. Affected groups in the binding interface (most expose to solvent ~31-55 residues).

Currently, our lab is performing neuronal growth functional assay to test the therapeutic effects of Ali3 and Ali4+Ali7 on neuron axonal regeneration. Next, we are going to do analysis for the rest of selected pool (Nogo-66 with lipid and Nogo $\Delta$ 20) and perform functional assays.

**Chapter 3**  
**Glutamate Provides a Key Structural Contact Between**  
**Reticulon-4 (Nogo-66) and Phosphocholine**

This chapter published in BBA: Biomembranes (2014) vol 1838, p 2350-6

Ali Alhoshani<sup>a</sup>, Rosemarie Vithayathil<sup>b</sup>, Jonathan Bandong<sup>b</sup>, Katherine M. Chrnyk<sup>b</sup>,  
Gabriel O. Moreno<sup>b</sup>, Gregory A. Weiss<sup>b,c</sup> and Melanie J. Cocco<sup>a,b\*</sup>

<sup>a</sup>Department of Pharmaceutical Sciences; <sup>b</sup>Department of Molecular Biology and Biochemistry; <sup>c</sup>Department of Chemistry University of California, Irvine, CA 9269

## Abstract

Human reticulon 4 (RTN-4) has been identified as the neurite outgrowth inhibitor (Nogo). This protein contains a span of 66 amino acids (Nogo-66) flanked by two membrane helices at the C-terminus. We previously determined the NMR structure of Nogo-66 in a native-like environment and defined the regions of Nogo-66 expected to be membrane embedded. We hypothesize that aromatic groups and a negative charge hyperconserved among RTNs (Glu26) drive the remarkably strong association of Nogo-66 with a phosphocholine surface. Glu26 is an isolated charge with no counter ion provided by nearby protein groups. We modeled the docking of dodecylphosphocholine (DPC) with Nogo-66 and found that a lipid choline group could form a stable salt bridge with Glu26 and serve as a membrane anchor point. To test the role of the Glu26 anion in binding choline, we mutated this residue to alanine and assessed the structural consequences, association with lipid and affinity for the Nogo receptor. In an aqueous environment, Nogo-66 Glu26Ala is more helical than WT and binds the Nogo receptor with higher affinity. Thus, we can conclude that in the absence of a neutralizing positive charge provided by lipid, the glutamate anion is destabilizing to the Nogo-66 fold. Although the Nogo-66 Glu26Ala free energy of transfer from water into lipid is similar to that of WT, NMR data reveal a dramatic loss of tertiary structure for the mutant in DPC micelles. These data show that Glu26 has a key role in defining the structure of Nogo-66 on a phosphocholine surface.

## Introduction

As discussed above, RTNs are involved in various functions. In ER, they are believed to maintain the membrane curvature (Voeltz, Prinz et al. 2006). Previously, we found that Nogo-66 was disordered in solution but folded into a structure that was 85% helical in the presence of DMPC vesicles (Vasudevan, Schulz et al. 2010). Thus, the structure of Nogo-66 is driven by lipid interactions. To develop a list of potential protein/lipid interactions that could contribute in defining the protein fold, we mapped conserved positions onto the Nogo-66 structure. RTN sequences include one position that is hyperconserved among all RHDs (Figure 3.1C red highlight) and other groups that are conserved within the RTNs of higher vertebrates (e.g., Figure 3.1 C yellow, green highlight) (Oertle, Klinger et al. 2003). The positions of proposed lipid-interacting groups conserved in higher vertebrates (Tyr3, Phe19, Phe56, Leu61) and the hyperconserved Glu26 are depicted in the structure of Nogo-66 in (Figure 3.1 A-B). There are other groups conserved in higher vertebrates that appear to participate in intra-molecular helix-helix interactions (Arg1-Asp/Glu32, Leu65) or modulate secondary structure (Gly16, Pro18). These may play a role in folding the RHD-66 but do not appear to interact directly with lipid based on our previous study of accessibility and NOE contacts to DPC.

Inspection of the Nogo-66/DPC structure reveals that the hyperconserved Glu26 side chain is positioned at the base of a cavity and it is not involved in any interactions with charged functional groups from the protein that could neutralize the carboxylate. A model of PC binding in the Glu26 cavity shows that the choline group fits very well (Figure 3.2A). In fact, NOEs were previously found between protein groups and the DPC headgroup (Figure 3.2B). Other examples of PC-protein binding are shown in Figure 3.2 C-G. Since it appears plausible that the



Glu26 cavity in Nogo-66 could similarly bind PC, we hypothesized that Glu26 could play a role in the determining the protein structure; we tested this by mutation of Glu26 to Ala, a group unable to bind choline through ionic interactions.

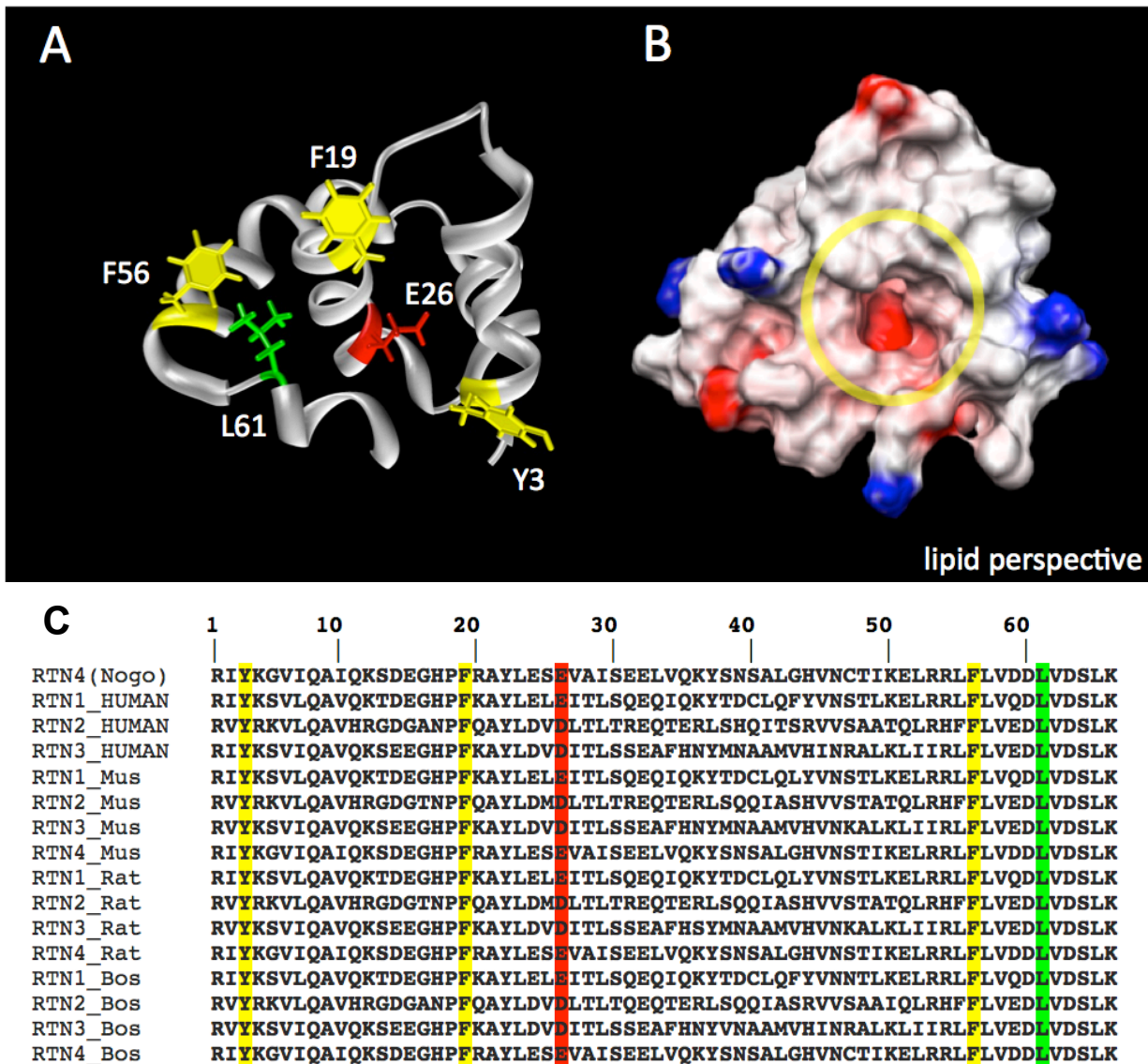


Figure 3.1. Structure and homology of Nogo-66. A) Ribbon diagram of Nogo-66 showing the lipid-protein interface of Nogo-66 (PDB ID: 2KO2); groups conserved among higher vertebrate RHDs are highlighted (yellow: Y3, F19, F56; green: L61); a negative charge is hyperconserved (E or D) among all RHDs at position 26 (red: E26). B) surface representation of Nogo66 colored according to electrostatic potential; facing the phosphocholine surface, E26 is visible at the base of a cavity (yellow circle) with no protein counter ion nearby. C) Sequence Alignment of RHD-66 (extracellular region) of selected higher vertebrates; conserved groups that contact lipid (featured in A and B) are highlighted.

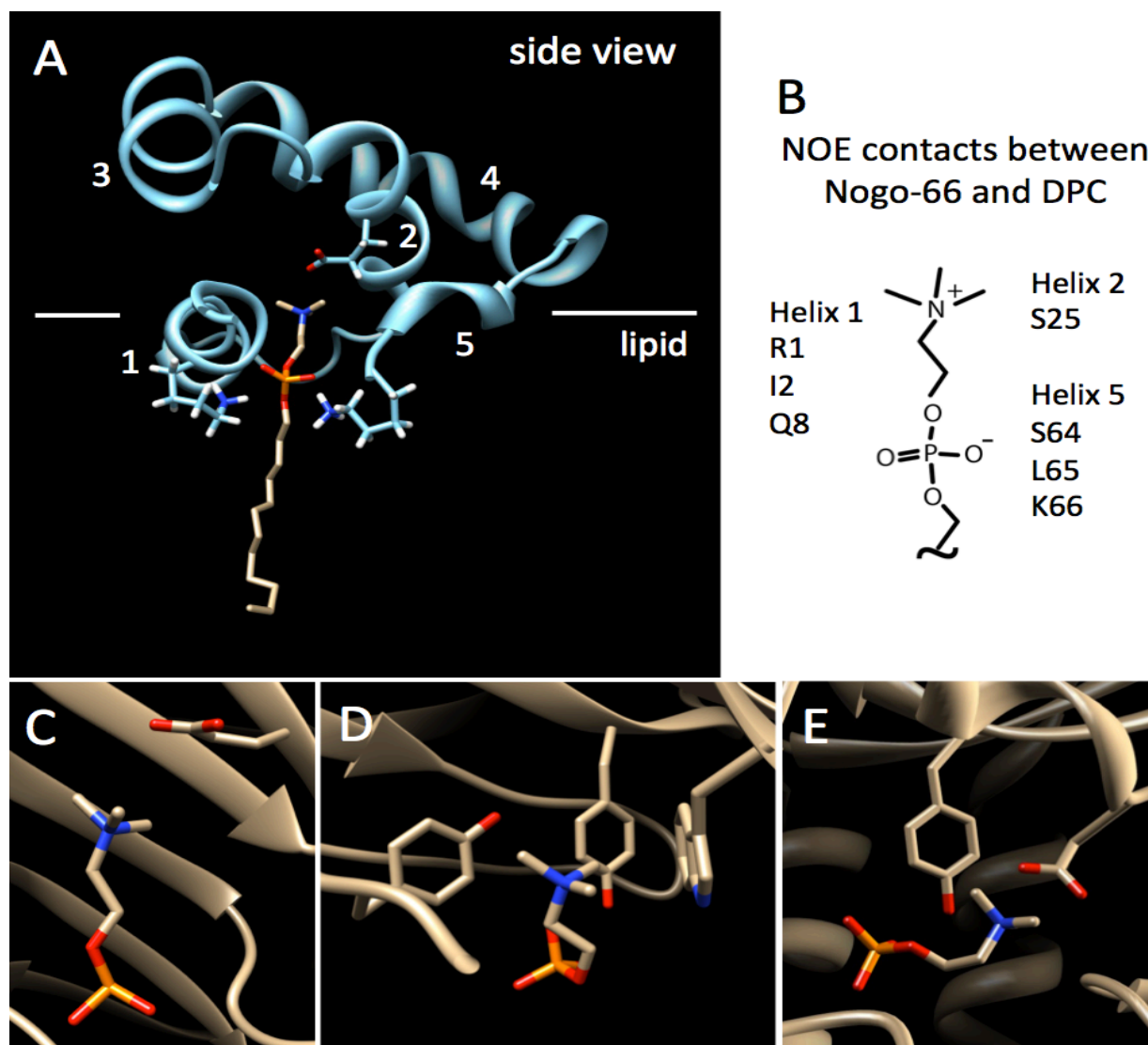


Figure 3.2: A) Model of a single DPC molecule docked into the Nogo-66 Glu26 cavity by manually adjusting the position of DPC and cationic side chains. Helices 1-5 are numbered. B) NOEs previously determined between protein and DPC guide placement of the DPC phosphocholine in contact with helices 1 and 5 and in proximity to Glu26 (Vasudevan, Schulz et al. 2010). Several other proteins are known to bind the choline cation of a phosphocholine group via interaction with either a Glu or Asp carboxylate and/or aromatic p-cation bonding. C) Human C-reactive protein (PDB ID: 1B09) binds a PC at the protein surface through ionic interactions forming a salt bridge between choline and Glu81. D) The antibody MC/Pc603 Fab-PC complex (PDB ID: 2MCP) binds the choline using aromatic ring p-cation interactions. E) The enzyme PfPMT (PDB ID: 3UJC) produces PC as a product. In this case, the protein binds choline using both p-cation and ionic interactions.

### ***Secondary structure and partitioning of E26A into the lipid phase***

The structural features of Nogo-66 wild type (WT) have been described by circular dichroism (CD) and NMR spectroscopies (Vasudevan, Schulz et al. 2010). These experiments were performed in the aqueous phase where functional assays have shown Nogo-66 is active as an axonal growth inhibitor, and in the presence of lipid or detergent. We mutated Glu26 to alanine and compared CD spectra of this sample to Nogo-66 WT in both the aqueous phase and in the presence of DMPC lipid vesicles. We assessed the secondary structure of E26A using CD in Figure 3.3 A. The CD spectrum of Nogo-66 WT in water features little helical content (15%) and a substantial contribution of random coil below 205 nm. In contrast, the CD spectrum of the mutant E26A shows a canonical helical signature, estimated to be 38% helix (Figure 3.3 A blue). Previously, we demonstrated that addition of lipid vesicles to Nogo-66 WT induces a dramatic increase in helical content (to 85% helix) (Vasudevan, Schulz et al. 2010). We performed a similar measurement for E26A but found a more modest increase in helical content when lipid was added, E26A is estimated to be 64% helical in DMPC. Based on these CD data, E26A is ~23% more helical in water but ~21% less structured in the presence of lipid compared to WT; transfer of E26A into the lipid phase only increases the helical content by ~16%. Since the lipid bilayer is a liquid phase, the partition coefficient,  $K_x$  is the correct term to compare the affinities of Nogo-66 WT and E26A with the lipid phase (White, Wimley et al. 1998). This can be calculated from a change in ellipticity ( $\theta$ , mdeg) if a peptide or protein shows substantial folding in the presence of lipid. We measured CD spectra of WT and E26A with increasing DMPC lipid concentration and normalized the change in ellipticity at 222 nm between the two samples to determine the fraction of protein ( $f_l$ ) partitioned into lipid. Figure

3.3B shows the partitioning of E26A compared to WT. Notably, the two proteins transfer favorably into the lipid phase with very similar partition coefficients (WT:  $K_x = 1.8 \times 10^5$ ; E26A:  $K_x = 1.2 \times 10^5$ ). The corresponding free energies of transfer are virtually identical:  $\Delta G = -5.8$  kcal/mol for WT and  $\Delta G = -5.6$  kcal/mol for E26A.

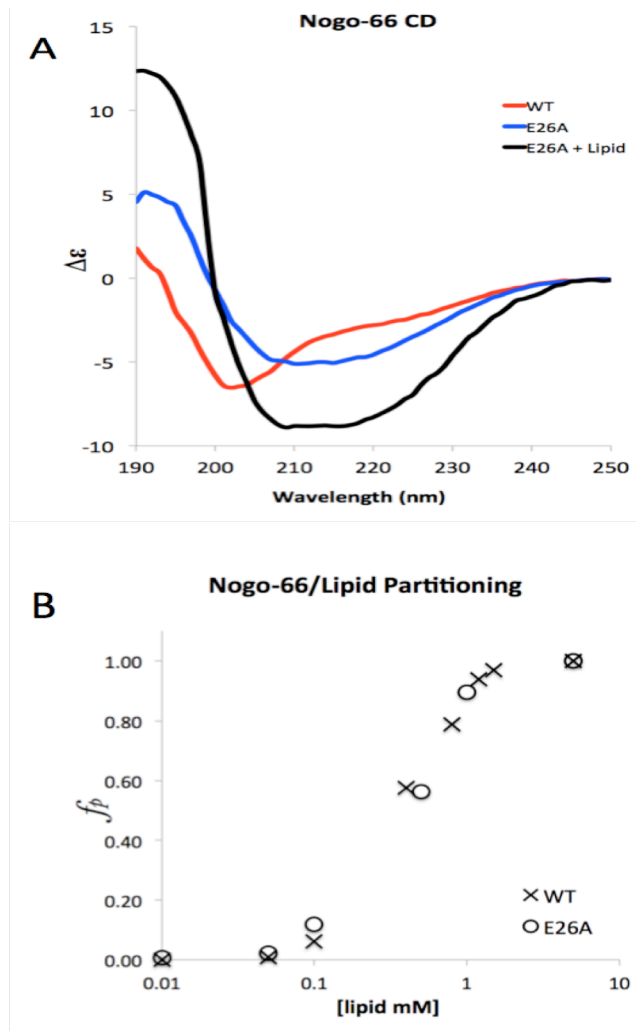


Figure 3.3. Secondary structure and lipid partitioning of WT and E26A Nogo-66 determined by CD spectroscopy. A) Comparison of CD spectra of WT (red) and E26A (blue) in an aqueous environment (5 mM NaAcetate, pH 5.0, 25°C). An increase in helical content (signal at 222nm) is visible in the mutant spectra, WT is approximately 15% helical; E26A is calculated to be 38%. Addition of DMPC lipid vesicles (100 nm diameter) to E26A resulted in a significant increase in helical secondary structure (64%), but less than the increase seen for WT (85%) (Vasudevan, Schulz et al. 2010). B) A plot of the fraction of protein in the lipid phase (calculated as 1 - normalized  $q_{222nm}$ ) with increasing lipid concentrations. The partition coefficient for E26A ( $K_x = 1.2 \times 10^5$ ) is only slightly lower than that of WT ( $K_x = 1.8 \times 10^5$ ).

### ***NMR characterization of E26A***

We prepared a  $^{15}\text{N}$ -labeled sample of Nogo-66 E26A and collected  $^{15}\text{N}$ -HSQC NMR spectra as a measure of tertiary structure. Although CD data described above indicate that E26A is more helical in an aqueous environment compared to WT, we found no long range NOEs in NMR experiments performed on E26A in water (this is similar to the results of NMR experiments on WT in an aqueous environment (Vasudevan, Schulz et al. 2010)). In addition, the protein amide groups of E26A exchange immediately with  $\text{D}_2\text{O}$ , indicating a lack of stable structure. Previously, WT Nogo-66 was found to be highly ordered in DPC, giving one set of strong NMR signals with many long-range NOEs (Vasudevan, Schulz et al. 2010). In contrast, the  $^{15}\text{N}$ -HSQC spectra of E26A in DPC is disordered with broad signals in the random coil region (Figure 3.4). The protein in DPC appears to be molten and we find only a few NOEs in the E26A NOESY spectrum. Although Nogo-66 WT samples remained soluble for weeks at low pH, the E26A mutant is prone to aggregation under the same conditions. Comparison of NMR spectra for WT and E26A show a dramatic change in structure; the mutant spectra reveal conformational heterogeneity for this species.

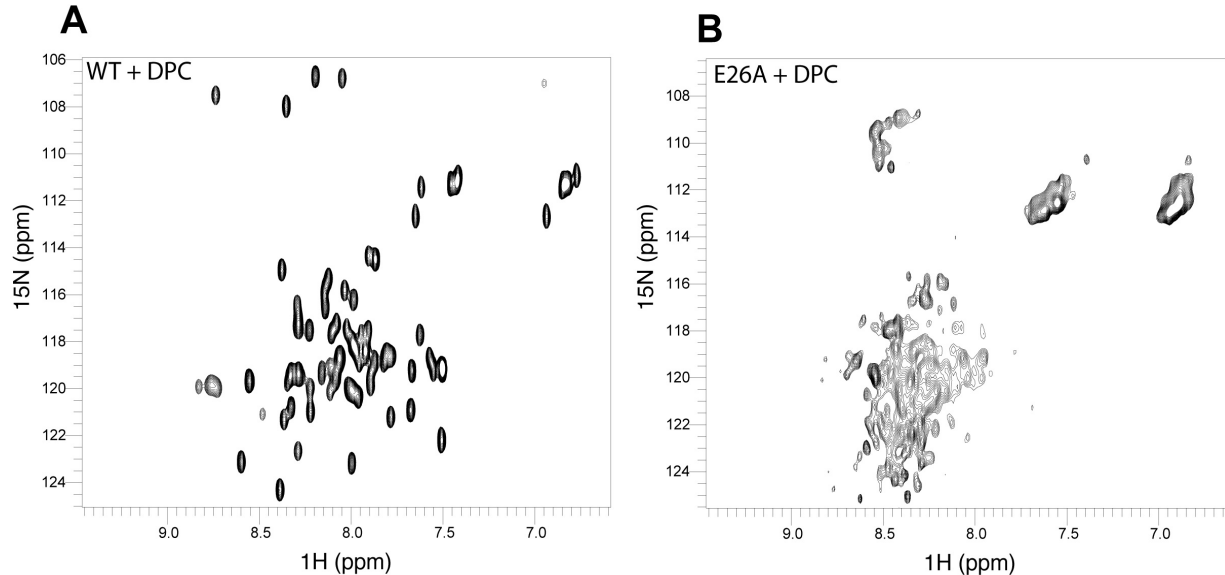


Figure 3.4: Tertiary structure of WT and E26A Nogo-66 in DPC assessed by NMR spectroscopy. 800 MHz  $^{15}\text{N}$  HSQC spectra of A) WT and B) E26A Nogo-66 in 200 mM DPC.

### ***Nogo receptor binding***

Functional assays have largely been performed on Nogo-66 in the aqueous phase. Although Nogo-66 is disordered in water, it is active in blocking neuronal outgrowth. It is possible that Nogo-66 folds into a helical bundle on the receptor surface with a conformation similar to that of the lipid-bound state. Since E26A was found to stabilize a helical conformation for Nogo-66 (Figure 3.3 A), we chose to assess receptor binding for this mutant under conditions similar to functional assays (aqueous phase). The use of phage display has proven a sensitive indicator of Nogo-66 binding to the receptor (Chen, Huber et al. 2000). Nogo-66 and the NgR are not soluble at the same pH; this presents a challenge for binding assays. We have determined that the NgR is unfolded at the pH optimal for Nogo-66 solubility (pH 4) and Nogo-66 begins to precipitate



above pH 5 where the receptor is stable. Phage display is a powerful technique in determining binding of a large library of mutant proteins in a single measurement. Display of the protein Nogo-66 on a phage particle offers another significant advantage: the phage particle is an enormous solubility tag. Phage can be concentrated to a point where they form liquid crystals and still remain soluble. Expression of Nogo-66 on the phage surface keeps Nogo-66 in solution and monodisperse, allowing for robust binding assays.

Monotopic membrane proteins, like Nogo-66, can be displayed consistently using a mutant helper phage, termed M13-KO7<sup>+</sup> or KO7<sup>+</sup>, to package the phage. KO7<sup>+</sup> incorporates an extra positively charged functionality into the phage coat, which can better mimic the zwitterionic composition of phospholipid head groups (Vithayathil, Hooy et al. 2011). In the experiments reported here, Nogo-66 is displayed as a fusion to the major coat protein, P8 on the surface of KO7<sup>+</sup> packaged phage particles. A FLAG epitope fused to the N-terminus allows estimation of relative levels of the displayed proteins.

After successful mutagenesis of the Nogo-66 WT phagemid to incorporate the E26A point mutation, a phage-based ELISA confirmed the display of the Nogo-66 E26A variant. In this assay, an anti-FLAG antibody was immobilized on a 96-well microtiter plate. Subsequent to the wells being blocked with BSA, Nogo-66 E26A-displayed phage was incubated with the anti-FLAG antibody. The wells were washed to remove any unbound phage. Anti-M13 antibody specific to the phage was then incubated, and the relative levels of displayed Nogo-66 WT and E26A variant were measured by HRP activity (Figure 3.6). Following confirmation of the successful display of the Nogo-66 variant, the binding of the phage-displayed Nogo-66 E26A to NgR was examined (Figure 2.6). In order to determine the relative binding affinity of the Nogo-66 variant

from the absorbance levels, the display levels and binding levels were measured on the same ELISA plate (Figure 3.5 and 3.6). Negative controls included binding to NgR by KO7<sup>+</sup> phage without Nogo-66 displayed and binding of phage-displayed Nogo-66, wild-type and variant to the blocking agent, BSA; as expected, the negative controls for the Nogo-66 variants displayed essentially no binding (Figure 3.6).

As shown previously (Rossenu, Leyman et al. 2003), the ratio of the Nogo-66 binding levels ( $A$ ) to display levels ( $A^0$ ) has a linear correlation to the  $K_A$  for the interaction, provided the concentration of the target protein (NgR) greatly exceeds the concentration of the displayed protein. This is a reasonable assumption for a phage-displayed 7.5 kD protein. Thus, a correlation likely exists between the apparent and actual  $K_A$  of the NgR binding to Nogo66 wild-type and the variant. The binding affinity as apparent  $K_A$  of the Nogo-66 E26A relative to wild-type is represented in Figure 3.5. The mutation of Glu26 to Ala resulted in a four-fold increase in affinity to the receptor.

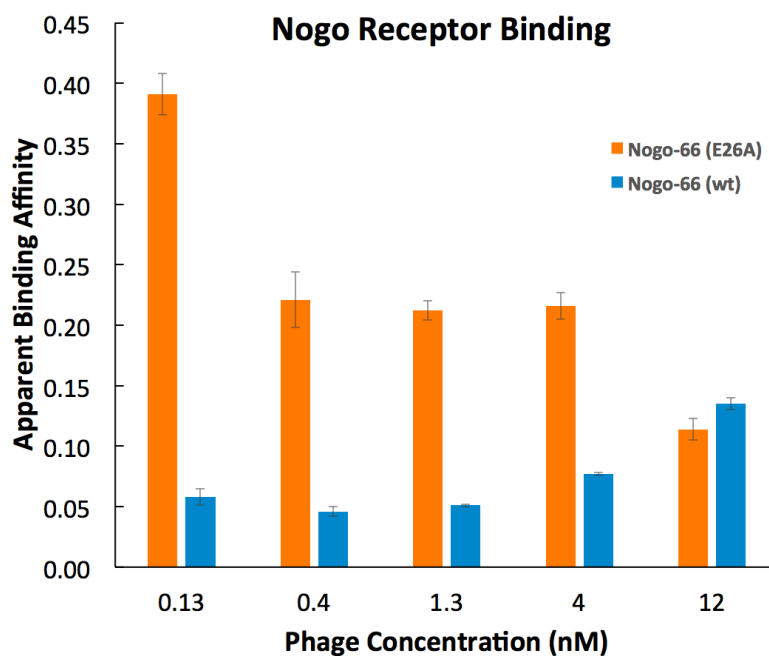


Figure 3.5: Apparent Binding Affinity of Nogo-66 WT and E26A mutant to the Nogo receptor. The apparent binding affinity is calculated as the apparent  $K_A$  of the ligand-receptor interaction. The apparent  $K_A$  is determined as the ratio of the binding levels of the protein (Nogo-66 WT or E26A) with its target (NgR) ( $A$ ) to the amount of displayed protein (Nogo-66 WT or E26A) on the phage surface ( $A^0$ ) (Rossenu, Leyman et al. 2003). A single microtiter plate was used to simultaneously measure display levels and binding levels of Nogo-66 WT and E26A mutant. Each concentration was in triplicate and the average plotted. Standard errors are shown. In the range where the apparent  $K_A$  is linear, the mutant E26A shows a binding affinity for NgR that is four-fold higher than that of WT.

### Receptor Binding Affinity of E26A mutant and WtNg66

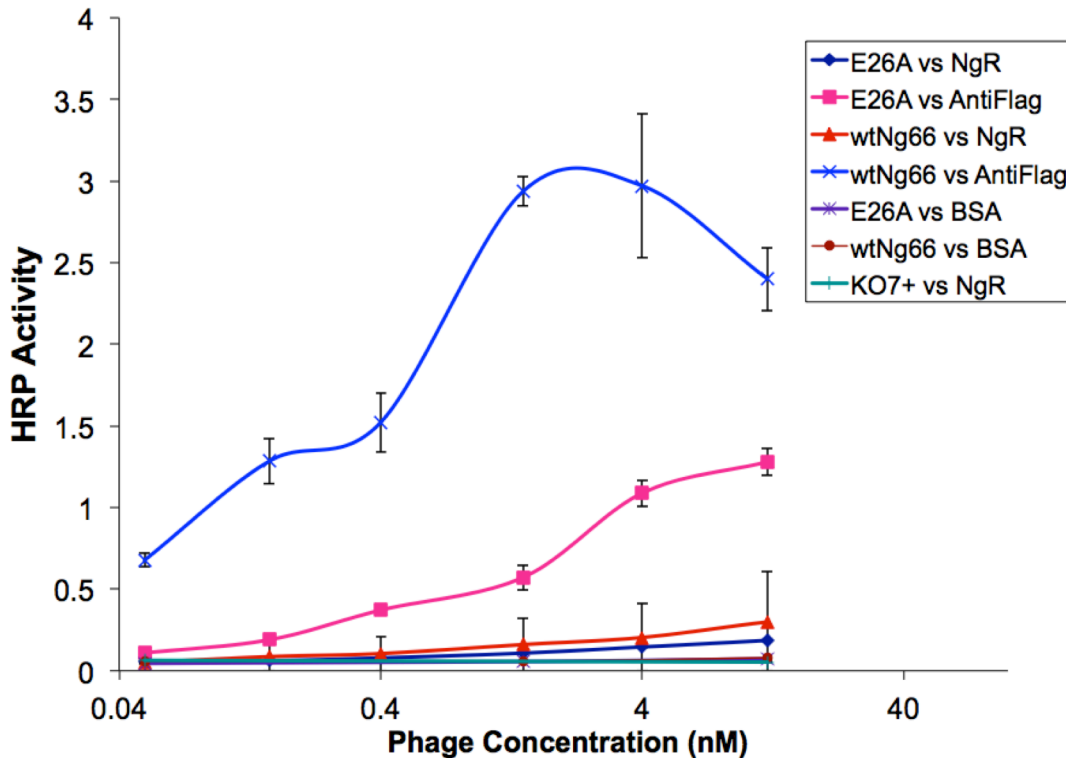


Figure 3.6: Nogo-66 E26A has a higher binding affinity to the Nogo receptor (NgR) than WT (raw data). In this phage-based ELISA, HRP activity provides a measure of the amount of phage-Nogo associated with NgR. Levels of displayed Nogo-66 were assayed through immobilized anti-FLAG ( $\alpha$ -Flag) antibody binding to a FLAG epitope fused to the N-terminus of the phage-displayed protein. The negative controls for this ELISA include Nogo-displayed phage binding to the blocking agent BSA, and the helper phage KO7<sup>+</sup> binding to the Nogo receptor (NgR).

## Discussion

Many proteins that act at the membrane interface would be expected to recognize and bind PC. Interactions between positively charged Arg and Lys side chains and the phosphate or other lipid anion have been studied in detail, most notably for antimicrobial peptides. However, choline binding is has been less characterized. Protein crystal structures with good density

describing the position of the PC reveal two major contributors to binding choline: aromatic p-cation interactions and Glu or Asp carboxylate-choline ionic interactions. The first structure showing a bound PC was an antibody determined by the Davies laboratory (Figure 3.2D, (Satow, Cohen et al. 1986)). In that structure, three aromatic residues Trp107, Tyr33, Tyr100 form a perfect pocket for the positively-charged choline group, highlighting p-cation binding. Human C-reactive protein (CRP) levels are elevated in response to acute infection, and it binds to PC on the surface of dead cells to initiate clearance. From the crystal structure of CRP, it is clear that the positively charged choline moiety of PC is in contact with the negatively charged Glu81 side chain, whereas the phosphate group interacts with protein-bound calcium (Figure 2.2C, (Thompson, Pepys et al. 1999)). Another example of PC binding is seen in the structure of phosphoethanolaminemethyltransferase from *Plasmodium falciparum* (PfPMT). In this case, a mixed p and anion pair: Tyr160 and Asp128, interact with choline to stabilize the PC enzyme product. (Figure 3.2E, (Lee, Kim et al. 2012)).

Although we previously performed NMR experiments of Nogo-66 in DPC, the NMR structure calculation relied only on NOE distance constraints between protein groups; no distance constraints to DPC molecules were included and the structure calculation was performed on the protein molecule alone (without lipid) (Vasudevan, Schulz et al. 2010). Notably, the NOE constraints limited to protein-protein contacts created a cavity near Glu26 that can accommodate exactly one PC molecule in the Nogo-66 structure. Tyr22 is one helical turn from Glu26 and is positioned to p-cation bond with choline in Nogo-66 providing additional stabilization in PC docking; however, this Tyr is not conserved in all RHDs.

The results presented here show that structural influence of Glu26 depends on the

environment of the protein – when either dissolved in an aqueous solvent or partially embedded at a PC surface. A summary of the structural features present under each condition is shown in Figure 3.7. Both WT and E26A Nogo-66 have similar partition coefficients ( $K_x$ ) of transfer from water into the lipid phase, but dramatically different structures on a PC surface. WT folds into a single conformer in DPC but E26A, unable to form a stable salt bridge to choline, is disordered and less helical. The similarity in transfer energy between WT and mutant when partitioning into lipid could be accounted for by compensating effects; an energetically favorable increase in entropy of disordered E26A in DPC could compensate for the destabilization resulting from a lost salt bridge between Glu and the lipid headgroup.

In an aqueous environment, Nogo-66 WT is active in functional assays but maintains a very disordered structure. In contrast, mutation of the buried Glu26 charge to Ala stabilizes helical conformations and increases helical content by ~23% in E26A. Moreover, Nogo-66 E26A has a much higher affinity for the receptor than WT in an aqueous environment; this effect is most likely a consequence of stabilized secondary structure in the lipid-free state. Although a complete structure of the complex between NgR, Nogo-66 and lipid has not been determined, these studies provide insight into the state of Nogo-66 when binding the receptor. We observe that the interaction of Glu26 with lipid stabilizes the WT protein fold. In contrast, when lipid is absent Glu26 destabilizes both the helical fold and receptor binding. The region 31-55 is known to contain residues sufficient for Nogo-66 function; Glu26 is positioned on the opposite protein face compared to the functional groups. The ability of a position within the interior of a compact helical bundle (Glu26) to affect receptor binding when it is not among the residues expected to make up the binding interface suggests a model where Nogo-66 folds on the

receptor into a structure similar to that induced by lipid.

The RHD-66 domain is flanked by two membrane-embedded helices that are believed to induce curvature of the ER membrane. These structures would be expected to stabilize the RHD-66 structure, both in anchoring the protein to the membrane and in extending the N- and C-terminal helices. It is also expected that the RHD-66 would be more stable in a natural membrane than in DPC micelles. Compared to planar bilayers, micelles are highly curved and much more dynamic. It is possible that the loss in structure seen in the lipid-associated state for the E26A mutant is not as pronounced in the context of the full-length protein and natural cell membranes. Nevertheless, a system that is on the cusp of stability is actually very useful in understanding protein folding. Proteins that are extremely stable will often not show a measurable effect from a single mutation; this can make it difficult to determine the relative contributions of individual amino acids to the overall protein stability. In deconstructing the RHD, we have found that Nogo-66 is an excellent model for testing the forces that drive protein folding at a lipid interface as well as providing specific detail on the RHD-66 fold. The structure of Nogo-66 in DPC is entirely consistent with functional assays and these studies show that Nogo-66 is an autonomous folding unit that uses a negative charge at position 26 to anchor the protein to the membrane surface. Nearby aromatic rings can also anchor Nogo-66 in the membrane and contribute to the lipid-induced fold. In addition, there are several other Glu/Asp side chains conserved in higher vertebrates that could interact with choline and drive docking into the membrane leaflet. Studies are ongoing to extend the structure of Nogo-66 with the flanking membrane embedded regions and define a complete RHD structure.

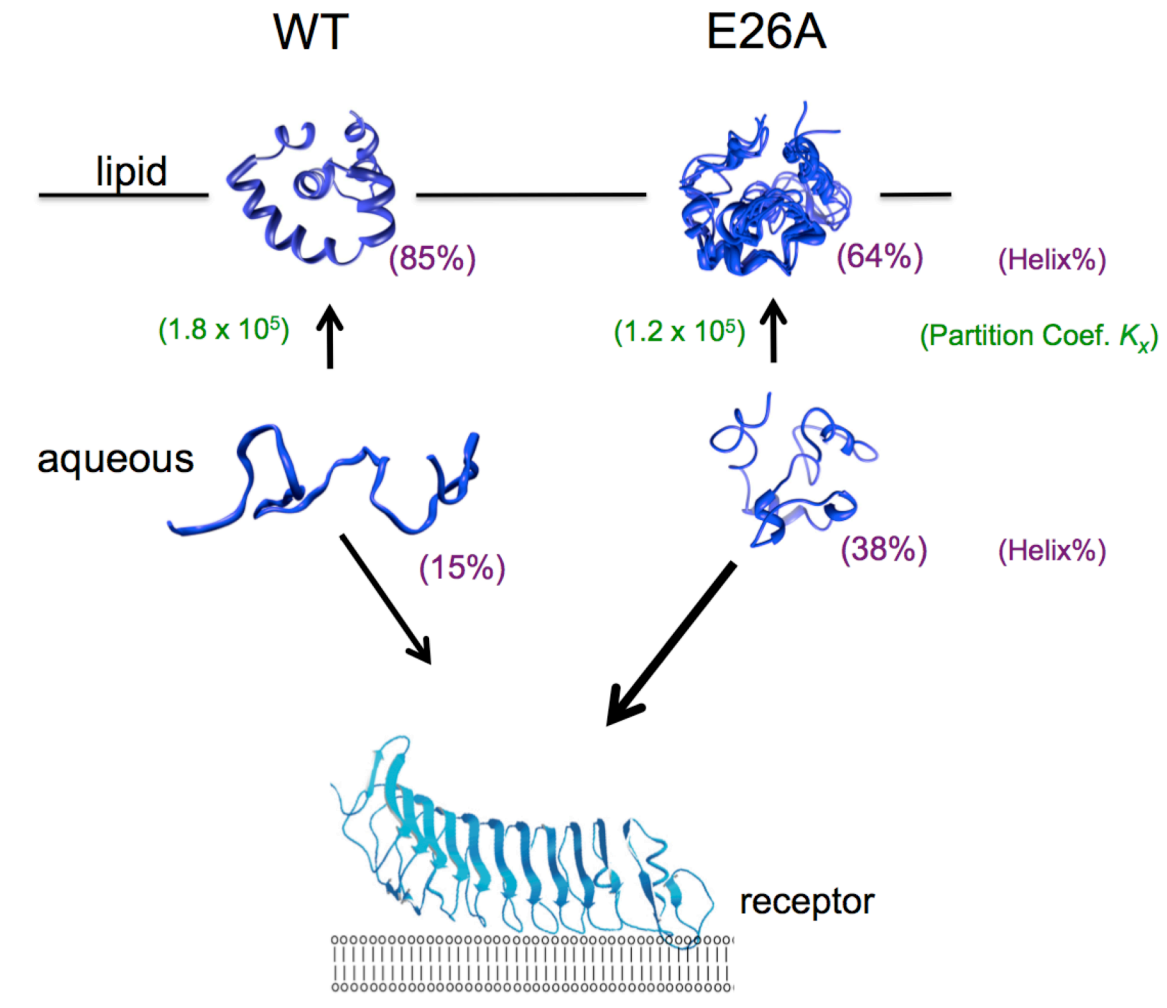


Figure 2.7. Summary of the effect of Glu26 mutation in Nogo-66. Although both proteins are strongly associated with lipid, E26A is more disordered than WT. In contrast, E26A is more helical in the aqueous phase than WT and binds the receptor with higher affinity.



## **Chapter 4**

### **JSRV envelope protein cytoplasmic tail and transmembrane domain structure determination**

## Abstract

Jaagsiekte sheep retrovirus (JSRV) is the etiologic agent of a transmissible lung cancer in sheep, ovine pulmonary adenocarcinoma (OPA). OPA resembles bronchiole-alveolar carcinoma in humans, and it is an excellent animal model for this disease. A unique feature of JSRV is that the viral envelope (Env) protein also functions as an oncogene, in that the expression of the JSRV Env protein causes morphological transformation of fibroblast and epithelial cell lines, and vectored Env expression induces epithelial tumors in several animals. Previous studies showed that the region containing the short 46 amino acid C-terminal cytoplasmic tail (CT) of JSRV Env is essential for the ability of JSRV to transform cells. Residues in the cytoplasmic tail include a tyrosine (Y590), which is present in a consensus motif YXXM, which could potentially bind the regulatory subunit of phosphatidylinositol 3-kinase (PI3K) if the Y590 is phosphorylated. Alanine scanning mutagenesis on the JSRV transmembrane (TM) and CT has been conducted. Mutation of some residues abolished Env transformation potential, while mutation of other residues had no effect or partial effects. To further understand the mechanism of JSRV transformation, structure-function analysis of the TM cytoplasm tail (CT) is important. We have determined the structure of the JSRV CT using NMR spectroscopy. This data allows us to interpret the alanine scanning mutagenesis, and allows better understanding of previous studies. Interestingly, using both CD and NMR, we find that the CT is only structured in the presence of a phosphocholine surface. The results validated some aspects of the predicted structure, and they also provided a basis for evaluating models of transformation.

## **Introduction:**

Historically, retroviruses have been known to cause cancer. Retroviruses consist of RNA surrounded by capsid (lipid envelope). They are classified into simple or complex retroviruses according to their genome. The oncogenic properties of retroviruses is either acute which induce tumors rapidly, or non-acute that induce tumors slowly (Hofacre and Fan 2010).

Jaagsiekte sheep retrovirus (JSRV) is a simple betaretrovirus with (acute) transforming ability of peripheral lung epithelial cells inducing Ovine pulmonary adenocarcinoma (OPA) in sheep. Ovine pulmonary adenocarcinoma is considered one of the most common transmissible lung tumors in sheep. Based on some studies, 80% of the flock can be lost after first virus exposure and the economic impact on the agriculture is high. To date, ovine pulmonary adenocarcinoma occurs in sheep farming worldwide. Because of the resemblance between the OPA and bronchiole-alveolar carcinoma in humans (BAC), resulting from smoking, OPA offers an excellent model for the study of the human lung tumor (Hofacre and Fan 2010).

JSRV encodes Gag, Pro, Pol, and Env proteins. The Env protein is enough to induce morphological transformation in epithelial cells. Active form of JSRV Env is composed of surface unit (SU) N-terminal and transmembrane unit (TM) C-terminal, spans the viral envelope (Figure 4.1). Disulfide bonds connect these two units. The surface unit is responsible for binding to the host cell receptor while the transmembrane unit plays a role in infection, mainly by the 46 amino acid cytoplasmic tail (Figure 4.2). The cytoplasmic tail contains a motif YXXM (Y590), which is considered a potential binding site to PI3K/p85 regulatory subunit, if phosphorylated. Alanine scanning mutagenesis studies showed that mutation at specific sites abolished the Env transformation ability, while others show no or partially no effect. In addition, four sites

potentiate the transformation more than wild type (Hull and Fan 2006).

Structural studies of transmembrane cytoplasmic tail (CT) of JSRV would further our understanding about its mechanism of action.

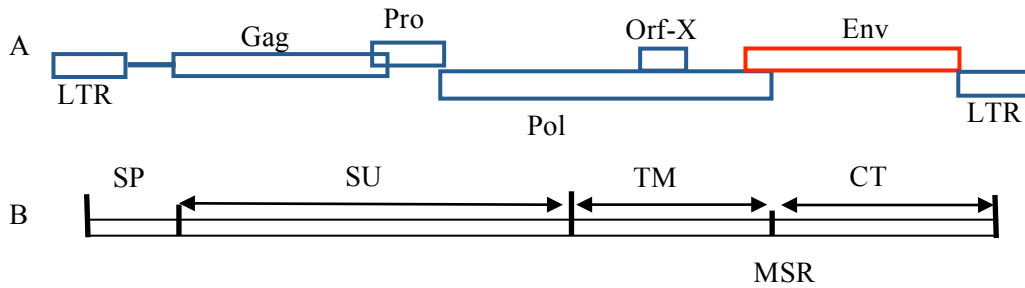


Figure 4.1: (A) JSRV Genome contains only essential gene gag, pol, orf and env. (B) Env structure: SU, Surface unit, MSR, Membrane spanning region (i) TM, Transmembrane (ii) CT, cytoplasmic tail(Liu and Miller 2007).

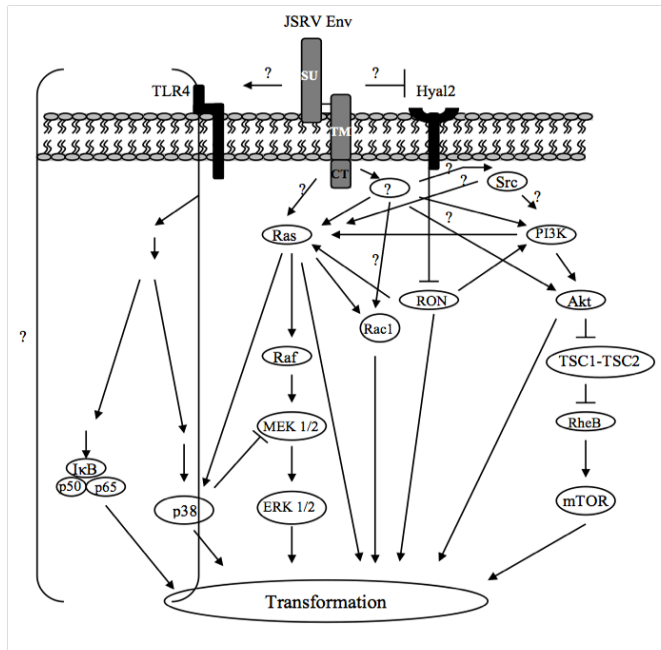
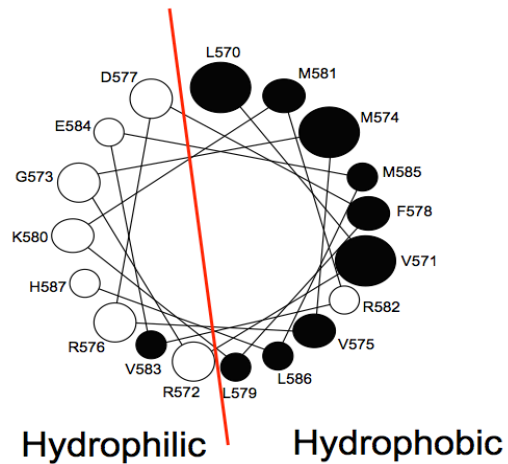


Figure 4.2: Downstream effect of JSRV. Depending on the cell line, Three different pathways have showed to be activated (i) Hyal2-RON pathway, (ii) PI3K pathway, (iii) Ras pathway(Hofacre and Fan 2010).



### Helical Wheel

Figure 4.3: portion of CT-JSRV Helical Wheel Plot. 18 residues plotted on a helical wheel. Those residues can potentially form an amphipathic helix and interact with the lipid (Hull and Fan 2006).

#### Understanding how CT-JSRV presents groups to the cytoplasm of the host cell:

The cytoplasmic tail of JSRV env protein is a key for transformation (Palmarini, Maeda et al. 2001). The CT-JSRV encompasses 46 amino acids. The first 18 amino acids (570-587) form an amphipathic helix with two sides after plotted as a helical wheel (Figure 4.3) (Hull and Fan 2006). According to the predicted model, one side is associated with the membrane while the other extends into the cytoplasm (Figure 4.4). The C-terminal (607-615) is nonessential. The YXXM motif (588-606), within CT domain, was believed to be responsible for its mode of action upon the phosphorylation of tyrosine (Y590). However, according to a mutational analysis study conducted in Dr. Fan's laboratory, the function of this motif may not be related to kinase phosphorylation activity (Figure 4.5) (Hull and Fan 2006). A large range of amino acids within

the cytoplasmic tail of JSRV env protein are implicated in transformation and there is no evidence of phosphorylation of Y590 at this time. Thus, studying the CT-JSRV in the structural setting would help to elaborate the mechanism of transformation by allowing us to define which groups are accessible to cellular proteins.

A previous graduate student in the Cocco laboratory, Jessica Schulz, characterized the CT-JSRV. First,  $^{15}\text{N}$ -labeled peptide was synthesized to incorporate specific labels. Then, a series of 2D and 3D NMR data was acquired for the sample in phosphate buffer at pH 7. The NMR  $^{15}\text{N}$  HSQC spectrum of CT protein in aqueous solution was not dispersed, indicating the protein was not correctly folded (Figure 4.6). This was in agreement with circular dichroism (CD) data (Figure 4.7). It has been suggested that proteins with amphipathic helix would become more folded in a hydrophobic environment. Next, dodecylphosphocholine (DPC) micelles were added to the protein and CD spectra recollected (Figure 4.7). Significant changes in the CD spectra indicates that the protein became more structured with DPC. An NMR experiment confirms the result where the spectrum shows more dispersed peaks compare to the ones in aqueous solution (Figure 4.7).

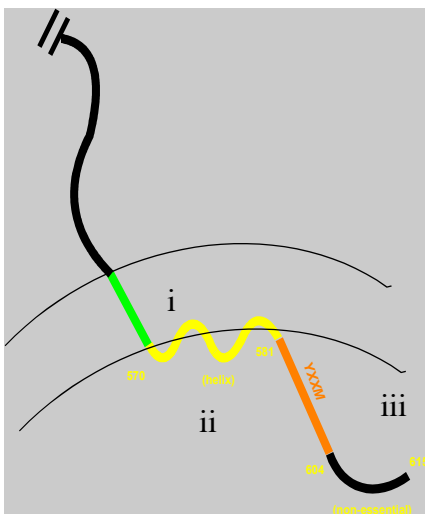


Figure 4.4: Model of JSRV Env protein when interacting with host cell membrane (i) membrane spanning region (ii) cytoplasmic tail (iii) YXXM motif (iv) non structure C-terminal (Hull, S. and H. Fan (2006))

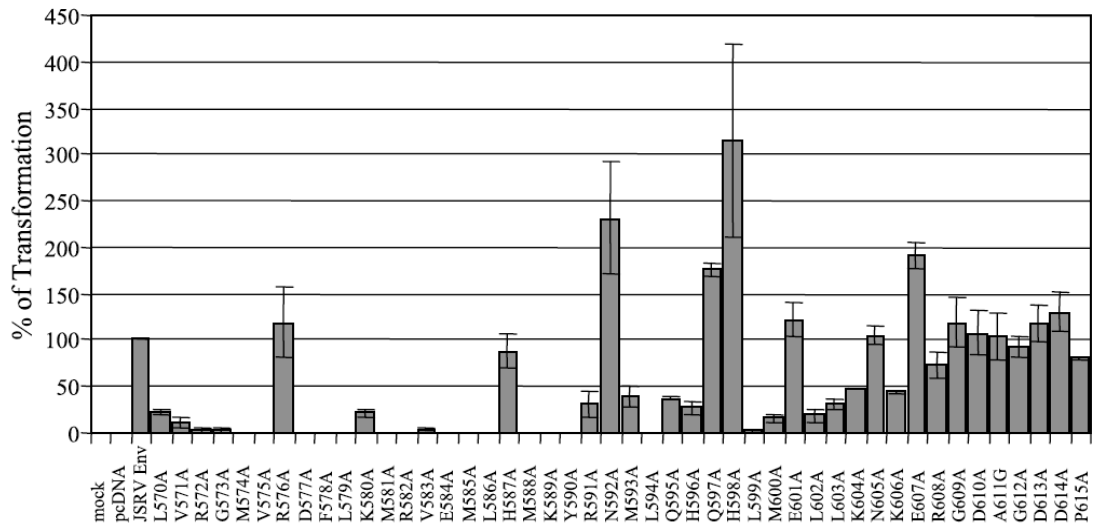


Figure 4.5 : Mutagenesis studies test transformation efficiencies of cytoplasmic tail mutants. Alanine mutations at each of the residues in the cytoplasmic tail (CT) were compared to that of wild-type JSRV Env(Hull and Fan 2006).

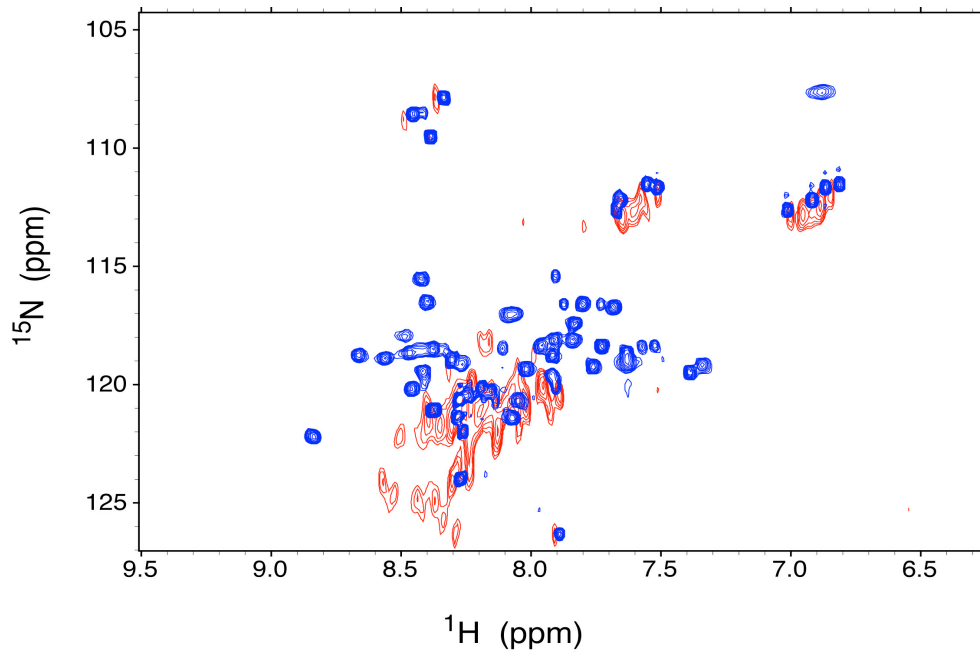


Figure 4.6: CT-JSRV  $^{15}\text{N}$  HSQC: (Red) CT-JSRV in aqueous solution (Blue) CT in presence of DPC. The peaks in red are clustered in small region, the lines width are wider. However, peaks with DPC are sharper and dispersed(Schulz 2009)

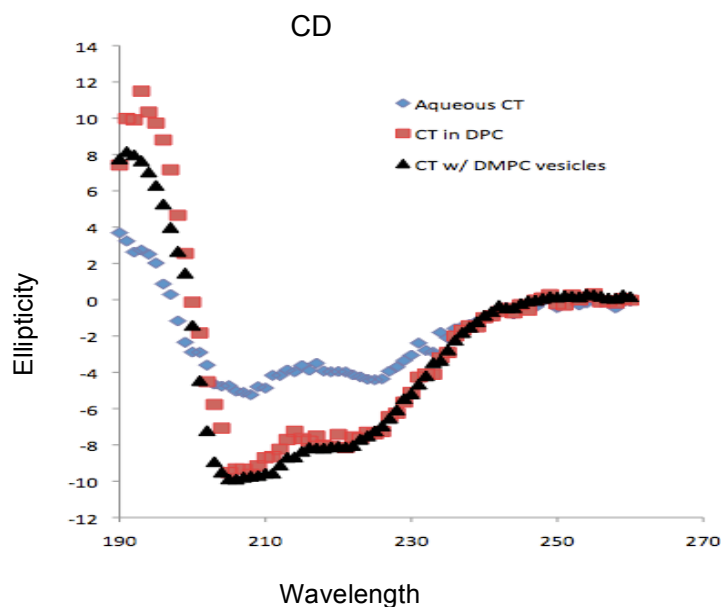


Figure 4.7: CT-JSRV Circular Dichroism. (Blue) CT-JSRV in aqueous solution (Red) CT in presence of DPC (Black) CT with lipid, DMPC(Schulz 2009).

After confirmation of the presence of helical secondary structure, and that the protein is in a folded state, we performed other experiments on a Varian 800 Mhz NMR spectrometer to help the sequential assignment of the backbone and side chains, and to get distance constraints from NOEs. These include HSQC, NOESY, TOCSY, and COSY. Data was collected on samples in 90% H<sub>2</sub>O and 10% D<sub>2</sub>O. nmrDraw, a graphical interface for NMRPipe, was used for processing the data and Ccpnmr Analysis 2.1 software for assignment, visualizing the spectra, and creating constraints list (Delaglio, Grzesiek et al. 1995, Vranken, Boucher et al. 2005). Almost 50% of cytoplasmic tail was composed of only five amino acids (Arg, Asp, Leu, Lys, Met). Thus, assigning all peaks is quite difficult due to the overlap and ambiguity. To overcome this problem, three



different approaches were proposed: (i) producing a  $^{15}\text{N}$ - and  $^{13}\text{C}$ -labelled sample, (ii) producing a selectively labelled synthetic sample, by which we can choose which residues would be labelled, and (iii) collecting the spectra at different temperatures where the peaks will shift and/or resolve issues with ambiguity. Because the JSRV CT does not express well, the option (i)  $^{13}\text{C}$ -labelled sample was not prepared. The selectively labelled sample assisted in unambiguous assignment (Figure 4.8). Moreover, the spectra at different temperatures helped identify overlapping residues (Figure 4.9).

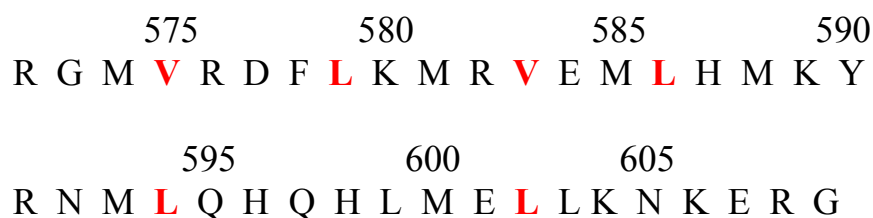


Figure 4.8: CT-JSRV sequences: Residues in red indicate the selectively  $^{15}\text{N}$ -labeled residues.

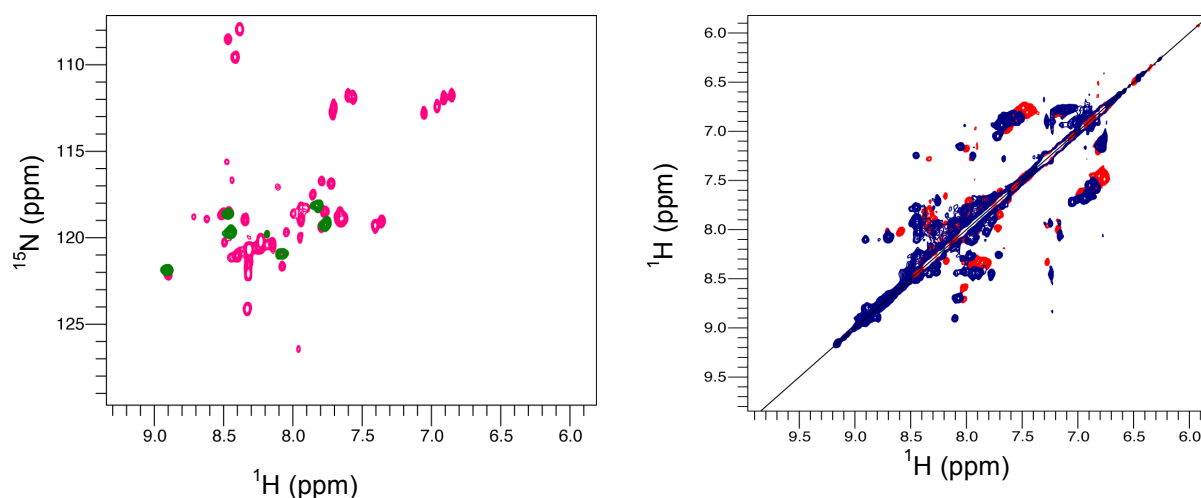


Figure 4.9:  $^{15}\text{N}$  HSQC and  $^{15}\text{N}$  NOESY-HSQC: A) overlaid HSQC spectra of full length cytoplasmic tail (pink) and selectively labeled residues (green) B) overlaid NOESY-HSQC spectra at two different temperature  $30^\circ\text{C}$  (blue) and  $40^\circ\text{C}$  (red)

**Assignments:**

Assigning the peaks in NMR spectra is essential for studying protein structure and function. To link the backbone residues through sequential (i, i+1) NOEs, we started by looking for amide proton (HN) backbone sequential connectivities using 20°C and 40°C NOESY experiments. Based on the previous CD data, we looked for helical NOE signatures. Canonical alpha-helical connections are defined by NH-NH (i, i+1) and NH-C<sup>α</sup>H(i, i+4). These were found between 575-578 and 599-603 ( Figure 4.10 A). Leucine and valine side chains present similar spin system patterns and can be difficult to distinguish. Assigning their side chains in NOESY spectra is a challenge. Thus, we used a specifically <sup>15</sup>N labeled sample to assign four leucines and two valines. This step was done by correlating the <sup>1</sup>H HSQC chemical shift of the residue with a peak at the same <sup>1</sup>H chemical shift on the NOESY experiment. Also we used the TOCSY experiment to help assign through-bond interaction. We overlaid the NOESY and TOCSY spectra to determine the interaction between alpha carbon protons C<sup>α</sup>H and amid protons NH to help assign the neighboring amino acid (Figure 4.10 B). Then, we generated a list of NOEs for assigned residues and used NIH-Xplor software to generate set of structures by simulated annealing script (Schwieters, Kuszewski et al. 2003). The simulated annealing script heats up the protein until 3500°C and cools it down in 25 steps. The preliminary generated structures were not in a correct 3-D conformation (Figure 4.11). This was because not all residues were assigned, or because few numbers of constraints per residues.

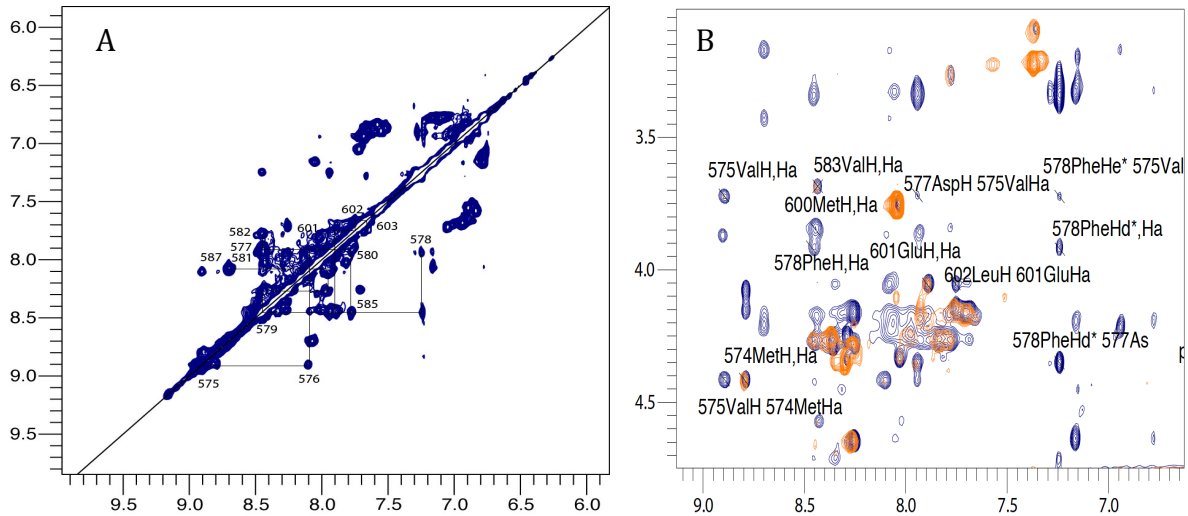


Figure 4.10 : A) NOESY backbone walk for residues V575- H587 and L599-L603 B) Part of the NOESY and TOCSY spectra of CT-JSRV. The NOESY is shown in Blue with the TOCSY overlaid in orange (M. Cocco, unpublished). This area of the spectra describes where the HN and C<sup>α</sup>H protons resonate. By using a combination of these connectivities one can assign adjacent amino acids as shown in the above spectra.

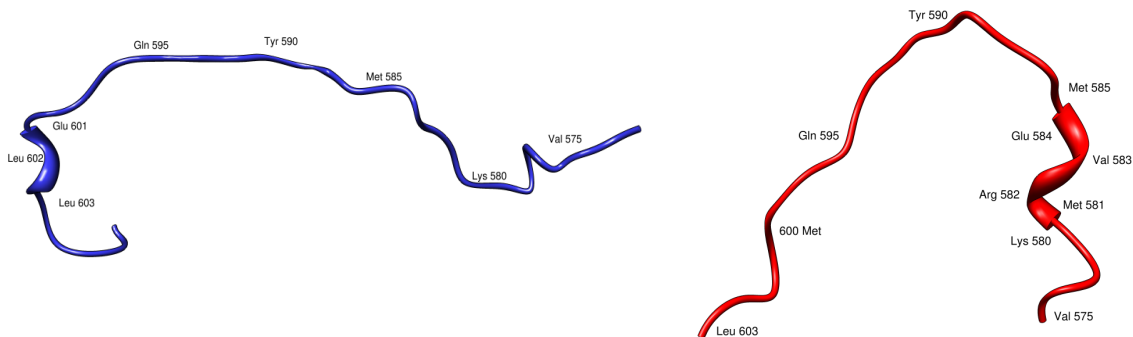


Figure 4.11 : preliminary structure of JSRV cytoplasmic tail

While we were trying to assign more residues and optimize the NIH-Xplor run, recent mutations studies in MSR of TM of env JSRV protein have shown great transformation efficiency by CT. However, replacing exTM with enTM does not show any effect. To confirm whether CT alone is responsible for transformation, we decided to solve the structure in the presence of MSR. Then, we will compare any conformational changes and find how TM could participate in the transformation process (Hull and Fan unpublished).

**Solving the structure of TM JSRV:**

The constructs for expressing JSRV were provided by the laboratory of Professor Henry Fan (Figure 4.12). First, we tried to grow CT-JSRV alone. In order to produce isotopic <sup>15</sup>N labeled protein, we over expressed the optimized CT pTE15b vector in Escherichia coli BL21 (pLysS) in minimal media. Then, the protein was purified and eluted in 8M urea. The concentration was measured by UV spectrophotometry and the size was confirmed by mass spectrometry MALDI-TOF (Figure 4.13)

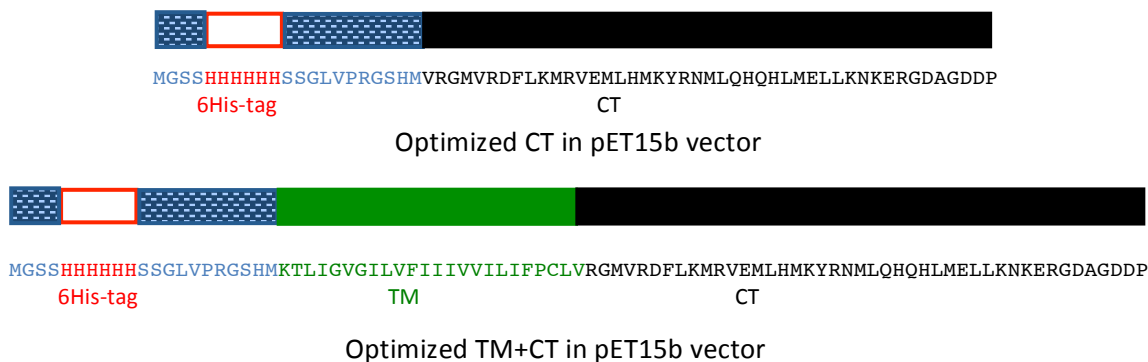


Figure 4.12: Optimized JSRV in pET15b vector

To get rid of the urea, we dialyzed the protein against water for 24 hours at pH 7.5. The UV-scan showed light scattering, indicating that the protein was aggregated. We tried using a 0.45  $\mu\text{m}$  syringe filter to trap the aggregation (Figure 4.14). Then, we tried different dialysis conditions summarized in (Table 4.1). Unfortunately, all conditions resulted in precipitation and aggregation of the protein.

Condition	pH 7.5	pH 6	pH 5	pH 4	Results
Water	X	X	X	X	Precipitation
5 mM Na.Phos	X				Precipitation
5 mM Tris	X				Precipitation
Table 4.1 : Dialysis conditions for CT-JSRV ( X, tested condition).					

The optimized CT pTE15b is a hexahistidine tagged construct. Woestenenk *et al.* tested the effect of His tag on the solubility of purified proteins. They found that His tag has a negative impact on protein solubility (Woestenenk, Hammarstrom et al. 2004). Based on these results, we needed to counteract the negative effect the His tag. One approach is to cut the His tag off. For CT-JSRV and MT-JSRV full parameters see (Appendix B).

Improving the solubility will help to prepare the CD and NMR sample to characterize and solve the structure of recombinant CT alone and in presence of TM. To do so, we will run a series of 2D and 3D NMR experiments, including NOESY with TOCSY and COSY to assign the spin system by following specific pattern for each amino acid and assign all peaks. Once these assignments are completed, NOE distance constraints list will be generated. Then, we will apply it to the structure calculation software (NIH-Xplor) to generate set number of structures, with low energy, fewer violations, and low RMSD. Later, we will move to the next step and start the refinement. In this step, the NOE constraints list will be used along with the finest structure

from the previous step. Then again, pick the structure with low energy, none or fewer violations, and low RMSD.

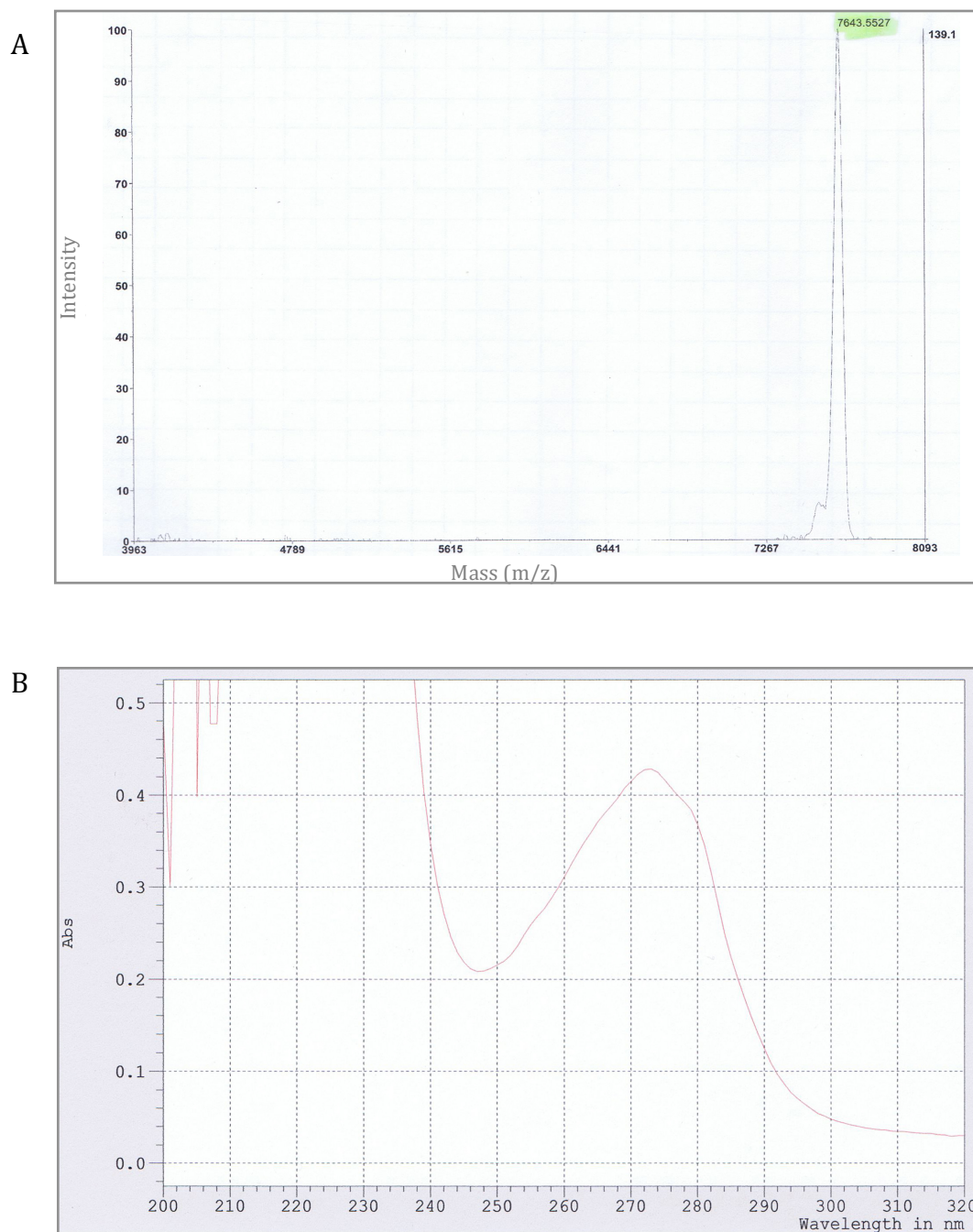


Figure 4.13:  $^{15}\text{N}$  CT-JSRV molecular weight is 7661.8 Da. (A) Mass spectrometry (MALDI-TOF) shows CT-JSRV corresponding molecular weight (B) UV-spectrophotometry scan for purified CT-JSRV, in 8M urea. Ext. coefficient  $1490 \text{ M}^{-1} \text{ cm}^{-1}$

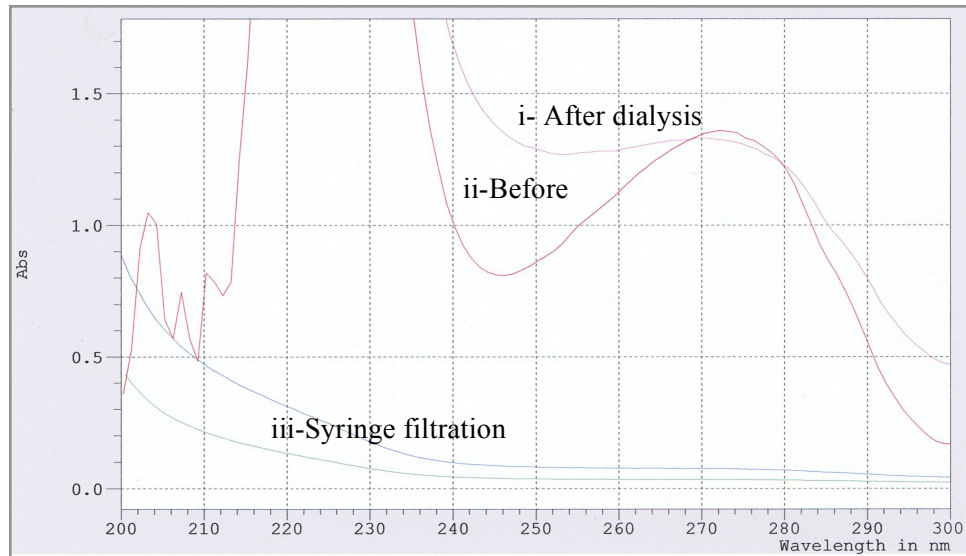


Figure 4.14: UV-spectrophotometry scan (i and ii) before and after dialysis against water, pH 7.5. (iii) UV scan after syringe filtration, sample was trapped in the filter.

## Chapter 5

### Materials and Methods

Part of this chapter published in BBA: Biomembranes (2014) vol 1838, p 2350-6

Ali Alhoshani<sup>a</sup>, Rosemarie Vithayathil<sup>b</sup>, Jonathan Bandong<sup>b</sup>, Katherine M. Chrnyk<sup>b</sup>,  
Gabriel O. Moreno<sup>b</sup>, Gregory A. Weiss<sup>b,c</sup> and Melanie J. Cocco<sup>a,b\*</sup>

<sup>a</sup>Department of Pharmaceutical Sciences; <sup>b</sup>Department of Molecular Biology and Biochemistry;

<sup>c</sup>Department of Chemistry University of California, Irvine, CA 92697



## HADDOCK

We have used the HADDOCK server, Expert interface for the docking studies (de Vries, van Dijk et al. 2010). HADDOCK is a server created for the more experienced user. One of the foremost differences between the HADDOCK software as compared to less advanced options is

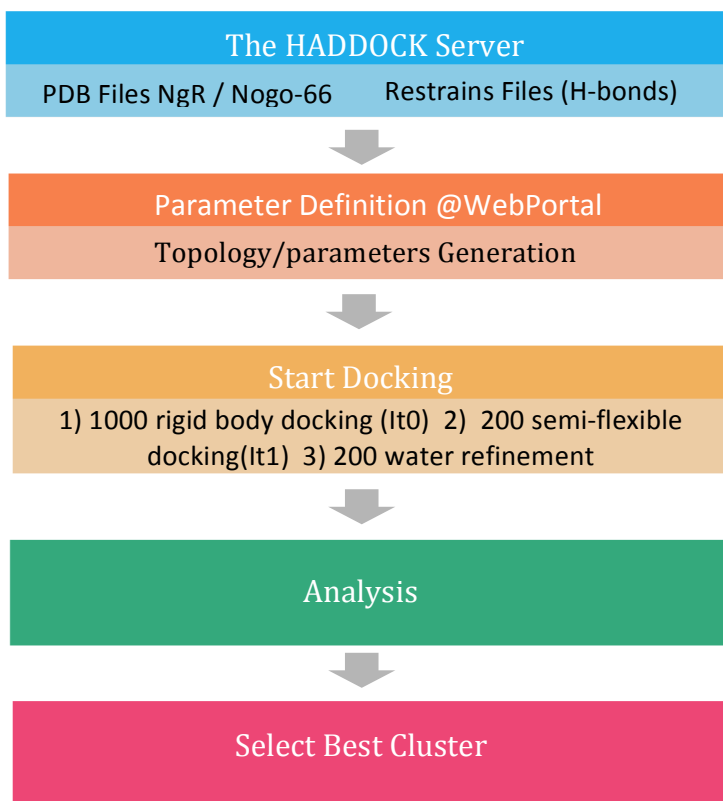


Figure 4.1: HADDOCK protocol (High Ambiguity Driven DOCKing) is an experimental-driven docking approach for bimolecular complexes. It uses information from identified/predicted protein interfaces in ambiguous interaction restraints (AIRs) to drive the docking process. This flowchart illustrates HADDOCK protocol used in this study.

that HADDOCK can handle a major class of modeling issues such as protein-protein, protein-nucleic acid, and protein-ligand compounds. HADDOCK software also provides a path for the user to upload a hydrogen bond, create and identify a custom distance, and lastly recognize dihedral angle restraint files. Utilizing this type of docking system permits the user to perform a variety of tasks. The user is able to choose the number of structures/complexes to be calculated, while also allowing the user to define and delineate the flexible segments and protonation states within the various histidine proteins. The HADDOCK web server supports the established guidelines set forth by the HADDOCK program thus allowing for the same docking mechanisms to be completed with improved efficiency and ease as compared to using the HADDOCK on a local machine. (de Vries, van Dijk et al. 2010).

Before starting the docking studies, PDB files of the crystal structure of NgR (ID 1OZN) and the NMR solution structure of Nogo-66 (ID 2KO2) were uploaded into the sever (first molecule, second molecule). We used hydrogen bonds as restraint to guide the docking process. H-bonds restraint syntax file for Nogo-66 and all images were created by UCSF Chimera software (Appendix B.5) (Pettersen, Goddard et al. 2004). In Nogo-66, residues Arg53, Arg54, Ser38, Asn39, Ser40 were selected as active residues. In NgR, residues Asp 111, Asp 114, Asp 163 were selected as active residues (Schimmele and Pluckthun 2005). Passive residues were automatically selected for both Nogo-66 and NgR. HADDOCK uses active and passive residues in both molecules, along with H-bonds, to generate the ambiguous interaction restraints (Air's) for the interaction interface. At this point, the generation of a structure topology is created which selects the specific molecules to be docked. Docking is completed in three steps (1) rigid body minimization (it0). During the first step, a minimum of 25 Å s are used as a division between the

molecules (Nogo-66 and NgR). These molecules are then rotated around their center of mass. Then thousands of structures are generated. Only the top structures are selected to be refined in (2) semi-flexible simulating annealing (SA) in torsion angle space refinement (it1) step followed by (3) explicit solvent refinement, water (W). HADDOCK scored and ranked the best structures. The HADDOCK score is calculated by the summation of the van der Waals, electrostatic, desolvation and restraint violation reactions, while also giving ample consideration to the surface area. HADDOCK automatically defined all parameters that governed the docking process such as temperature, number of time steps, and structures after each steps. In this study, the number of initial best structures from rigid-body docking was 1000. Among those 1000 structures, we retained 200 best structures for the next step.

After the explicit solvent refinement step, structures are clustered on the basis of a backbone root mean square deviation tolerance at the binding interface. The best-docked complex structure was the structure that had the lowest intermolecular interaction energy (sum of all energy terms) within the cluster of the lowest average intermolecular interaction energy (de Vries, van Dijk et al. 2010).

### ***CD measurements***

The secondary structure of Nogo- $\Delta$ 20 and E26A were analyzed by CD spectroscopy in the far UV (185–250 nm) regions. Solutions of the proteins (Nogo- $\Delta$ 20 and E26A) were dialyzed against 5 mM sodium phosphate and 5 mM sodium acetate, pH 7.0 and pH 5.0 respectively. For Nogo-66, we choose pH 5 to balance the solubility of the protein with maintaining the Glu side

chain above the pKa. We also collected pH 7 data at a lower protein concentration and found the same spectral features. 1mg/ml Nogo-Δ20 and 1.9 mg/ml WT and 1.3 mg/ml E26A Nogo-66 samples were analyzed at 20°C and 25°C respectively. 1.0 nm wavelength intervals used in JASCO Model 720 CD spectropolarimeter (JASCO, Easton, MD) with a scan speed of 50 nm/min and average response time of 5 s. A total of 10 consecutive scans were accumulated for analysis. To minimize light scattering inherent in lipid vesicles samples, data was collected with a 0.1-mm path-length cell (NSG Precision Cells, Inc., Farmingdale, NY). Dichroweb, an online server providing various CD analysis programs, was used to analyze E26A data (Whitmore and Wallace 2004). The program ContinLL was used to fit the data and estimate the content of secondary structure present using reference set SP175 (Lees, Miles et al. 2006).

### ***Lipid partitioning assays***

To determine the partition coefficient for the transfer of Nogo-66 WT and E26A from water into lipid, CD wavelength spectra were collected at varying lipid concentrations and the change in ellipticity at 222nm ( $\theta$ , mdegrees) was analyzed (White, Wimley et al. 1998). DMPC vesicles were extruded to 100nm diameter particles at 35 °C. Proteins and lipids were diluted into separate tubes to maintain a final protein concentration of approximately 0.5 mg/ml, 5 mM sodium acetate, pH 5.0 with varying concentration of lipid (0.01 – 10 mM). CD spectra were collected at 25 °C The fraction of protein partitioned into the lipid phase ( $f_p$ ) plotted as a function of lipid concentration was fit to the following equation to determine the partition coefficient,  $K_x$ .

$$f_p = \frac{K_x[L]}{[W] + K_x[L]} \quad (1)$$

The free energy of transfer from water into lipid bilayer was calculated from the equation:

$$\Delta G = -RT \ln K_x \quad (2)$$

### ***NMR measurements***

NMR experiments were performed on a Varian Inova 800 MHz NMR spectrometer equipped with a 5 mm xyz, pulse-field gradient triple resonance probe. <sup>15</sup>N HSQC experiments were performed on 1 mM WT and E26A Nogo-66 in presence of 200mM DPC at 35 °C, pH 4.5 in 90% H<sub>2</sub>O/10%D<sub>2</sub>O. Data was processed using NMRPipe (Delaglio, Grzesiek et al. 1995).

### ***Cloning and Expression of NgR***

The protocol for production of the receptor, NgR was adapted from a previously described report (He, Bazan et al. 2003) A pCRII-TOPO (Invitrogen) vector for expression in mammalian cell culture, containing a mouse Nogo receptor was provided to us by Dr. Binhai Zheng (UCSD). The sequence of NgR was verified and the Nogo ligand binding domain (residues 26-310) was PCR amplified before subcloning into Pharmingen's pAcGp67A secretion vector, which was designed to produce a His<sub>6</sub> tag fused to the C-terminus of NgR. The glycosylated, folded material was successfully produced in Sf9 insect cells (Novagen), which were grown in BacVector Insect cell Media (Novagen) as suspension cultures in a spinner flask at 28 °C. The culture was infected with recombinant baculovirus at a cell density of 1 x 10<sup>6</sup> cells/ml. The MOI (multiplicity of infection) determined for optimal expression was 5 pfu/ml, and the optimal

period of infection was 96 hrs. Cells were sedimented and the media supernatant with secreted NgR was concentrated 10-fold. Nickel resin was added to the concentrated media, and the standard protocol described by Qiagen for purification of His<sub>6</sub> tag proteins under native conditions was used. The receptor was dialyzed into HBS buffer (HEPES buffered saline pH 7.2, 5 mM HEPES), and concentrated to 2-3 mg/ml.

### ***Receptor Binding Assay***

The phage-Nogo-66 vector has been described previously (Vithayathil, Hooy et al. 2011). The mutation E26A was made using Quikchange mutagenesis, and the mutation was confirmed by DNA sequencing. Phage production and isolation have been described in (Vithayathil, Hooy et al. 2011). A phage-based ELISA was used to assess display levels of WT Nogo-66 on the surface of the M13-KO7<sup>+</sup> phage by immobilizing an anti-FLAG antibody on the ELISA plate. Followed phage-based ELISA protocol as described in (Vithayathil, Hooy et al. 2011). A single microtiter plate was used to assay simultaneously the display levels ( $A^0$ ) as well as binding ( $A$ ) of Nogo-66 wild-type and variant to immobilized NgR. The ratio ( $A/A^0$ ) represents the apparent binding affinity,  $K_A$ :

$$K_A = \frac{A}{A^0} \quad (3)$$

where

$A^0$  = The absorbances measured in wells coated with the AntiFlag antibody. This value quantifies display levels of Nogo-66 wild-type and variant on the phage surface.

$A$  = The absorbances measured in wells coated with NgR. This value quantifies binding levels of Nogo-66 wild-type and variant to NgR (Rossenu, Leyman et al. 2003).

## ***Nogo-66 and Nogo Δ20 preparation***

### **Luria-Bertani media (LB)**

Nogo-66 and Nogo Δ20 constructs were inserted into pET16b vector and over expressed in *Escherichia coli* BL21 (DE3) as N-terminal hexahistidine tag, separately (Appendix B3 and B4). For full protein parameters and transformation protocol see Appendix B6. For expression, Luria-Bertani media (LB) was used in the presence of ampicillin. Cells were grown at 37°C to an optical density (OD) of 1 at 600nm. Then, induced with 1mM IPTG. 5 hours later, cells were harvested by centrifugation at 3000xg for 15 minutes. Then lysed by using a buffer containing 8M urea, 10 mM Tris; and 100 mM NaH<sub>2</sub>PO<sub>4</sub>; pH 8.0 (25 ml / ~5g of cells), sonicated at 20-25Ω for 15 minutes, and centrifuged at 30000xg for 15 minutes. The cell's debris was discarded, and the supernatant was mixed with pretreated Nickel- Nitrilotriacetic acid (Ni-NTA) resin with a lysis buffer for 1 hour to allow binding of the hexahistidine tag. The resin was loaded into a gravity column and washed with the lysis buffer now pH 6.3 to remove any contaminating protein. Then eluted using pH 4.5 lysis buffer. Eluted protein was dialyzed into pH 4.5 for Nogo-66 and pH 7 for Nogo Δ20 water to remove the urea. Upon removal the protein was then concentrated to 2mg/ml and stored at -20 °C.

UV/Vis spectroscopy was used to estimate the concentration  $A=\epsilon/c$ . ProtParam tool at [expasy.org](http://expasy.org) was used to calculate the extinction coefficient ( $\epsilon$ ). The value of  $\epsilon$  is 4470 M<sup>-1</sup> cm<sup>-1</sup> for Nogo-66 and 8940 M<sup>-1</sup> cm<sup>-1</sup> for Nogo Δ20.

### **Minimal Media (MM) for isotope label protein**

<sup>15</sup>N Nogo-66 isotope labeled was prepared in the same way as unlabeled Nogo-66, except for the expression media. <sup>15</sup>N Nogo-66 overexpressed in minimal media instead of LB. The minimal media was supplemented with <sup>15</sup>N-ammonium chloride (<sup>15</sup>NH<sub>4</sub>Cl) as a source of amine.

### **SELEX**


Selection was done for 14 rounds. Each round, we first immobilized NogoΔ20 to (Ni-NTA) beads by (a) wash 100 μL of the Ni-NTA beads with 400μl binding buffer 4x (20 mM Tris, 150 mM NaCl, 1 mM MgCl<sub>2</sub>, pH 8.0) (b) add ~23 μl of NogoΔ20 (2 mg/ml stock) pH 7.5 to the Ni-NTA beads and incubate for 45 min to 1 hour at 25 °C (c) wash the beads with 100 μl binding buffer (20 mM Tris, 150 mM NaCl, 1 mM MgCl<sub>2</sub>, pH 8.0) for 3x (to remove unbound protein and excess urea). Second, we annealed the ssDNA library (provided by Dr.Luptak), Starting pool

5'**CATCGATGCTAGTCGTAACGATCC**-N<sub>44</sub>-**TTTCTCTCTCTCCCTATAGTGAGTCGTATTA**3',

by incubating it at 90°C for 3 min, then at 4°C for one hour. Then 92°C for 5 min then on ice for 10 min. After that, I incubated it at 25°C for 20 min (allow DNA to gradually fold). Third is to bind the ssDNA to NogoΔ20 by adding the annealed DNA into NogoΔ20+Ni-NTA beads (first step) and then incubate the mixture for a minimum of 1.5 hr, with gentle agitation at 25°C. After 1.5 hr I loaded the mixture to mini-column and wash for 3x with 400 μl binding buffer to remove unbound DNA. Then, add 200 μl of elution buffer (20 mM Tris, 150 mM NaCl, 1 mM MgCl<sub>2</sub>, 300 mM imidazole, pH 8.0) let it sit overnight, then collect the flow in new 0.5 ml tube. Next, precipitate the elution by adding 300 μl 100% ethanol, 1 μl GlycoBlue, incubate for ~15 min, spin at max at 4°C for 30 min, then discard the supernatant. Then, suspend it in 50 μl-distilled



water; set up asymmetric (1:10) PCR in a 40  $\mu$ L volume using PCR primers (synthesized by Eurofins) specific for the library,

PCR Mixture	
DreamTaq * PCR Master Mix (2x) is a ready-to-use solution containing DreamTaq DNA Polymerase, optimized DreamTaq buffer, MgCl <sub>2</sub> , and dNTPs	20 $\mu$ l
Primer F 40 $\mu$ M	0.2 $\mu$ l
Primer R 40 $\mu$ M	2 $\mu$ l
ssDNA	1 $\mu$ l
dH <sub>2</sub> O	16.8 $\mu$ l
Total	40 $\mu$ l

Forward primer (377) 5' **CATCGATGCTAGTCGTAACGATCC** 3'

Reverse primer (488) 5' **TAATACGACTCACTATAGGGAGAGGAGAGAAA** 3' Reverse primer

PCR conditions: 30 Cycles

1. 94°C 1 minute
2. 95°C 30 sec
3. 63°C 30 sec
4. 72°C 30 sec
5. Repeat steps 2-4 14 times, collect 10  $\mu$ L of reaction (30 min)
6. Repeat steps 2-4 5 times, collect 10  $\mu$ L of reaction (9 min)
7. Repeat steps 2-4 5 times, collect 10  $\mu$ L of reaction (9 min)

8. Repeat steps 2-4 5 times (9 min)
9. Finish with 45 sec at 72°C, remove last 10 µL of reaction from the machine

Then I determined which fraction contains the fully amplified pool, by loading 3 µL of each collected fraction on a 2% agarose gel to according to the following steps:

1. To 3 µl of each fraction add 1 µl of 6x Loading dye (6 µl Glycerol+20µl 6x loading dye).
2. Ladder: 3 µl of 20bp ladder (Sigma Aldrich) + 1 µl loading dye (Bio-Rad).
3. Place the gel in the electrophoresis chamber. (DNA is -ve).
4. Add 1x TBE Buffer (Tris-borate-EDTA) until the max. (Note 1 contains the recipe for 10x TBE)
5. Load 3.5-4 µl on 2% Agarose gel. (Note 2 is how to make Gel)
6. Cover the chamber; turn on; set the Voltage to 100; running time 35-40 min; hit run.

\* I did the same steps for Nogo-66

### ***Material for protein purification***

- LB
- Ampicillin (100 mg/ml @-20C) ( 1 ul /ml LB or MM )

#### **-Minimal Media (1L) should be prepared fresh or stored**

Thiamine•HCl (Anhydrous)	0.0500 g= 50 mg	(MW: 337.3 g/mol )
Potassium Phosphate K <sub>2</sub> HPO <sub>4</sub> , Dibasic	0.230 g = 230 mg	(MW: 174.18 g/mol)
Sodium Bicarbonate NaHCO <sub>3</sub>	0.8401 g = 840.1 mg	(MW: 84.03 g/mol )
Ammonium Chloride <sup>15</sup> NH <sub>4</sub> Cl	1.0163 g N = 1016.3 mg	(MW: 53.49 g/mol )

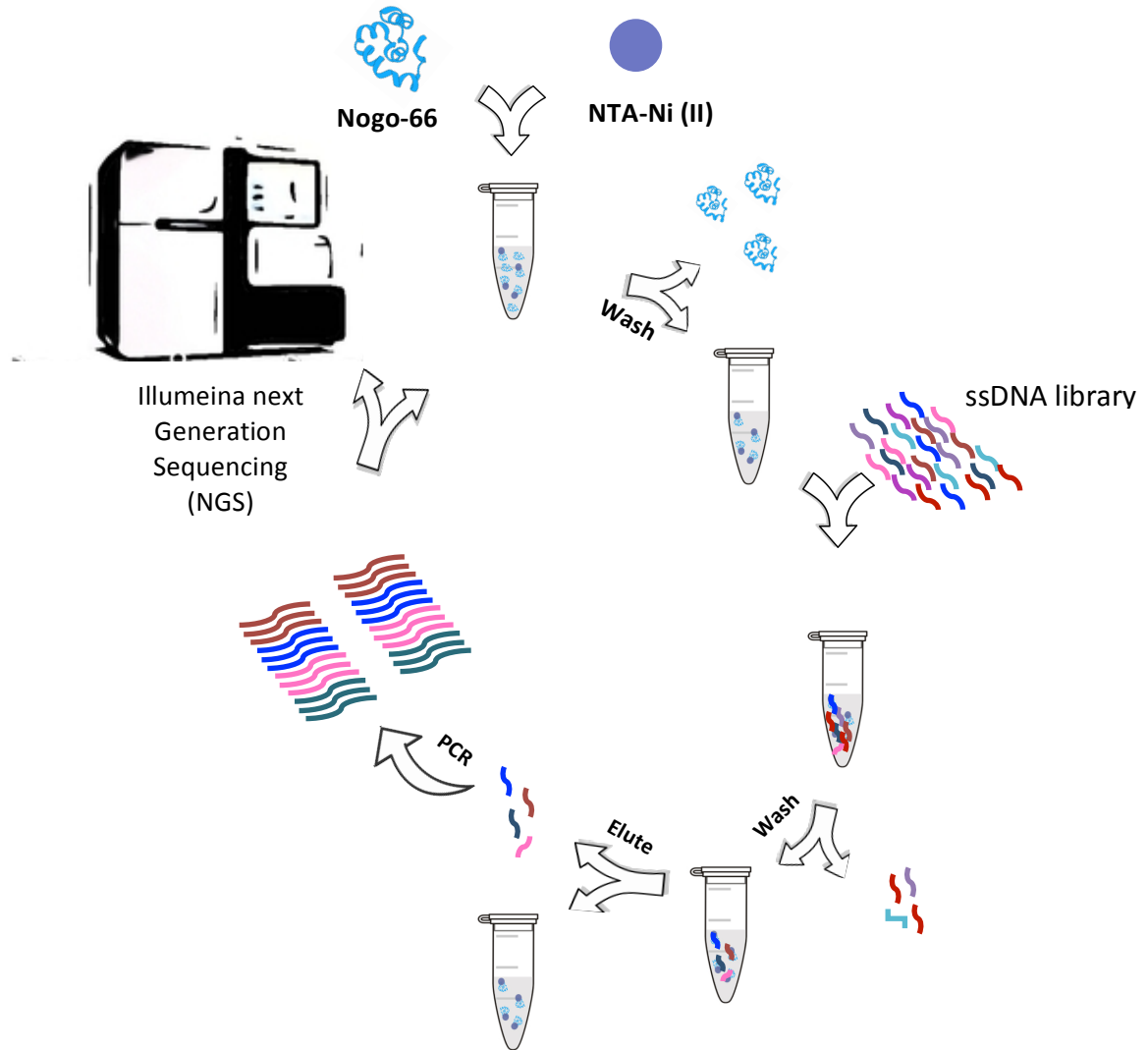
Glucose C <sub>6</sub> H <sub>6</sub> O <sub>6</sub> (Anhydrous) Dextrose	10.00 g	(MW: 180.16 g/mol)
10x Neidhart's	100 mL 10 <sup>x</sup> Stock / or 50ml for 20x	
Amp	1 ml (100 mg /1 ml)	
pH	7.4 ,then filter 0.22 μm	

**Purification buffers for membrane protein under Denatured Condition 500 ml**

(Source: "The QIAexpressionist handbook" <http://web.mnstate.edu/provost/QiaExpressionist.pdf>)

- Lysis buffer (B):
  - 100 mM NaH<sub>2</sub>PO<sub>4</sub> 6.9 g (MW: 137.99 g/mol)
  - 10 mM Tis.Cl 0.6 g (MW 121.1 g/mol)
  - 8 M Urea 240.25 g (MW 60.06 g/mol)
  - pH 8.0 , Adjust using NaOH before use
  
- Wash Buffer (C) : 500 ml
  - 100 mM NaH<sub>2</sub>PO<sub>4</sub> 6.9 g (MW: 137.99 g/mol)
  - 10 mM Tis.Cl 0.6 g (MW 121.1 g/mol)
  - 8 M Urea 240.25 g (MW 60.06 g/mol)
  - pH 6.3 using HCL before use
  
- Elution Buffer (E)
  - 100 mM NaH<sub>2</sub>PO<sub>4</sub> 6.9 g (MW: 137.99 g/mol)
  - 10 mM Tis.Cl 0.6 g (MW 121.1 g/mol)
  - 8 M Urea 240.25 g (MW 60.06 g/mol)
  - pH 4.5 using HCL before use

Figure 4.2 :Method of SELEX



## References

- Burmeister, P. E., C. Wang, J. R. Killough, S. D. Lewis, L. R. Horwitz, A. Ferguson, K. M. Thompson, P. S. Pendergrast, T. G. McCauley, M. Kurz, J. Diener, S. T. Cload, C. Wilson and A. D. Keefe (2006). "2'-Deoxy purine, 2'-O-methyl pyrimidine (dRmY) aptamers as candidate therapeutics." *Oligonucleotides* **16**(4): 337-351.
- Chen, M. S., A. B. Huber, M. E. van der Haar, M. Frank, L. Schnell, A. A. Spillmann, F. Christ and M. E. Schwab (2000). "Nogo-A is a myelin-associated neurite outgrowth inhibitor and an antigen for monoclonal antibody IN-1." *Nature* **403**(6768): 434-439.
- Chen, M. S., A. B. Huber, M. E. van der Haar, M. Frank, L. Schnell, A. A. Spillmann, F. Christ and M. E. Schwab (2000). "Nogo-A is a myelin-associated neurite outgrowth inhibitor and an antigen for monoclonal antibody IN-1." *Nature* **403**(6768): 434-439.
- Das, R., J. Karanicolas and D. Baker (2010). "Atomic accuracy in predicting and designing noncanonical RNA structure." *Nat Methods* **7**(4): 291-294.
- de Vries, S. J., M. van Dijk and A. M. Bonvin (2010). "The HADDOCK web server for data-driven biomolecular docking." *Nat Protoc* **5**(5): 883-897.
- Dominguez, C., R. Boelens and A. M. Bonvin (2003). "HADDOCK: a protein-protein docking approach based on biochemical or biophysical information." *J Am Chem Soc* **125**(7): 1731-1737.
- Ellington, A. D. and J. W. Szostak (1990). "In vitro selection of RNA molecules that bind specific ligands." *Nature* **346**(6287): 818-822.
- Fournier, A. E., T. GrandPre and S. M. Strittmatter (2001). "Identification of a receptor mediating Nogo-66 inhibition of axonal regeneration." *Nature* **409**(6818): 341-346.
- Fu, L., B. Niu, Z. Zhu, S. Wu and W. Li (2012). "CD-HIT: accelerated for clustering the next-generation sequencing data." *Bioinformatics* **28**(23): 3150-3152.
- GrandPre, T., F. Nakamura, T. Vartanian and S. M. Strittmatter (2000). "Identification of the Nogo inhibitor of axon regeneration as a Reticulon protein." *Nature* **403**(6768): 439-444.
- He, X. L., J. F. Bazan, G. McDermott, J. B. Park, K. Wang, M. Tessier-Lavigne, Z. He and K. C. Garcia (2003). "Structure of the Nogo receptor ectodomain: a recognition module implicated in myelin inhibition." *Neuron* **38**(2): 177-185.
- Jayasena, S. D. (1999). "Aptamers: An emerging class of molecules that rival antibodies in diagnostics." *Clinical Chemistry* **45**(9): 1628-1650.
- Joset, A., D. A. Dodd, S. Haleboua and M. E. Schwab (2010). "Pincher-generated Nogo-A endosomes mediate growth cone collapse and retrograde signaling." *Journal of Cell Biology* **188**(2): 271-285.
- Keefe, A. D., S. Pai and A. Ellington (2010). "Aptamers as therapeutics (vol 9, pg 537, 2010)." *Nature Reviews Drug Discovery* **9**(8).
- Kempf, A. and M. E. Schwab (2013). "Nogo-A represses anatomical and synaptic plasticity in the central nervous system." *Physiology (Bethesda)* **28**(3): 151-163.
- Kempf, A., B. Tews, M. E. Arzt, O. Weinmann, F. J. Obermair, V. Pernet, M. Zagrebelsky, A. Delekate, C. Iobbi, A. Zemmar, Z. Ristic, M. Gullo, P. Spies, D. Dodd, D. Gyax, M. Korte and M. E. Schwab (2014). "The Sphingolipid Receptor S1PR2 Is a Receptor for Nogo-A Repressing Synaptic Plasticity." *PLoS Biol* **12**(1): e1001763.
- Khalid K. Alam, J. L. C. D. H. B. (2014). FASTAptamer: A Bioinformatic Toolkit for High-Throughput Sequence Analysis of Combinatorial Selections, University of Missouri, Columbia, MO USA.

Kikin, O., L. D'Antonio and P. S. Bagga (2006). "QGRS Mapper: a web-based server for predicting G-quadruplexes in nucleotide sequences." Nucleic Acids Res **34**(Web Server issue): W676-682.

Kulbachinskiy, A. V. (2007). "Methods for selection of aptamers to protein targets." Biochemistry (Mosc) **72**(13): 1505-1518.

Lee, S. W. and B. A. Sullenger (1997). "Isolation of a nuclease-resistant decoy RNA that can protect human acetylcholine receptors from myasthenic antibodies." Nat Biotechnol **15**(1): 41-45.

Li, M., J. Shi, Z. Wei, F. Y. Teng, B. L. Tang and J. Song (2004). "Structural characterization of the human Nogo-A functional domains. Solution structure of Nogo-40, a Nogo-66 receptor antagonist enhancing injured spinal cord regeneration." Eur J Biochem **271**(17): 3512-3522.

Li, M. and J. Song (2007). "The N- and C-termini of the human Nogo molecules are intrinsically unstructured: bioinformatics, CD, NMR characterization, and functional implications." Proteins **68**(1): 100-108.

Lyskov, S., F. C. Chou, S. O. Conchuir, B. S. Der, K. Drew, D. Kuroda, J. Xu, B. D. Weitzner, P. D. Renfrew, P. Sripakdeevong, B. Borgo, J. J. Havranek, B. Kuhlman, T. Kortemme, R. Bonneau, J. J. Gray and R. Das (2013). "Serverification of molecular modeling applications: the Rosetta Online Server that Includes Everyone (ROSIE)." PLoS One **8**(5): e63906.

McKerracher, L., S. David, D. L. Jackson, V. Kottis, R. J. Dunn and P. E. Braun (1994). "Identification of myelin-associated glycoprotein as a major myelin-derived inhibitor of neurite growth." Neuron **13**(4): 805-811.

Mi, S., X. Lee, Z. H. Shao, G. Thill, B. X. Ji, J. Relton, M. Levesque, N. Allaire, S. Perrin, B. Sands, T. Crowell, R. L. Cate, J. M. McCoy and R. B. Pepinsky (2004). "LINGO-1 is a component of the Nogo-66 receptor/p75 signaling complex." Nature Neuroscience **7**(3): 221-228.

Mosyak, L., A. Wood, B. Dwyer, M. Buddha, M. Johnson, A. Aulabaugh, X. Zhong, E. Presman, S. Benard, K. Kelleher, J. Wilhelm, M. L. Stahl, R. Kriz, Y. Gao, Z. Cao, H. P. Ling, M. N. Pangalos, F. S. Walsh and W. S. Somers (2006). "The structure of the Lingo-1 ectodomain, a module implicated in central nervous system repair inhibition." J Biol Chem **281**(47): 36378-36390.

Oertle, T., M. E. van der Haar, C. E. Bandtlow, A. Robeva, P. Burfeind, A. Buss, A. B. Huber, M. Simonen, L. Schnell, C. Brosamle, K. Kaupmann, R. Vallon and M. E. Schwab (2003). "Nogo-A inhibits neurite outgrowth and cell spreading with three discrete regions." J Neurosci **23**(13): 5393-5406.

Park, J. B., G. Yiu, S. Kaneko, J. Wang, J. F. Chang, X. L. L. He, K. C. Garcia and Z. G. He (2005). "A TNF receptor family member, TROY, is a coreceptor with nogo receptor in mediating the inhibitory activity of myelin inhibitors (vol 45, pg 345, 2005)." Neuron **45**(5): 815-815.

Pendergrast PS, T. K., Ferguson A, Kilough J, Horwitz L, et al (2006). "Aptamers that discriminate between IL-23 and IL-12 are specific inhibitors of IL-23 and IL-12 are specific inhibitors of IL-23 activity in vitro." GTC Bio 4th Annual Conference on Cytokines and Inflammation. San Diego California: pp 109-111.

Pernet, V. and M. E. Schwab (2012). "The role of Nogo-A in axonal plasticity, regrowth and repair." Cell Tissue Res **349**(1): 97-104.

Pettersen, E. F., T. D. Goddard, C. C. Huang, G. S. Couch, D. M. Greenblatt, E. C. Meng and T. E. Ferrin (2004). "UCSF Chimera--a visualization system for exploratory research and analysis." J Comput Chem **25**(13): 1605-1612.

Rentmeister, A., A. Bill, T. Wahle, J. Walter and M. Famulok (2006). "RNA aptamers selectively modulate protein recruitment to the cytoplasmic domain of beta-secretase BACE1 in vitro." *RNA* **12**(9): 1650-1660.

Schimmele, B. and A. Pluckthun (2005). "Identification of a functional epitope of the Nogo receptor by a combinatorial approach using ribosome display." *J Mol Biol* **352**(1): 229-241.

Schmandke, A., A. Schmandke and S. M. Strittmatter (2007). "ROCK and Rho: biochemistry and neuronal functions of Rho-associated protein kinases." *Neuroscientist* **13**(5): 454-469.

Schwab, M. E. (2010). "Functions of Nogo proteins and their receptors in the nervous system." *Nat Rev Neurosci* **11**(12): 799-811.

Seo, H., Lee SW (2000). "In vitro selection of the 29-fluor-29deoxyribonucleotide decoy RNA inhibitor of myasthenia autoantibodies." *J Microbiol Biotechnol* **10**: 7070-7073.

Varma, A. K., A. Das, G. t. Wallace, J. Barry, A. A. Vertegel, S. K. Ray and N. L. Banik (2013). "Spinal cord injury: a review of current therapy, future treatments, and basic science frontiers." *Neurochem Res* **38**(5): 895-905.

Vasudevan, S. V., J. Schulz, C. Zhou and M. J. Cocco (2010). "Protein folding at the membrane interface, the structure of Nogo-66 requires interactions with a phosphocholine surface." *Proc Natl Acad Sci U S A* **107**(15): 6847-6851.

Vithayathil, R. (2012). *Unlocking the Secrets of Membrane Proteins with Phage Display*. Ph.D Dissertation, UNIVERSITY OF CALIFORNIA, IRVINE.

Wan, Y., Y. T. Kim, N. Li, S. K. Cho, R. Bachoo, A. D. Ellington and S. M. Iqbal (2010). "Surface-immobilized aptamers for cancer cell isolation and microscopic cytology." *Cancer Res* **70**(22): 9371-9380.

Wang, K. C., J. A. Kim, R. Sivasankaran, R. Segal and Z. G. He (2002). "p75 interacts with the Nogo receptor as a co-receptor for Nogo, MAG and OMgp." *Nature* **420**(6911): 74-78.

Wang, K. C., V. Koprivica, J. A. Kim, R. Sivasankaran, Y. Guo, R. L. Neve and Z. He (2002). "Oligodendrocyte-myelin glycoprotein is a Nogo receptor ligand that inhibits neurite outgrowth." *Nature* **417**(6892): 941-944.

Wang, Y. X., Z. Z. Khaing, N. Li, B. Hall, C. E. Schmidt and A. D. Ellington (2010). "Aptamer Antagonists of Myelin-Derived Inhibitors Promote Axon Growth." *Plos One* **5**(3).

Yiu, G. and Z. He (2006). "Glial inhibition of CNS axon regeneration." *Nat Rev Neurosci* **7**(8): 617-627.

Ylera, F., R. Lurz, V. A. Erdmann and J. P. Furste (2002). "Selection of RNA aptamers to the Alzheimer's disease amyloid peptide." *Biochem Biophys Res Commun* **290**(5): 1583-1588.

Zhou, J., M. L. Bobbin, J. C. Burnett and J. J. Rossi (2012). "Current progress of RNA aptamer-based therapeutics." *Front Genet* **3**: 234.

Zuker, M. (2003). "Mfold web server for nucleic acid folding and hybridization prediction." *Nucleic Acids Res* **31**(13): 3406-3415.

Bai, Y., J. J. Englander, L. Mayne, J. S. Milne and S. W. Englander (1995). "Thermodynamic parameters from hydrogen exchange measurements." *Methods Enzymol* **259**: 344-356.

Bai, Y., J. S. Milne, L. Mayne and S. W. Englander (1993). "Primary structure effects on peptide group hydrogen exchange." *Proteins* **17**(1): 75-86.

Baroni, T. E., T. Wang, H. Qian, L. R. Dearth, L. N. Truong, J. Zeng, A. E. Denes, S. W. Chen and R. K. Brachmann (2004). "A global suppressor motif for p53 cancer mutants." *Proc Natl Acad Sci U S A* **101**(14): 4930-4935.

Bullock, A. N. and A. R. Fersht (2001). "Rescuing the function of mutant p53." Nat Rev Cancer **1**(1): 68-76.

Canadillas, J. M., H. Tidow, S. M. Freund, T. J. Rutherford, H. C. Ang and A. R. Fersht (2006). "Solution structure of p53 core domain: structural basis for its instability." Proc Natl Acad Sci U S A **103**(7): 2109-2114.

Delaglio, F., S. Grzesiek, G. W. Vuister, G. Zhu, J. Pfeifer and A. Bax (1995). "NMRPipe: a multidimensional spectral processing system based on UNIX pipes." J Biomol NMR **6**(3): 277-293.

Englander, S. and N. Kallenbach (1984). "Hydrogen exchange and structural dynamics of proteins and nucleic-acids." Q Rev Biophys **16**: 521-655.

Joerger, A. C., M. D. Allen and A. R. Fersht (2004). "Crystal structure of a superstable mutant of human p53 core domain. Insights into the mechanism of rescuing oncogenic mutations." J Biol Chem **279**(2): 1291-1296.

Joerger, A. C. and A. R. Fersht (2008). "Structural biology of the tumor suppressor p53." Annu Rev Biochem **77**: 557-582.

Khoo, K. H., A. C. Joerger, S. M. Freund and A. R. Fersht (2009). "Stabilising the DNA-binding domain of p53 by rational design of its hydrophobic core." Protein Eng Des Sel **22**(7): 421-430.

Lane, D. P. and P. M. Fischer (2004). "Turning the key on p53." Nature **427**(6977): 789-790.

Maity, H., W. K. Lim, J. N. Rumbley and S. W. Englander (2003). "Protein hydrogen exchange mechanism: local fluctuations." Protein Sci **12**(1): 153-160.

Raschke, T. M. and S. Marqusee (1998). "Hydrogen exchange studies of protein structure." Curr Opin Biotechnol **9**(1): 80-86.

Tan, Y. H., Y. M. Chen, X. Ye, Q. Lu, V. Tretyachenko-Ladokhina, W. Yang, D. F. Senear and R. Luo (2009). "Molecular mechanisms of functional rescue mediated by P53 tumor suppressor mutations." Biophysical Chemistry **145**(1): 37-44.

Vogelstein, B., D. Lane and A. J. Levine (2000). "Surfing the p53 network." Nature **408**(6810): 307-310.

Whibley, C., P. D. Pharoah and M. Hollstein (2009). "p53 polymorphisms: cancer implications." Nat Rev Cancer **9**(2): 95-107.

Wong, K. B., B. S. DeDecker, S. M. Freund, M. R. Proctor, M. Bycroft and A. R. Fersht (1999). "Hot-spot mutants of p53 core domain evince characteristic local structural changes." Proc Natl Acad Sci U S A **96**(15): 8438-8442.

Acevedo, L., J. Yu, H. Erdjument-Bromage, R. Q. Miao, J. E. Kim, D. Fulton, P. Tempst, S. M. Strittmatter and W. C. Sessa (2004). "A new role for Nogo as a regulator of vascular remodeling." Nat Med **10**(4): 382-388.

Anatrace, I. "DETERGENTS AND THEIR USES IN MEMBRANE PROTEIN SCIENCE."

Chen, M. S., A. B. Huber, M. E. van der Haar, M. Frank, L. Schnell, A. A. Spillmann, F. Christ and M. E. Schwab (2000). "Nogo-A is a myelin-associated neurite outgrowth inhibitor and an antigen for monoclonal antibody IN-1." Nature **403**(6768): 434-439.

Chong, S. Y., S. S. Rosenberg, S. P. Fancy, C. Zhao, Y. A. Shen, A. T. Hahn, A. W. McGee, X. Xu, B. Zheng, L. I. Zhang, D. H. Rowitch, R. J. Franklin, Q. R. Lu and J. R. Chan (2011). "Neurite outgrowth inhibitor Nogo-A establishes spatial segregation and extent of oligodendrocyte myelination." Proc Natl Acad Sci U S A.



de Vries, S. J., M. van Dijk and A. M. Bonvin (2010). "The HADDOCK web server for data-driven biomolecular docking." *Nat Protoc* **5**(5): 883-897.

Delaglio, F., S. Grzesiek, G. W. Vuister, G. Zhu, J. Pfeifer and A. Bax (1995). "NMRPipe: a multidimensional spectral processing system based on UNIX pipes." *J Biomol NMR* **6**(3): 277-293.

Di Sano, F., P. Bernardoni and M. Piacentini (2012). "The reticulons: guardians of the structure and function of the endoplasmic reticulum." *Exp Cell Res* **318**(11): 1201-1207.

Diaz, A. and P. Ahlquist (2012). "Role of host reticulon proteins in rearranging membranes for positive-strand RNA virus replication." *Curr Opin Microbiol* **15**(4): 519-524.

GrandPre, T., F. Nakamura, T. Vartanian and S. M. Strittmatter (2000). "Identification of the Nogo inhibitor of axon regeneration as a Reticulon protein." *Nature* **403**(6768): 439-444.

He, W., Y. Lu, I. Qahwash, X. Y. Hu, A. Chang and R. Yan (2004). "Reticulon family members modulate BACE1 activity and amyloid-beta peptide generation." *Nat Med* **10**(9): 959-965.

He, W., Q. Shi, X. Hu and R. Yan (2007). "The membrane topology of RTN3 and its effect on binding of RTN3 to BACE1." *J Biol Chem* **282**(40): 29144-29151.

Hofacre, A. and H. Fan (2010). "Jaagsiekte sheep retrovirus biology and oncogenesis." *Viruses* **2**(12): 2618-2648.

Hofacre, A. and H. Fan (2010). "Jaagsiekte Sheep Retrovirus Biology and Oncogenesis." *Viruses* **2**(12): 2618-2648.

Hull, S. and H. Fan (2006). "Mutational analysis of the cytoplasmic tail of jaagsiekte sheep retrovirus envelope protein." *J Virol* **80**(16): 8069-8080.

Kempf, A. and M. E. Schwab (2013). "Nogo-A represses anatomical and synaptic plasticity in the central nervous system." *Physiology (Bethesda)* **28**(3): 151-163.

Kempf, A., B. Tews, M. E. Arzt, O. Weinmann, F. J. Obermair, V. Pernet, M. Zagrebelsky, A. Delekate, C. Iobbi, A. Zemmar, Z. Ristic, M. Gullo, P. Spies, D. Dodd, D. Gyax, M. Korte and M. E. Schwab (2014). "The Sphingolipid Receptor S1PR2 Is a Receptor for Nogo-A Repressing Synaptic Plasticity." *PLoS Biol* **12**(1): e1001763.

Kiseleva, E., K. N. Morozova, G. K. Voeltz, T. D. Allen and M. W. Goldberg (2007). "Reticulon 4a/NogoA locates to regions of high membrane curvature and may have a role in nuclear envelope growth." *J Struct Biol* **160**(2): 224-235.

Lee, S. G., Y. Kim, T. D. Alpert, A. Nagata and J. M. Jez (2012). "Structure and reaction mechanism of phosphoethanolamine methyltransferase from the malaria parasite *Plasmodium falciparum*: an antiparasitic drug target." *J Biol Chem* **287**(2): 1426-1434.

Liu, S. L. and A. D. Miller (2007). "Oncogenic transformation by the jaagsiekte sheep retrovirus envelope protein." *Oncogene* **26**(6): 789-801.

Oertle, T., M. Klinger, C. A. Stuermer and M. E. Schwab (2003). "A reticular rhapsody: phylogenetic evolution and nomenclature of the RTN/Nogo gene family." *FASEB J* **17**(10): 1238-1247.

Palmarini, M., N. Maeda, C. Murgia, C. De-Fraja, A. Hofacre and H. Fan (2001). "A phosphatidylinositol 3-kinase docking site in the cytoplasmic tail of the Jaagsiekte sheep retrovirus transmembrane protein is essential for envelope-induced transformation of NIH 3T3 cells." *J Virol* **75**(22): 11002-11009.

Pernet, V. and M. E. Schwab (2012). "The role of Nogo-A in axonal plasticity, regrowth and repair." *Cell Tissue Res* **349**(1): 97-104.

Rossenu, S., S. Leyman, D. Dewitte, D. Peelaers, V. Jonckheere, M. Van Troys, J. Vandekerckhove and C. Ampe (2003). "A phage display-based method for determination of

relative affinities of mutants. Application of the actin-binding motifs in thymosin beta 4 and the villin headpiece." *J Biol Chem* **278**(19): 16642-16650.

Satow, Y., G. H. Cohen, E. A. Padlan and D. R. Davies (1986). "Phosphocholine Binding Immunoglobulin Fab Mcpc603 an X-Ray-Diffraction Study at 2.7 Å." *Journal of Molecular Biology* **190**(4): 593-604.

Schmandke, A., A. Schmandke and M. E. Schwab (2014). "Nogo-A: Multiple Roles in CNS Development, Maintenance, and Disease." *Neuroscientist*.

Schulz, J. R. (2009). The Structural Characterization of Three Membrane Associated Proteins: Nogo66, Cryptdin-3, and the Cytoplasmic Tail of JSRV. DOCTOR OF PHILOSOPHY, University of Claifornia , Irvine.

Schwieters, C. D., J. J. Kuszewski, N. Tjandra and G. M. Clore (2003). "The Xplor-NIH NMR molecular structure determination package." *J Magn Reson* **160**(1): 65-73.

Tagami, S., Y. Eguchi, N. Kinoshita, Y. Takeda and Y. Tsujimoto (2000). "A novel protein, RTN-XS, interacts with both Bcl-XL and Bcl-2 on endoplasmic reticulum and reduces their anti-apoptotic activity." *Oncogene* **19**: 5736-5746.

Thompson, D., M. B. Pepys and S. P. Wood (1999). "The physiological structure of human C-reactive protein and its complex with phosphocholine." *Structure* **7**(2): 169-177.

Vasudevan, S. V., J. Schulz, C. Zhou and M. J. Cocco (2010). "Protein folding at the membrane interface, the structure of Nogo-66 requires interactions with a phosphocholine surface." *Proc Natl Acad Sci U S A* **107**(15): 6847-6851.

Vithayathil, R., R. M. Hooy, M. J. Cocco and G. A. Weiss (2011). "The scope of phage display for membrane proteins." *J Mol Biol* **414**(4): 499-510.

Voeltz, G. K., W. A. Prinz, Y. Shibata, J. M. Rist and T. A. Rapoport (2006). "A class of membrane proteins shaping the tubular endoplasmic reticulum." *Cell* **124**(3): 573-586.

Vranken, W. F., W. Boucher, T. J. Stevens, R. H. Fogh, A. Pajon, M. Llinas, E. L. Ulrich, J. L. Markley, J. Ionides and E. D. Laue (2005). "The CCPN data model for NMR spectroscopy: development of a software pipeline." *Proteins* **59**(4): 687-696.

Walchli, T., V. Pernet, O. Weinmann, J. Y. Shiu, A. Guzik-Kornacka, G. Decrey, D. Yuksel, H. Schneider, J. Vogel, D. E. Ingber, V. Vogel, K. Frei and M. E. Schwab (2013). "Nogo-A is a negative regulator of CNS angiogenesis." *Proc Natl Acad Sci U S A* **110**(21): E1943-1952.

White, S. H., W. C. Wimley, A. S. Ladokhin and K. Hristova (1998). "Protein folding in membranes: determining energetics of peptide-bilayer interactions." *Methods Enzymol* **295**: 62-87.

Woestenenk, E. A., M. Hammarstrom, S. van den Berg, T. Hard and H. Berglund (2004). "His tag effect on solubility of human proteins produced in Escherichia coli: a comparison between four expression vectors." *J Struct Funct Genomics* **5**(3): 217-229.

Yang, Y. S. and S. M. Strittmatter (2007). "The reticulons: a family of proteins with diverse functions." *Genome Biol* **8**(12): 234.

Zhu, L., R. Xiang, W. Dong, Y. L. Liu and Y. P. Qi (2007). "Anti-apoptotic activity of Bcl-2 is enhanced by its interaction with RTN3." *Cell Biology International* **31**(8): 825-830.

Acevedo, L., J. Yu, H. Erdjument-Bromage, R. Q. Miao, J. E. Kim, D. Fulton, P. Tempst, S. M. Strittmatter and W. C. Sessa (2004). "A new role for Nogo as a regulator of vascular remodeling." *Nat Med* **10**(4): 382-388.

Anatrace, I. "DETERGENTS AND THEIR USES IN MEMBRANE PROTEIN SCIENCE."

Bai, Y., J. J. Englander, L. Mayne, J. S. Milne and S. W. Englander (1995). "Thermodynamic parameters from hydrogen exchange measurements." *Methods Enzymol* **259**: 344-356.

Bai, Y., J. S. Milne, L. Mayne and S. W. Englander (1993). "Primary structure effects on peptide group hydrogen exchange." *Proteins* **17**(1): 75-86.

Baroni, T. E., T. Wang, H. Qian, L. R. Dearth, L. N. Truong, J. Zeng, A. E. Denes, S. W. Chen and R. K. Brachmann (2004). "A global suppressor motif for p53 cancer mutants." *Proc Natl Acad Sci U S A* **101**(14): 4930-4935.

Bullock, A. N. and A. R. Fersht (2001). "Rescuing the function of mutant p53." *Nat Rev Cancer* **1**(1): 68-76.

Canadillas, J. M., H. Tidow, S. M. Freund, T. J. Rutherford, H. C. Ang and A. R. Fersht (2006). "Solution structure of p53 core domain: structural basis for its instability." *Proc Natl Acad Sci U S A* **103**(7): 2109-2114.

Chen, M. S., A. B. Huber, M. E. van der Haar, M. Frank, L. Schnell, A. A. Spillmann, F. Christ and M. E. Schwab (2000). "Nogo-A is a myelin-associated neurite outgrowth inhibitor and an antigen for monoclonal antibody IN-1." *Nature* **403**(6768): 434-439.

Chong, S. Y., S. S. Rosenberg, S. P. Fancy, C. Zhao, Y. A. Shen, A. T. Hahn, A. W. McGee, X. Xu, B. Zheng, L. I. Zhang, D. H. Rowitch, R. J. Franklin, Q. R. Lu and J. R. Chan (2011). "Neurite outgrowth inhibitor Nogo-A establishes spatial segregation and extent of oligodendrocyte myelination." *Proc Natl Acad Sci U S A*.

de Vries, S. J., M. van Dijk and A. M. Bonvin (2010). "The HADDOCK web server for data-driven biomolecular docking." *Nat Protoc* **5**(5): 883-897.

Delaglio, F., S. Grzesiek, G. W. Vuister, G. Zhu, J. Pfeifer and A. Bax (1995). "NMRPipe: a multidimensional spectral processing system based on UNIX pipes." *J Biomol NMR* **6**(3): 277-293.

Di Sano, F., P. Bernardoni and M. Piacentini (2012). "The reticulons: guardians of the structure and function of the endoplasmic reticulum." *Exp Cell Res* **318**(11): 1201-1207.

Diaz, A. and P. Ahlquist (2012). "Role of host reticulon proteins in rearranging membranes for positive-strand RNA virus replication." *Curr Opin Microbiol* **15**(4): 519-524.

Englander, S. and N. Kallenbach (1984). "Hydrogen exchange and structural dynamics of proteins and nucleic-acids." *Q Rev Biophys* **16**: 521-655.

GrandPre, T., F. Nakamura, T. Vartanian and S. M. Strittmatter (2000). "Identification of the Nogo inhibitor of axon regeneration as a Reticulon protein." *Nature* **403**(6768): 439-444.

He, W., Y. Lu, I. Qahwash, X. Y. Hu, A. Chang and R. Yan (2004). "Reticulon family members modulate BACE1 activity and amyloid-beta peptide generation." *Nat Med* **10**(9): 959-965.

He, W., Q. Shi, X. Hu and R. Yan (2007). "The membrane topology of RTN3 and its effect on binding of RTN3 to BACE1." *J Biol Chem* **282**(40): 29144-29151.

Hofacre, A. and H. Fan (2010). "Jaagsiekte sheep retrovirus biology and oncogenesis." *Viruses* **2**(12): 2618-2648.

Hofacre, A. and H. Fan (2010). "Jaagsiekte Sheep Retrovirus Biology and Oncogenesis." *Viruses* **2**(12): 2618-2648.

Hull, S. and H. Fan (2006). "Mutational analysis of the cytoplasmic tail of jaagsiekte sheep retrovirus envelope protein." *J Virol* **80**(16): 8069-8080.

Joerger, A. C., M. D. Allen and A. R. Fersht (2004). "Crystal structure of a superstable mutant of human p53 core domain. Insights into the mechanism of rescuing oncogenic mutations." *J Biol Chem* **279**(2): 1291-1296.

Joerger, A. C. and A. R. Fersht (2008). "Structural biology of the tumor suppressor p53." *Annu Rev Biochem* **77**: 557-582.

Kempf, A. and M. E. Schwab (2013). "Nogo-A represses anatomical and synaptic plasticity in the central nervous system." *Physiology (Bethesda)* **28**(3): 151-163.

Kempf, A., B. Tews, M. E. Arzt, O. Weinmann, F. J. Obermair, V. Pernet, M. Zagrebelsky, A. Delekate, C. Iobbi, A. Zemmar, Z. Ristic, M. Gullo, P. Spies, D. Dodd, D. Gyax, M. Korte and M. E. Schwab (2014). "The Sphingolipid Receptor S1PR2 Is a Receptor for Nogo-A Repressing Synaptic Plasticity." *PLoS Biol* **12**(1): e1001763.

Khoo, K. H., A. C. Joerger, S. M. Freund and A. R. Fersht (2009). "Stabilising the DNA-binding domain of p53 by rational design of its hydrophobic core." *Protein Eng Des Sel* **22**(7): 421-430.

Kiseleva, E., K. N. Morozova, G. K. Voeltz, T. D. Allen and M. W. Goldberg (2007). "Reticulon 4a/NogoA locates to regions of high membrane curvature and may have a role in nuclear envelope growth." *J Struct Biol* **160**(2): 224-235.

Lane, D. P. and P. M. Fischer (2004). "Turning the key on p53." *Nature* **427**(6977): 789-790.

Lee, S. G., Y. Kim, T. D. Alpert, A. Nagata and J. M. Jez (2012). "Structure and reaction mechanism of phosphoethanolamine methyltransferase from the malaria parasite *Plasmodium falciparum*: an antiparasitic drug target." *J Biol Chem* **287**(2): 1426-1434.

Liu, S. L. and A. D. Miller (2007). "Oncogenic transformation by the jaagsiekte sheep retrovirus envelope protein." *Oncogene* **26**(6): 789-801.

Maity, H., W. K. Lim, J. N. Rumbley and S. W. Englander (2003). "Protein hydrogen exchange mechanism: local fluctuations." *Protein Sci* **12**(1): 153-160.

Oertle, T., M. Klinger, C. A. Stuermer and M. E. Schwab (2003). "A reticular rhapsody: phylogenetic evolution and nomenclature of the RTN/Nogo gene family." *FASEB J* **17**(10): 1238-1247.

Palmarini, M., N. Maeda, C. Murgia, C. De-Fraja, A. Hofacre and H. Fan (2001). "A phosphatidylinositol 3-kinase docking site in the cytoplasmic tail of the Jaagsiekte sheep retrovirus transmembrane protein is essential for envelope-induced transformation of NIH 3T3 cells." *J Virol* **75**(22): 11002-11009.

Pernet, V. and M. E. Schwab (2012). "The role of Nogo-A in axonal plasticity, regrowth and repair." *Cell Tissue Res* **349**(1): 97-104.

Raschke, T. M. and S. Marqusee (1998). "Hydrogen exchange studies of protein structure." *Curr Opin Biotechnol* **9**(1): 80-86.

Rossenu, S., S. Leyman, D. Dewitte, D. Peelaers, V. Jonckheere, M. Van Troys, J. Vandekerckhove and C. Ampe (2003). "A phage display-based method for determination of relative affinities of mutants. Application of the actin-binding motifs in thymosin beta 4 and the villin headpiece." *J Biol Chem* **278**(19): 16642-16650.

Satow, Y., G. H. Cohen, E. A. Padlan and D. R. Davies (1986). "Phosphocholine Binding Immunoglobulin Fab Mcpc603 an X-Ray-Diffraction Study at 2.7 Å." *Journal of Molecular Biology* **190**(4): 593-604.

Schmandke, A., A. Schmandke and M. E. Schwab (2014). "Nogo-A: Multiple Roles in CNS Development, Maintenance, and Disease." *Neuroscientist*.

Schulz, J. R. (2009). The Structural Characterization of Three Membrane Associated Proteins: Nogo66, Cryptdin-3, and the Cytoplasmic Tail of JSRV. DOCTOR OF PHILOSOPHY, University of Claifornia , Irvine.

Schwieters, C. D., J. J. Kuszewski, N. Tjandra and G. M. Clore (2003). "The Xplor-NIH NMR molecular structure determination package." *J Magn Reson* **160**(1): 65-73.

Tagami, S., Y. Eguchi, N. Kinoshita, Y. Takeda and Y. Tsujimoto (2000). "A novel protein, RTN-XS, interacts with both Bcl-XL and Bcl-2 on endoplasmic reticulum and reduces their anti-apoptotic activity." *Oncogene* **19**: 5736-5746.

Tan, Y. H., Y. M. Chen, X. Ye, Q. Lu, V. Tretyachenko-Ladokhina, W. Yang, D. F. Senear and R. Luo (2009). "Molecular mechanisms of functional rescue mediated by P53 tumor suppressor mutations." *Biophysical Chemistry* **145**(1): 37-44.

Thompson, D., M. B. Pepys and S. P. Wood (1999). "The physiological structure of human C-reactive protein and its complex with phosphocholine." *Structure* **7**(2): 169-177.

Vasudevan, S. V., J. Schulz, C. Zhou and M. J. Cocco (2010). "Protein folding at the membrane interface, the structure of Nogo-66 requires interactions with a phosphocholine surface." *Proc Natl Acad Sci U S A* **107**(15): 6847-6851.

Vithayathil, R., R. M. Hooy, M. J. Cocco and G. A. Weiss (2011). "The scope of phage display for membrane proteins." *J Mol Biol* **414**(4): 499-510.

Voeltz, G. K., W. A. Prinz, Y. Shibata, J. M. Rist and T. A. Rapoport (2006). "A class of membrane proteins shaping the tubular endoplasmic reticulum." *Cell* **124**(3): 573-586.

Vogelstein, B., D. Lane and A. J. Levine (2000). "Surfing the p53 network." *Nature* **408**(6810): 307-310.

Vranken, W. F., W. Boucher, T. J. Stevens, R. H. Fogh, A. Pajon, M. Llinas, E. L. Ulrich, J. L. Markley, J. Ionides and E. D. Laue (2005). "The CCPN data model for NMR spectroscopy: development of a software pipeline." *Proteins* **59**(4): 687-696.

Walchli, T., V. Pernet, O. Weinmann, J. Y. Shiu, A. Guzik-Kornacka, G. Decrey, D. Yuksel, H. Schneider, J. Vogel, D. E. Ingber, V. Vogel, K. Frei and M. E. Schwab (2013). "Nogo-A is a negative regulator of CNS angiogenesis." *Proc Natl Acad Sci U S A* **110**(21): E1943-1952.

Whibley, C., P. D. Pharoah and M. Hollstein (2009). "p53 polymorphisms: cancer implications." *Nat Rev Cancer* **9**(2): 95-107.

White, S. H., W. C. Wimley, A. S. Ladokhin and K. Hristova (1998). "Protein folding in membranes: determining energetics of peptide-bilayer interactions." *Methods Enzymol* **295**: 62-87.

Woestenenk, E. A., M. Hammarstrom, S. van den Berg, T. Hard and H. Berglund (2004). "His tag effect on solubility of human proteins produced in Escherichia coli: a comparison between four expression vectors." *J Struct Funct Genomics* **5**(3): 217-229.

Wong, K. B., B. S. DeDecker, S. M. Freund, M. R. Proctor, M. Bycroft and A. R. Fersht (1999). "Hot-spot mutants of p53 core domain evince characteristic local structural changes." *Proc Natl Acad Sci U S A* **96**(15): 8438-8442.

Yang, Y. S. and S. M. Strittmatter (2007). "The reticulons: a family of proteins with diverse functions." *Genome Biol* **8**(12): 234.

Zhu, L., R. Xiang, W. Dong, Y. L. Liu and Y. P. Qi (2007). "Anti-apoptotic activity of Bcl-2 is enhanced by its interaction with RTN3." *Cell Biology International* **31**(8): 825-830.

de Vries, S. J., M. van Dijk and A. M. Bonvin (2010). "The HADDOCK web server for data-driven biomolecular docking." *Nat Protoc* **5**(5): 883-897.

Delaglio, F., S. Grzesiek, G. W. Vuister, G. Zhu, J. Pfeifer and A. Bax (1995). "NMRPipe: a multidimensional spectral processing system based on UNIX pipes." *J Biomol NMR* **6**(3): 277-293.

He, X. L., J. F. Bazan, G. McDermott, J. B. Park, K. Wang, M. Tessier-Lavigne, Z. He and K. C. Garcia (2003). "Structure of the Nogo receptor ectodomain: a recognition module implicated in myelin inhibition." *Neuron* **38**(2): 177-185.

Lees, J. G., A. J. Miles, R. W. Janes and B. A. Wallace (2006). "Novel methods for secondary structure determination using low wavelength (VUV) circular dichroism spectroscopic data." *BMC Bioinformatics* **7**: 507.

Pettersen, E. F., T. D. Goddard, C. C. Huang, G. S. Couch, D. M. Greenblatt, E. C. Meng and T. E. Ferrin (2004). "UCSF Chimera--a visualization system for exploratory research and analysis." *J Comput Chem* **25**(13): 1605-1612.

Rossenu, S., S. Leyman, D. Dewitte, D. Peelaers, V. Jonckheere, M. Van Troys, J. Vandekerckhove and C. Ampe (2003). "A phage display-based method for determination of relative affinities of mutants. Application of the actin-binding motifs in thymosin beta 4 and the villin headpiece." *J Biol Chem* **278**(19): 16642-16650.

Schimmele, B. and A. Pluckthun (2005). "Identification of a functional epitope of the Nogo receptor by a combinatorial approach using ribosome display." *J Mol Biol* **352**(1): 229-241.

Vithayathil, R., R. M. Hooy, M. J. Cocco and G. A. Weiss (2011). "The scope of phage display for membrane proteins." *J Mol Biol* **414**(4): 499-510.

White, S. H., W. C. Wimley, A. S. Ladokhin and K. Hristova (1998). "Protein folding in membranes: determining energetics of peptide-bilayer interactions." *Methods Enzymol* **295**: 62-87.

Whitmore, L. and B. A. Wallace (2004). "DICHROWEB, an online server for protein secondary structure analyses from circular dichroism spectroscopic data." *Nucleic Acids Res* **32**(Web Server issue): W668-673.

Acevedo, L., J. Yu, H. Erdjument-Bromage, R. Q. Miao, J. E. Kim, D. Fulton, P. Tempst, S. M. Strittmatter and W. C. Sessa (2004). "A new role for Nogo as a regulator of vascular remodeling." *Nat Med* **10**(4): 382-388.

Anatrice, I. "DETERGENTS AND THEIR USES IN MEMBRANE PROTEIN SCIENCE."

Bai, Y., J. J. Englander, L. Mayne, J. S. Milne and S. W. Englander (1995). "Thermodynamic parameters from hydrogen exchange measurements." *Methods Enzymol* **259**: 344-356.

Bai, Y., J. S. Milne, L. Mayne and S. W. Englander (1993). "Primary structure effects on peptide group hydrogen exchange." *Proteins* **17**(1): 75-86.

Baroni, T. E., T. Wang, H. Qian, L. R. Dearth, L. N. Truong, J. Zeng, A. E. Denes, S. W. Chen and R. K. Brachmann (2004). "A global suppressor motif for p53 cancer mutants." *Proc Natl Acad Sci U S A* **101**(14): 4930-4935.

Bullock, A. N. and A. R. Fersht (2001). "Rescuing the function of mutant p53." *Nat Rev Cancer* **1**(1): 68-76.

Burmeister, P. E., C. Wang, J. R. Killough, S. D. Lewis, L. R. Horwitz, A. Ferguson, K. M. Thompson, P. S. Pendergrast, T. G. McCauley, M. Kurz, J. Diener, S. T. Cload, C. Wilson and A. D. Keefe (2006). "2'-Deoxy purine, 2'-O-methyl pyrimidine (dRmY) aptamers as candidate therapeutics." *Oligonucleotides* **16**(4): 337-351.

Canadillas, J. M., H. Tidow, S. M. Freund, T. J. Rutherford, H. C. Ang and A. R. Fersht (2006). "Solution structure of p53 core domain: structural basis for its instability." *Proc Natl Acad Sci U S A* **103**(7): 2109-2114.

Chen, M. S., A. B. Huber, M. E. van der Haar, M. Frank, L. Schnell, A. A. Spillmann, F. Christ and M. E. Schwab (2000). "Nogo-A is a myelin-associated neurite outgrowth inhibitor and an antigen for monoclonal antibody IN-1." *Nature* **403**(6768): 434-439.

Chen, M. S., A. B. Huber, M. E. van der Haar, M. Frank, L. Schnell, A. A. Spillmann, F. Christ and M. E. Schwab (2000). "Nogo-A is a myelin-associated neurite outgrowth inhibitor and an antigen for monoclonal antibody IN-1." *Nature* **403**(6768): 434-439.

Chong, S. Y., S. S. Rosenberg, S. P. Fancy, C. Zhao, Y. A. Shen, A. T. Hahn, A. W. McGee, X. Xu, B. Zheng, L. I. Zhang, D. H. Rowitch, R. J. Franklin, Q. R. Lu and J. R. Chan (2011). "Neurite outgrowth inhibitor Nogo-A establishes spatial segregation and extent of oligodendrocyte myelination." Proc Natl Acad Sci U S A.

Das, R., J. Karanicolas and D. Baker (2010). "Atomic accuracy in predicting and designing noncanonical RNA structure." Nat Methods **7**(4): 291-294.

de Vries, S. J., M. van Dijk and A. M. Bonvin (2010). "The HADDOCK web server for data-driven biomolecular docking." Nat Protoc **5**(5): 883-897.

Delaglio, F., S. Grzesiek, G. W. Vuister, G. Zhu, J. Pfeifer and A. Bax (1995). "NMRPipe: a multidimensional spectral processing system based on UNIX pipes." J Biomol NMR **6**(3): 277-293.

Di Sano, F., P. Bernardoni and M. Piacentini (2012). "The reticulons: guardians of the structure and function of the endoplasmic reticulum." Exp Cell Res **318**(11): 1201-1207.

Diaz, A. and P. Ahlquist (2012). "Role of host reticulon proteins in rearranging membranes for positive-strand RNA virus replication." Curr Opin Microbiol **15**(4): 519-524.

Dominguez, C., R. Boelens and A. M. Bonvin (2003). "HADDOCK: a protein-protein docking approach based on biochemical or biophysical information." J Am Chem Soc **125**(7): 1731-1737.

Ellington, A. D. and J. W. Szostak (1990). "In vitro selection of RNA molecules that bind specific ligands." Nature **346**(6287): 818-822.

Englander, S. and N. Kallenbach (1984). "Hydrogen exchange and structural dynamics of proteins and nucleic-acids." Q Rev Biophys **16**: 521-655.

Fournier, A. E., T. GrandPre and S. M. Strittmatter (2001). "Identification of a receptor mediating Nogo-66 inhibition of axonal regeneration." Nature **409**(6818): 341-346.

GrandPre, T., F. Nakamura, T. Vartanian and S. M. Strittmatter (2000). "Identification of the Nogo inhibitor of axon regeneration as a Reticulon protein." Nature **403**(6768): 439-444.

He, W., Y. Lu, I. Qahwash, X. Y. Hu, A. Chang and R. Yan (2004). "Reticulon family members modulate BACE1 activity and amyloid-beta peptide generation." Nat Med **10**(9): 959-965.

He, W., Q. Shi, X. Hu and R. Yan (2007). "The membrane topology of RTN3 and its effect on binding of RTN3 to BACE1." J Biol Chem **282**(40): 29144-29151.

He, X. L., J. F. Bazan, G. McDermott, J. B. Park, K. Wang, M. Tessier-Lavigne, Z. He and K. C. Garcia (2003). "Structure of the Nogo receptor ectodomain: a recognition module implicated in myelin inhibition." Neuron **38**(2): 177-185.

Hofacre, A. and H. Fan (2010). "Jaagsiekte Sheep Retrovirus Biology and Oncogenesis." Viruses **2**(12): 2618-2648.

Hofacre, A. and H. Fan (2010). "Jaagsiekte sheep retrovirus biology and oncogenesis." Viruses **2**(12): 2618-2648.

Hull, S. and H. Fan (2006). "Mutational analysis of the cytoplasmic tail of jaagsiekte sheep retrovirus envelope protein." J Virol **80**(16): 8069-8080.

Jayasena, S. D. (1999). "Aptamers: An emerging class of molecules that rival antibodies in diagnostics." Clinical Chemistry **45**(9): 1628-1650.

Joerger, A. C., M. D. Allen and A. R. Fersht (2004). "Crystal structure of a superstable mutant of human p53 core domain. Insights into the mechanism of rescuing oncogenic mutations." J Biol Chem **279**(2): 1291-1296.

Joerger, A. C. and A. R. Fersht (2008). "Structural biology of the tumor suppressor p53." Annu Rev Biochem **77**: 557-582.

Joset, A., D. A. Dodd, S. Halegoua and M. E. Schwab (2010). "Pincher-generated Nogo-A endosomes mediate growth cone collapse and retrograde signaling." *Journal of Cell Biology* **188**(2): 271-285.

Keefe, A. D., S. Pai and A. Ellington (2010). "Aptamers as therapeutics (vol 9, pg 537, 2010)." *Nature Reviews Drug Discovery* **9**(8).

Kempf, A. and M. E. Schwab (2013). "Nogo-A represses anatomical and synaptic plasticity in the central nervous system." *Physiology (Bethesda)* **28**(3): 151-163.

Kempf, A., B. Tews, M. E. Arzt, O. Weinmann, F. J. Obermair, V. Pernet, M. Zagrebelsky, A. Delekate, C. Iobbi, A. Zemmar, Z. Ristic, M. Gullo, P. Spies, D. Dodd, D. Gyax, M. Korte and M. E. Schwab (2014). "The Sphingolipid Receptor S1PR2 Is a Receptor for Nogo-A Repressing Synaptic Plasticity." *PLoS Biol* **12**(1): e1001763.

Khalid K. Alam, J. L. C. D. H. B. (2014). FASTAptamer: A Bioinformatic Toolkit for High-Throughput Sequence Analysis of Combinatorial Selections, University of Missouri, Columbia, MO USA.

Khoo, K. H., A. C. Joerger, S. M. Freund and A. R. Fersht (2009). "Stabilising the DNA-binding domain of p53 by rational design of its hydrophobic core." *Protein Eng Des Sel* **22**(7): 421-430.

Kikin, O., L. D'Antonio and P. S. Bagga (2006). "QGRS Mapper: a web-based server for predicting G-quadruplexes in nucleotide sequences." *Nucleic Acids Res* **34**(Web Server issue): W676-682.

Kiseleva, E., K. N. Morozova, G. K. Voeltz, T. D. Allen and M. W. Goldberg (2007). "Reticulon 4a/NogoA locates to regions of high membrane curvature and may have a role in nuclear envelope growth." *J Struct Biol* **160**(2): 224-235.

Kulbachinskiy, A. V. (2007). "Methods for selection of aptamers to protein targets." *Biochemistry (Mosc)* **72**(13): 1505-1518.

Lane, D. P. and P. M. Fischer (2004). "Turning the key on p53." *Nature* **427**(6977): 789-790.

Lee, S. G., Y. Kim, T. D. Alpert, A. Nagata and J. M. Jez (2012). "Structure and reaction mechanism of phosphoethanolamine methyltransferase from the malaria parasite *Plasmodium falciparum*: an antiparasitic drug target." *J Biol Chem* **287**(2): 1426-1434.

Lee, S. W. and B. A. Sullenger (1997). "Isolation of a nuclease-resistant decoy RNA that can protect human acetylcholine receptors from myasthenic antibodies." *Nat Biotechnol* **15**(1): 41-45.

Lees, J. G., A. J. Miles, R. W. Janes and B. A. Wallace (2006). "Novel methods for secondary structure determination using low wavelength (VUV) circular dichroism spectroscopic data." *BMC Bioinformatics* **7**: 507.

Li, M., J. Shi, Z. Wei, F. Y. Teng, B. L. Tang and J. Song (2004). "Structural characterization of the human Nogo-A functional domains. Solution structure of Nogo-40, a Nogo-66 receptor antagonist enhancing injured spinal cord regeneration." *Eur J Biochem* **271**(17): 3512-3522.

Li, M. and J. Song (2007). "The N- and C-termini of the human Nogo molecules are intrinsically unstructured: bioinformatics, CD, NMR characterization, and functional implications." *Proteins* **68**(1): 100-108.

Liu, S. L. and A. D. Miller (2007). "Oncogenic transformation by the jaagsiekte sheep retrovirus envelope protein." *Oncogene* **26**(6): 789-801.

Lyskov, S., F. C. Chou, S. O. Conchuir, B. S. Der, K. Drew, D. Kuroda, J. Xu, B. D. Weitzner, P. D. Renfrew, P. Sripakdeevong, B. Borgo, J. J. Havranek, B. Kuhlman, T. Kortemme, R. Bonneau,



J. J. Gray and R. Das (2013). "Serverification of molecular modeling applications: the Rosetta Online Server that Includes Everyone (ROSIE)." *PLoS One* **8**(5): e63906.

Maity, H., W. K. Lim, J. N. Rumbley and S. W. Englander (2003). "Protein hydrogen exchange mechanism: local fluctuations." *Protein Sci* **12**(1): 153-160.

McKerracher, L., S. David, D. L. Jackson, V. Kottis, R. J. Dunn and P. E. Braun (1994). "Identification of myelin-associated glycoprotein as a major myelin-derived inhibitor of neurite growth." *Neuron* **13**(4): 805-811.

Mi, S., X. Lee, Z. H. Shao, G. Thill, B. X. Ji, J. Relton, M. Levesque, N. Allaire, S. Perrin, B. Sands, T. Crowell, R. L. Cate, J. M. McCoy and R. B. Pepinsky (2004). "LINGO-1 is a component of the Nogo-66 receptor/p75 signaling complex." *Nature Neuroscience* **7**(3): 221-228.

Mosyak, L., A. Wood, B. Dwyer, M. Buddha, M. Johnson, A. Aulabaugh, X. Zhong, E. Presman, S. Benard, K. Kelleher, J. Wilhelm, M. L. Stahl, R. Kriz, Y. Gao, Z. Cao, H. P. Ling, M. N. Pangalos, F. S. Walsh and W. S. Somers (2006). "The structure of the Lingo-1 ectodomain, a module implicated in central nervous system repair inhibition." *J Biol Chem* **281**(47): 36378-36390.

Oertle, T., M. Klinger, C. A. Stuermer and M. E. Schwab (2003). "A reticular rhapsody: phylogenetic evolution and nomenclature of the RTN/Nogo gene family." *FASEB J* **17**(10): 1238-1247.

Oertle, T., M. E. van der Haar, C. E. Bandtlow, A. Robeva, P. Burfeind, A. Buss, A. B. Huber, M. Simonen, L. Schnell, C. Brosamle, K. Kaupmann, R. Vallon and M. E. Schwab (2003). "Nogo-A inhibits neurite outgrowth and cell spreading with three discrete regions." *J Neurosci* **23**(13): 5393-5406.

Palmarini, M., N. Maeda, C. Murgia, C. De-Fraja, A. Hofacre and H. Fan (2001). "A phosphatidylinositol 3-kinase docking site in the cytoplasmic tail of the Jaagsiekte sheep retrovirus transmembrane protein is essential for envelope-induced transformation of NIH 3T3 cells." *J Virol* **75**(22): 11002-11009.

Park, J. B., G. Yiu, S. Kaneko, J. Wang, J. F. Chang, X. L. L. He, K. C. Garcia and Z. G. He (2005). "A TNF receptor family member, TROY, is a coreceptor with nogo receptor in mediating the inhibitory activity of myelin inhibitors (vol 45, pg 345, 2005)." *Neuron* **45**(5): 815-815.

Pendergrast PS, T. K., Ferguson A, Kilough J, Horwitz L, et al (2006). "Aptamers that discriminate between IL-23 and IL-12 are specific inhibitors of IL-23 and IL-12 are specific inhibitors of IL-23 activity in vitro." *GTC Bio 4th Annual Conference on Cytokines and Inflammation. San Diego California*: pp 109-111.

Pernet, V. and M. E. Schwab (2012). "The role of Nogo-A in axonal plasticity, regrowth and repair." *Cell Tissue Res* **349**(1): 97-104.

Pettersen, E. F., T. D. Goddard, C. C. Huang, G. S. Couch, D. M. Greenblatt, E. C. Meng and T. E. Ferrin (2004). "UCSF Chimera--a visualization system for exploratory research and analysis." *J Comput Chem* **25**(13): 1605-1612.

Raschke, T. M. and S. Marqusee (1998). "Hydrogen exchange studies of protein structure." *Curr Opin Biotechnol* **9**(1): 80-86.

Rentmeister, A., A. Bill, T. Wahle, J. Walter and M. Famulok (2006). "RNA aptamers selectively modulate protein recruitment to the cytoplasmic domain of beta-secretase BACE1 in vitro." *RNA* **12**(9): 1650-1660.

Rossenu, S., S. Leyman, D. Dewitte, D. Peelaers, V. Jonckheere, M. Van Troys, J. Vandekerckhove and C. Ampe (2003). "A phage display-based method for determination of

relative affinities of mutants. Application of the actin-binding motifs in thymosin beta 4 and the villin headpiece." *J Biol Chem* **278**(19): 16642-16650.

Satow, Y., G. H. Cohen, E. A. Padlan and D. R. Davies (1986). "Phosphocholine Binding Immunoglobulin Fab Mcpc603 an X-Ray-Diffraction Study at 2.7 Å." *Journal of Molecular Biology* **190**(4): 593-604.

Schimmele, B. and A. Pluckthun (2005). "Identification of a functional epitope of the Nogo receptor by a combinatorial approach using ribosome display." *J Mol Biol* **352**(1): 229-241.

Schmandke, A., A. Schmandke and M. E. Schwab (2014). "Nogo-A: Multiple Roles in CNS Development, Maintenance, and Disease." *Neuroscientist*.

Schmandke, A., A. Schmandke and S. M. Strittmatter (2007). "ROCK and Rho: biochemistry and neuronal functions of Rho-associated protein kinases." *Neuroscientist* **13**(5): 454-469.

Schulz, J. R. (2009). The Structural Characterization of Three Membrane Associated Proteins: Nogo66, Cryptdin-3, and the Cytoplasmic Tail of JSRV. DOCTOR OF PHILOSOPHY, University of Claifornia , Irvine.

Schwab, M. E. (2010). "Functions of Nogo proteins and their receptors in the nervous system." *Nat Rev Neurosci* **11**(12): 799-811.

Schwieters, C. D., J. J. Kuszewski, N. Tjandra and G. M. Clore (2003). "The Xplor-NIH NMR molecular structure determination package." *J Magn Reson* **160**(1): 65-73.

Seo, H., Lee SW (2000). "In vitro selectin of the 29-fluor-29deoxyribonucleotide decoy RNA inhibitor of myasthenia autoantibodies." *J Microbiol Biotechnol* **10**: 7070-7073.

Tagami, S., Y. Eguchi, N. Kinoshita, Y. Takeda and Y. Tsujimoto (2000). "A novel protein, RTN-XS, interacts with both Bcl-XL and Bcl-2 on endoplasmic reticulum and reduces their anti-apoptotic activity." *Oncogene* **19**: 5736-5746.

Tan, Y. H., Y. M. Chen, X. Ye, Q. Lu, V. Tretyachenko-Ladokhina, W. Yang, D. F. Senear and R. Luo (2009). "Molecular mechanisms of functional rescue mediated by P53 tumor suppressor mutations." *Biophysical Chemistry* **145**(1): 37-44.

Thompson, D., M. B. Pepys and S. P. Wood (1999). "The physiological structure of human C-reactive protein and its complex with phosphocholine." *Structure* **7**(2): 169-177.

Tuerk, C. and L. Gold (1990). "Systematic evolution of ligands by exponential enrichment: RNA ligands to bacteriophage T4 DNA polymerase." *Science* **249**(4968): 505-510.

Varma, A. K., A. Das, G. t. Wallace, J. Barry, A. A. Vertegel, S. K. Ray and N. L. Banik (2013). "Spinal cord injury: a review of current therapy, future treatments, and basic science frontiers." *Neurochem Res* **38**(5): 895-905.

Vasudevan, S. V., J. Schulz, C. Zhou and M. J. Cocco (2010). "Protein folding at the membrane interface, the structure of Nogo-66 requires interactions with a phosphocholine surface." *Proc Natl Acad Sci U S A* **107**(15): 6847-6851.

Vithayathil, R. (2012). Unlocking the Secrets of Membrane Proteins with Phage Display. Ph.D Dissertation, UNIVERSITY OF CALIFORNIA, IRVINE.

Vithayathil, R., R. M. Hooy, M. J. Cocco and G. A. Weiss (2011). "The scope of phage display for membrane proteins." *J Mol Biol* **414**(4): 499-510.

Voeltz, G. K., W. A. Prinz, Y. Shibata, J. M. Rist and T. A. Rapoport (2006). "A class of membrane proteins shaping the tubular endoplasmic reticulum." *Cell* **124**(3): 573-586.

Vogelstein, B., D. Lane and A. J. Levine (2000). "Surfing the p53 network." *Nature* **408**(6810): 307-310.

Vranken, W. F., W. Boucher, T. J. Stevens, R. H. Fogh, A. Pajon, M. Llinas, E. L. Ulrich, J. L. Markley, J. Ionides and E. D. Laue (2005). "The CCPN data model for NMR spectroscopy: development of a software pipeline." *Proteins* **59**(4): 687-696.

Walchli, T., V. Pernet, O. Weinmann, J. Y. Shiu, A. Guzik-Kornacka, G. Decrey, D. Yuksel, H. Schneider, J. Vogel, D. E. Ingber, V. Vogel, K. Frei and M. E. Schwab (2013). "Nogo-A is a negative regulator of CNS angiogenesis." *Proc Natl Acad Sci U S A* **110**(21): E1943-1952.

Wan, Y., Y. T. Kim, N. Li, S. K. Cho, R. Bachoo, A. D. Ellington and S. M. Iqbal (2010). "Surface-immobilized aptamers for cancer cell isolation and microscopic cytology." *Cancer Res* **70**(22): 9371-9380.

Wang, K. C., J. A. Kim, R. Sivasankaran, R. Segal and Z. G. He (2002). "p75 interacts with the Nogo receptor as a co-receptor for Nogo, MAG and OMgp." *Nature* **420**(6911): 74-78.

Wang, K. C., V. Koprivica, J. A. Kim, R. Sivasankaran, Y. Guo, R. L. Neve and Z. He (2002). "Oligodendrocyte-myelin glycoprotein is a Nogo receptor ligand that inhibits neurite outgrowth." *Nature* **417**(6892): 941-944.

Wang, Y. X., Z. Z. Khaing, N. Li, B. Hall, C. E. Schmidt and A. D. Ellington (2010). "Aptamer Antagonists of Myelin-Derived Inhibitors Promote Axon Growth." *Plos One* **5**(3).

Whibley, C., P. D. Pharoah and M. Hollstein (2009). "p53 polymorphisms: cancer implications." *Nat Rev Cancer* **9**(2): 95-107.

White, S. H., W. C. Wimley, A. S. Ladokhin and K. Hristova (1998). "Protein folding in membranes: determining energetics of peptide-bilayer interactions." *Methods Enzymol* **295**: 62-87.

Whitmore, L. and B. A. Wallace (2004). "DICHROWEB, an online server for protein secondary structure analyses from circular dichroism spectroscopic data." *Nucleic Acids Res* **32**(Web Server issue): W668-673.

Woestenenk, E. A., M. Hammarstrom, S. van den Berg, T. Hard and H. Berglund (2004). "His tag effect on solubility of human proteins produced in Escherichia coli: a comparison between four expression vectors." *J Struct Funct Genomics* **5**(3): 217-229.

Wong, K. B., B. S. DeDecker, S. M. Freund, M. R. Proctor, M. Bycroft and A. R. Fersht (1999). "Hot-spot mutants of p53 core domain evince characteristic local structural changes." *Proc Natl Acad Sci U S A* **96**(15): 8438-8442.

Yang, Y. S. and S. M. Strittmatter (2007). "The reticulons: a family of proteins with diverse functions." *Genome Biol* **8**(12): 234.

Yiu, G. and Z. He (2006). "Glial inhibition of CNS axon regeneration." *Nat Rev Neurosci* **7**(8): 617-627.

Ylera, F., R. Lurz, V. A. Erdmann and J. P. Furste (2002). "Selection of RNA aptamers to the Alzheimer's disease amyloid peptide." *Biochem Biophys Res Commun* **290**(5): 1583-1588.

Zhou, J., M. L. Bobbin, J. C. Burnett and J. J. Rossi (2012). "Current progress of RNA aptamer-based therapeutics." *Front Genet* **3**: 234.

Zhu, L., R. Xiang, W. Dong, Y. L. Liu and Y. P. Qi (2007). "Anti-apoptotic activity of Bcl-2 is enhanced by its interaction with RTN3." *Cell Biology International* **31**(8): 825-830.

Zuker, M. (2003). "Mfold web server for nucleic acid folding and hybridization prediction." *Nucleic Acids Res* **31**(13): 3406-3415.

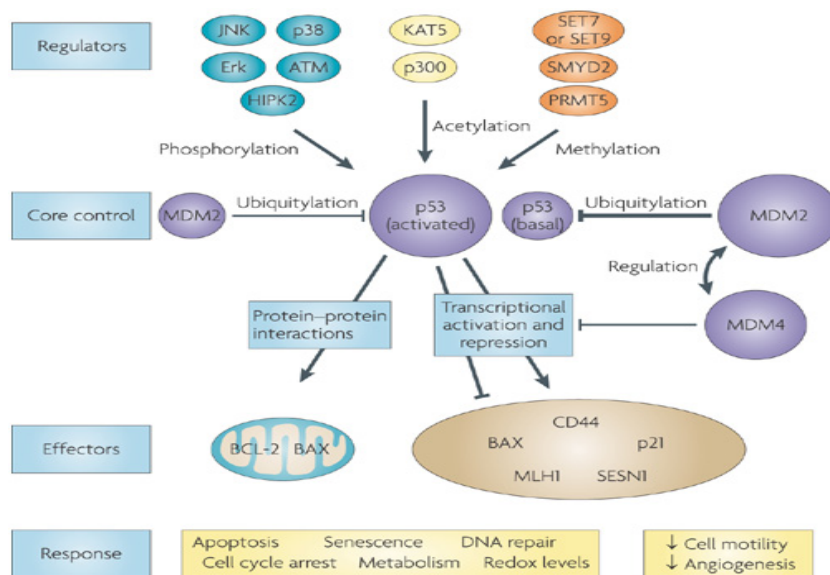
**Appendix A**  
**Revealing p53 rescue mutant mechanisms**

## **Abstract:**

p53 is a transcription factor with tumor suppressor activity that is triggered by various cellular stresses and functions to control genomic instability. Since p53 functions as a tetramer, any defect in either p53 allele would result in cancer. The importance of function of p53 and rescuing its mutations for cancer prevention has motivated researchers to find second-site suppressors, short peptides, and small molecules to restore wild type conformation. Bachmann and co-workers have identified the global suppressor motif involving amino acid N235, Y239, R240 restore the function by rescuing more than 50 % of the most p53 cancer mutations (Baroni, Wang et al. 2004). In order to understand the rescue mechanism I use NMR and monitor Hydrogen exchange (HX) to determine the most stable residues. I then calculated a protection factor (P) for each residue. p53 rescue mutants showed more protection than wild type, consistent with their mechanism of increasing stability. The average of protection factors for stable residues in N239Y compare to those in N235K and wild type i.e. N239Y ( $4.39 \times 10^6$ ) > N235K ( $1.68 \times 10^6$ ) > Wild type ( $6.94 \times 10^5$ ). The extreme protection in Asn-268 and Asp-259 in N239 and N235K is due to the involvement in a hydrogen bond network, which furthers their stability.

## Introduction/Background:

p53 is a transcription factor with a tumor suppressor activity that is triggered by various cellular stress signals, including DNA damage and metabolic and oxidative stresses (Vogelstein, Lane et al. 2000). Normally, p53 protein levels are low; once it is activated, the level of p53 is increased. It functions as a tetrameric transcription factor which preserves the integrity of the genome by controlling cell cycle, apoptosis (cell death), and/or DNA repair and differentiation (Lane and Fischer 2004), (Whibley, Pharoah et al. 2009). Furthermore, it can directly bind to several growth proteins. Therefore, any defect in p53, commonly by missense mutation, would overwhelm the regulation of cells growth and apoptosis and subsequently result in cancer (Figure A.1).



Nature Reviews | Cancer

Figure A.1: p53 pathway and downstream effect. (Whibley, Pharoah et al. 2009)

These mutations are centralized within a DNA core domain where p53 exerts its function and accounts for half of human cancers (Tan, Chen et al. 2009) (Figure A.2). The 393 amino acid proteins are divided into three domains: (i) the unstructured N-terminal transactivation domain; (ii) 218-amino acid DNA-binding core domain (DBD), formed by two beta-turn loops (L2-L3) and a loop-sheet-helix motif; and (iii) the C-terminal tetramerization domain (Joerger and Fersht 2008, Tan, Chen et al. 2009) (Figure A.2).

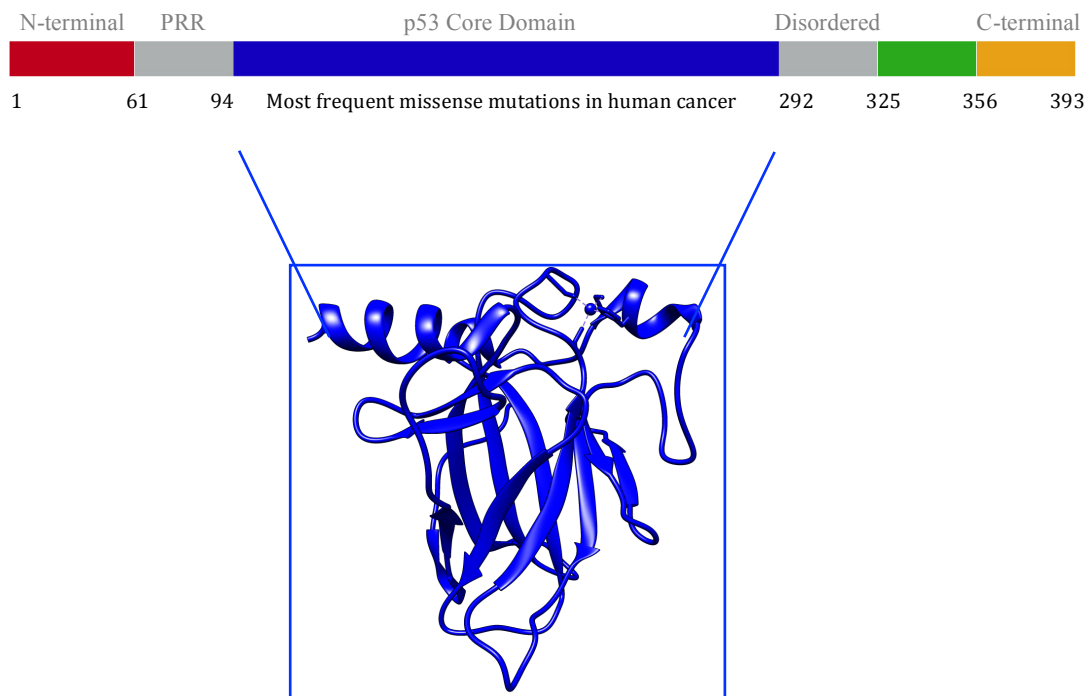


Figure A.2: p53 structural domains. Blue, the p53 core domain, p53C (DNA-binding domain, DBD). 175, 220, 245, 248, 249, 273, 282 are most frequent mutations in p53C. PRR, proline rich region.

Based on the DNA binding, three major classes describe the p53 core domain mutations missense: 1) mutations that prevent binding to DNA have little to no effect on structure; 2) mutations that unfold DBD reduce DNA binding abilities; 3) mutations induce structure conformational changes.

The importance of function of p53 for cancer prevention has motivated researchers to find second-site suppressors, short peptides, and small compounds to restore wild type conformation, and consequently reinstate p53 function (Bullock and Fersht 2001). Brachmann and co-workers have identified, by genetic approach, the global suppressor motif involving amino acids N235, N239, and R240 that refold the DNA Binding Domain (DBD) and restore the function by rescuing more than 50% of the most widespread p53 cancer mutations by stabilizing the protein without disturbing the DNA binding site (Baroni, Wang et al. 2004). The focus of this work is the rescue by mutation of N235 and N239. In order to understand how these mutations confer function to p53 cancer mutants, we should gain insight the basic structure and study the stability of p53 core domain. One approach is hydrogen exchange, which reveals site-specific information. p53 wild type and mutant structures have been determined by NMR and crystallography. However, hydrogen exchange (HX) has yet to be elucidated. This necessity leads us to another important part of this work. It's worth underlining that hydrogen exchange is a chemical reaction where the pH of the solvent plays an important role in catalyzing it. Acidic pH induces a momentary protonation of the backbone C=O, which leads to loss of N hydrogen, and then replaces it by deuterium



from the solvent. Basic pH directly removes N-H by solvent hydroxide, and subsequently replaces it by deuterium (Raschke and Marqusee 1998).

The rate of exchange of hydrogen atoms with deuterium gives information about protein structure and its dynamics. Amide hydrogens in the peptide bonds of protein backbone are particularly useful in providing information on the stability of secondary structural units (Bai, Englander et al. 1995). Hydrogen exchange has been useful in understanding protein stability, folding, binding and even protein interactions with DNA and/or other proteins. Hydrogen atoms exposed to solvent (e.g. loops) exchange faster than those that are buried within a hydrophobic core (Figure A.3). The intrinsic (random coil) exchange rates are predictable by their primary structure (Bai, Milne et al. 1993). Protein structure plays a role in protecting hydrogen atoms against exchange, and this is known as the protection factor (P), which is calculated for each residue in the protein. The protection factor is defined as  $P = k_{rc}/k_{ex}$ , where  $k_{rc}$  is the predicted HX rate constant from the random coil model, by referencing an alanine-based peptide (poly-DL-alanine, PDLA) (Table A.2 ), and  $k_{ex}$  is the experimental HX rate of a protein (Englander and Kallenbach 1984). Therefore, any mutations that change protein stability, even if they do not affect the protein's native structure, will change the hydrogen exchange at the residue and its adjacent ones. Thus, the high sensitivities of HX would sense any changes in protein dynamics that may not be noticeable in structure determination (Maity, Lim et al. 2003). Here, I determined the protection factor for WT p53 and its mutants,

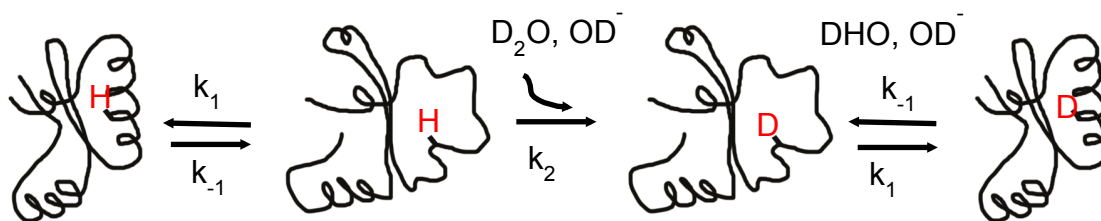


Figure A.3: Hydrogen-Deuterium Exchange mechanism (H-D exchange), it is pH dependent. Acidic pH is directly replaced the N-H by deuterium. Basic pH the N-H is transferred from H-bond to hydroxide ion then replaced by deuterium.

N235K and N239Y. Then, I elucidated the mechanism by which these mutants are stabilizing the functional domain of p53.

## Stability of p53 core domain determined by hydrogen exchange

### (HX):

To define specific positions within the rescue mutants that show increased stability, I measured the hydrogen-deuterium exchange rates and calculated the protection factors for each residue. The HSQC spectra were well dispersed and signals have previously been assigned (Wong, DeDecker et al. 1999). Our wild type spectrum was in good match with the published spectrum. The total p53 core domain is 218 residues. After initiation of exchange, 151 in p53 wild type, and 154 residues in N235K and N239Y exchanged with the solvent ( $D_2O$ ) too quickly to be followed, most of them are located in exposed regions. However, I was able to follow the slowly exchanging residues of the protein backbone in wild type, 67 residues, and its mutants, 64 residues

(Figure A.4). I calculated the hydrogen-deuterium exchange rates for the strong protected residues and then protection factors from these rates (Figure A.5 i and ii, A.6) (Bai, Milne et al. 1993).

Protection factors are a way to assess how the structure around amide hydrogen protects it from hydrogen-deuterium exchange. Mutated p53 showed more protection than the wild type. There were considerable variations in the average of protection factors for stable residues in N239Y compared to those in N235K and wild type i.e. N239Y ( $4.39 \times 10^6$ ) > N235K ( $1.68 \times 10^6$ ) > wild type ( $6.94 \times 10^5$ ) (Figure A.7).

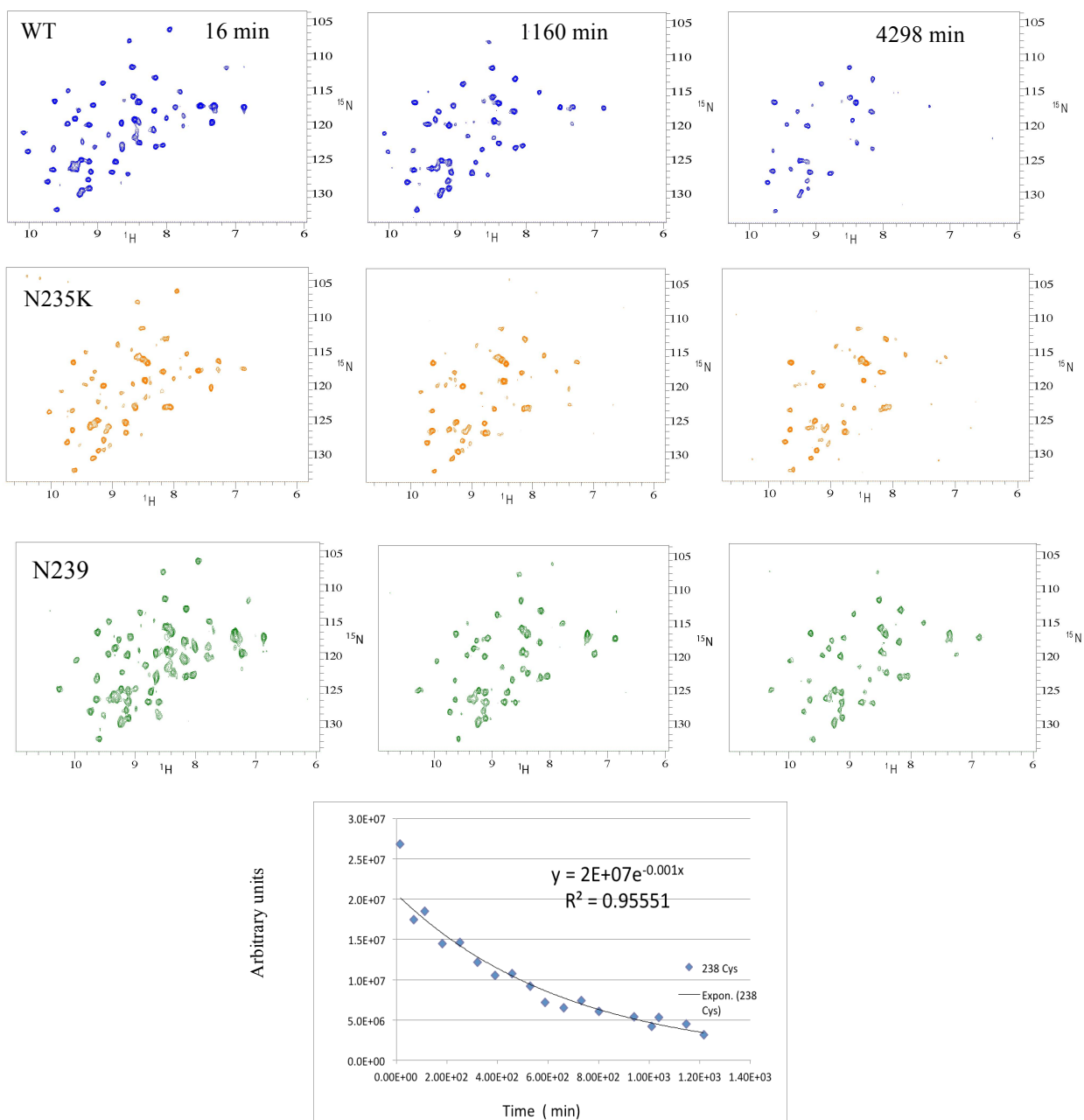


Figure A.4: HSQC after a different time period of exchange in D<sub>2</sub>O. (B) Exchange time of selected residues.

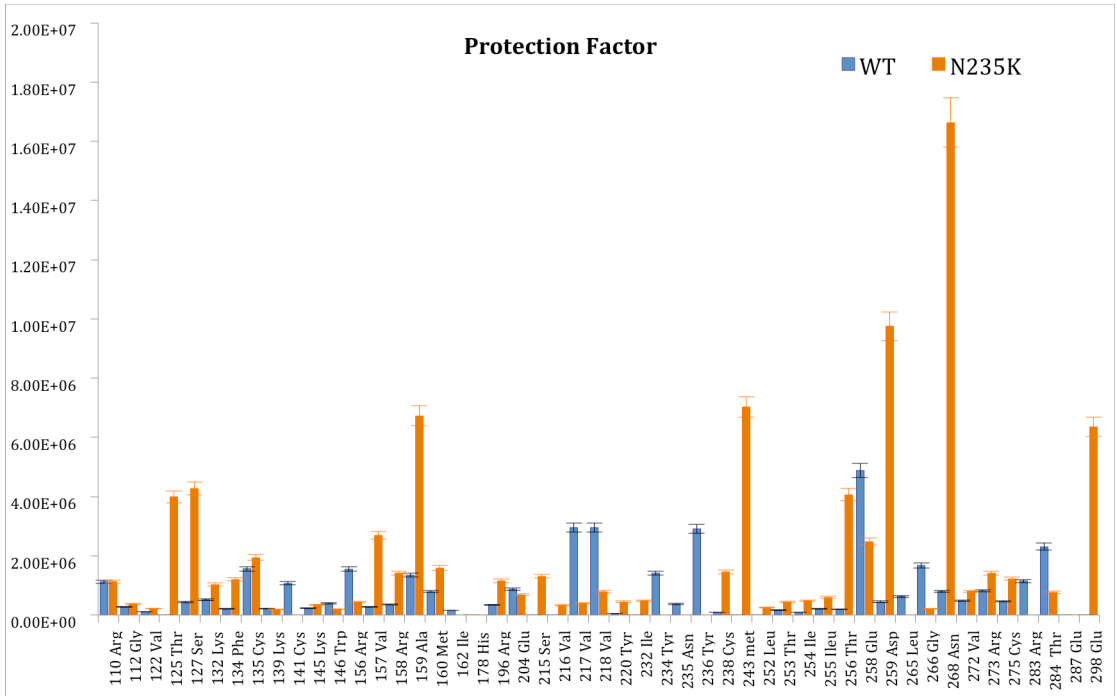


Figure A.5 (i) : Protection factor comparison wild type and N235K. Error bar is percentage error (5%)

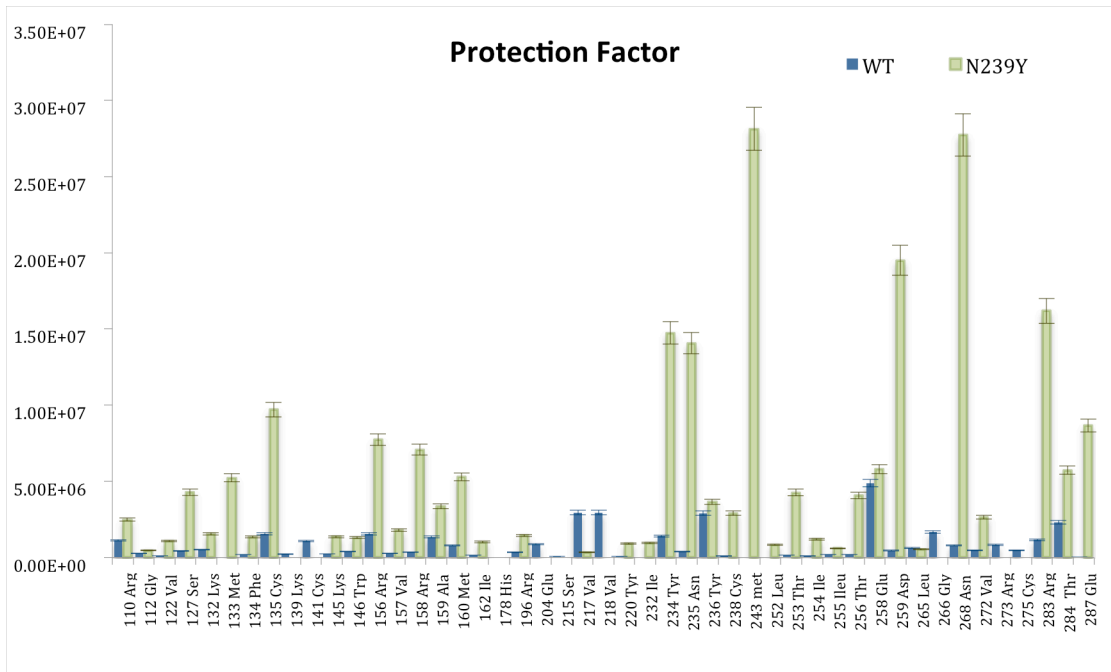


Figure A.5 (ii): Protection factor comparing wild type and N239Y. Error bar is percentage error (5%)

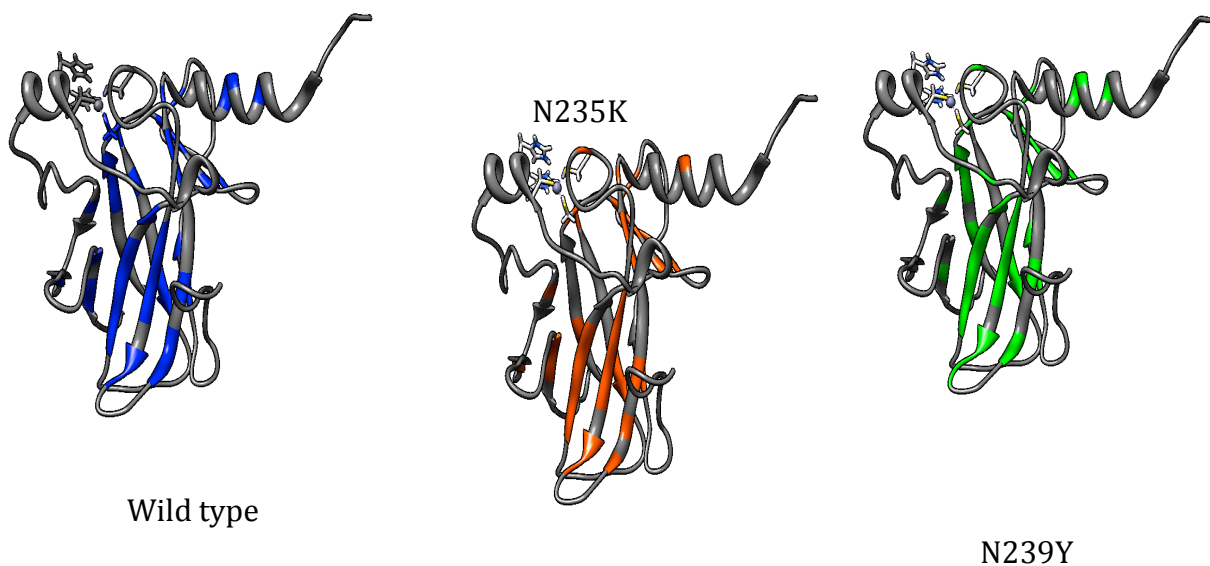


Figure A.6: highly protected residues, Shows the location of protected residues for wild type (blue), N235K (orange), and N239Y (green) mapped onto the crystal structure of p53 (PDB entry, 2FEJ)s

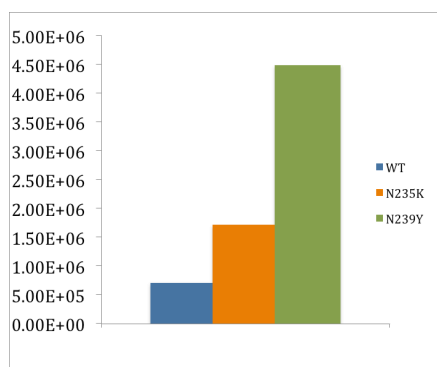


Figure A.7: Average of protection factors for WT, N235K, N239Y.

In N239Y, positions Y234, N235, M243, D259, N268 and R283 showed significantly greater protection against hydrogen-deuterium exchange compared to the wild type. In N235K, I found that only M243, D259, and N268 have increased protection compared to the wild type. In addition, A159 and Q298 showed increased protection in N235K indicating the mechanism of stabilization are different for these two rescue mutations. The maximum protection factor in N239Y was  $2.81 \times 10^7$  while in N235K and WT was  $1.66 \times 10^7$ , and  $4.88 \times 10^6$ , respectively.

The core domain of p53 is composed of a beta-sandwich with Greek key topology. This beta-sandwich consists of two anti-parallel beta sheets of four and five, where most of the highly protected residues are located (Figure A.6) (Joerger, Allen et al. 2004). This structure provides the platform for DNA contact surface L2 and L3 and loop-sheet-helix motifs. The p53 core domain has low thermodynamic stability compared to its homologs p63 and p73. Presence of polar groups (Y236-T253) in the hydrophobic core domain might contribute to the instability issue which has been suggested for the importance of the function of the protein (Canadillas, Tidow et al. 2006). Mutations in the p53 core domain are either stabilizing or destabilizing the protein, and so researchers have been investigating such mutants to maximize p53 stability for structural and biophysical studies. Nikolova and co-workers have identified a quadruple mutant (M133L/V203A/ N239Y / N268D) that stabilizes the p53 core domain by 2.65 kcal/mol and maintains wild-type p53 DNA-binding configuration. N239Y alone

stabilizes the core domain by 1.3 kcal/mol and N268D by 1.2 kcal/mol. Later, Khoo and co-workers generated a hexamutant (M133L/V203A/Y236F/N239Y/ T253I/N268D), which stabilized the p53 core domain by 1.9 kcal/mol at 37°C, compare to quadruple mutant (Khoo, Joerger et al. 2009). However, other mutants rescue destabilized p53 without adding significant contribution to global energy. For example, N235K increase p53's core domain stability by only 0.3 kcal/mol but still can rescue five of six of most common cancer mutants (Tan, Chen et al. 2009). The extreme protection I found for N268 in N239Y and N235K could be due to the participation in a hydrogen bonding network (Figure 4); N268 is located in beta strand S10. The nitrogen proton side chain is involved in a hydrogen bond with carbonyl-oxygen of F109 and R267 main chain (Joerger, Allen et al. 2004). Furthermore, the main chain nitrogen of N268 acts as a hydrogen donor by donating its proton to form a hydrogen bond with carbonyl-oxygen of I255, located in beta-strand S9. In addition, the carbonyl-oxygen of N268 accepts a proton from main chain I255 nitrogen. Notably, the crystal structures of both mutants show networks of hydrogen bonds, between stable residues in beta strand S9 and S8. These networks are less established in wild type. The existence of these hydrogen bonds in the rescue mutants further stabilizes the core domain and provides a reason to the extraordinary protection against hydrogen exchange in mutants. In the same way, D259, located in the hairpin connected S10 and S9, main chain proton amide hydrogen bond with carbonyl-oxygen of N263. The backbone nitrogen is pointed inward, which provided an extra protection and limited solvent accessibility. The nature of the hairpin turn is rigid. Two hydrogen bonds between E258, in hairpin connected S10 and S9, and



R156, in beta strand S8, limit the movement of backbone (Figure A.8). This explains the slow exchange with the solvent and the high protection against exchange. The side chain of M243 folds back onto the backbone in N239Y and N235K while in WT it is fully exposed to solvent.

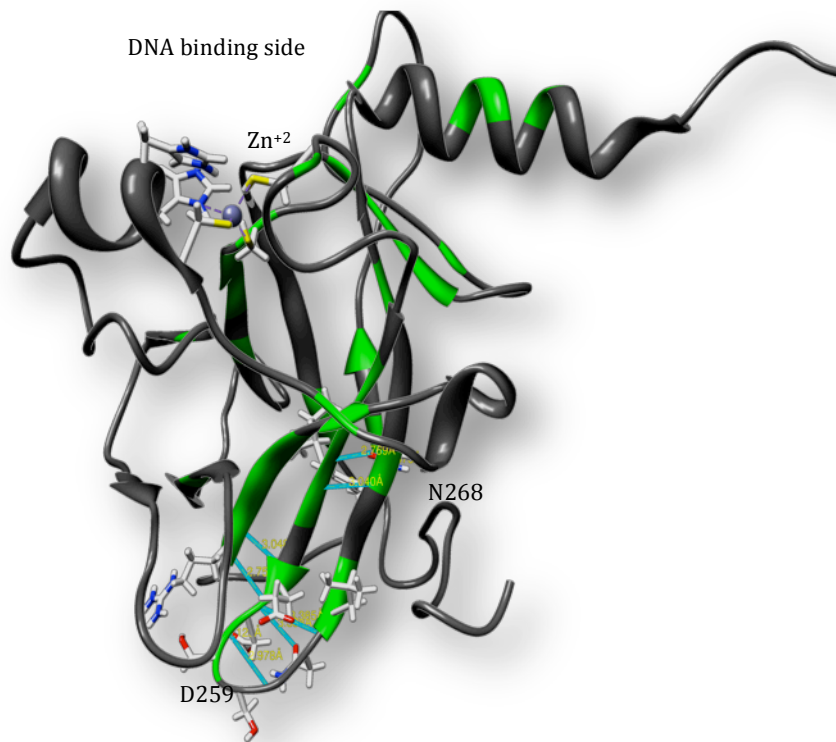


Figure A.8 : H-bonds involved in D259 and N268.

In summary, the global suppressor motif, N235K, N239Y, S240R, rescues 50% of most cancer mutants. N235K and N239Y are more stable than wild type; I find that most of the residues contributing to the stability are located in hydrophobic core domain (beta strands). These two rescue mutants have no effect on DNA-binding region. Analysis of

protection factor data helps to identify structural interaction. Hydrogen bonds could be the reason for higher protection in N239Y and N235K. Finding small molecules mimicking mutants will help to rescue the p53 wild type function.

## Methods:

### ***Data collection and:***

<sup>15</sup>N-labeled p53 wild type and its mutants were provided by Colleen Moody. They were in 335µl phosphate buffer (15 mM potassium chloride, 25 mM sodium phosphate, 10 mM BME) at 400 µM and pH 7.1. Samples were lyophilized and fully suspended in 100% D<sub>2</sub>O immediately before running the experiment to initiate the exchange. A two-dimensional <sup>1</sup>H-<sup>15</sup>N heteronuclear single quantum coherence (HSQC) NMR spectrum was recorded on Varian Inova 800 MHz for each sample every hour for 24 hours, and then every 3 hours for 48 hours at 20°C. The first 2D HSQC spectrum was recorded ~16 min after initiation of exchange. The total of 40 spectra were acquired in 72 hours for each samples. NMR data were processed using nmrDraw (Delaglio, Grzesiek et al. 1995). Residues assignment and rate measurements of the heights of peak in all 2D HSQC spectra were done using the software, Analysis

### ***Hydrogen-Deuterium Exchange and protection factor:***

To calculate the protection factor for each residues  $P = k_{rc}/k_{ex}$ , I need to determine  $k_{ex}$  and  $k_{rc}$ .  $k_{ex}$  determined by fitting the hydrogen-deuterium exchange intensities (A) from two-dimensional <sup>1</sup>H-<sup>15</sup>N HSQC as function of time to a time-dependent decreases function:

$$A = A_0 \exp(-k_{ex} X) \text{ ----- Eq (1)}$$

Where  $A_0$  is the initial intensity.

While  $k_{rc}$  was determined by (Bai, Milne et al. 1993):

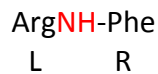
$$k_{rc} = \log k_a [H^+] + \log k_b [OH^-] + \log k_w \text{ -----Eq (2)}$$

$$\log k_a = \log k_{aref} + \log k_a R + \log k_a L - pD \text{ (7.5)}$$

$$\log k_b = \log k_{bref} + \log k_b R + \log k_b L - pOD \text{ (8.15)}$$

$$\log k_w = \log k_{wref} + \log k_b R + \log k_b$$

Where  $k_w$  is water rate constant,  $k_a$  is the acid catalyzed rate constant, and  $k_b$  is the base catalyzed rate constant. L, left R, right relative to the amide hydrogen. The size and polarity of neighboring amino acid side chain can directly affect the exchange rate of specific amino group in random coil (primary structure); thus, the exchange rate is amino acid sequence-dependent. Bai and coworker have quantified the effect of neighboring side chain as function of temperature and pH (Table A.1) (Bai, Milne et al. 1993). I used these values to calculate the  $k_{rc}$ . This is an example of how I calculated the  $k_{rc}$  in each residue. Phe and Arg side chains are on the right and the left of the Arg amide hydrogen, respectively. The acid catalysis values are marked in the table with blue square. The base catalysis values are marked in the table with red square. All reference rates constant values for  $k_a$ ,  $k_b$ , and  $k_w$  were acquired from Table A.2 (Bai, Milne et al. 1993). Then, I summed the result of  $\log k_a$ ,  $\log k_b$ ,  $\log k_w$  to get the  $k_{rc}$  for the Arg residue, see the Table A.4 for the rest of the residues.



$$\begin{aligned} \log k_a &= \log k_{a\text{ref}} (2.04) + \log k_a \text{ R } (-0.43) + \log k_a \text{ L } (-0.59) - pD(7.5) \\ \log k_b &= \log k_{b\text{ref}} (10.36) + \log k_b \text{ R } (0.06) + \log k_b \text{ L } (0.8) - pOD(8.15) \\ \log k_w &= \log k_{w\text{ref}} (-1.5) + \log k_b \text{ R } (0.06) + \log k_b \text{ L } (0.8) \end{aligned}$$

Side chain (X)	$\text{Log}k_{\text{ex}}(\text{X}) - \text{Log}k_{\text{ex}}(\text{Ala})$			
	Acid catalysis		Base catalysis	
	L	R	L	R
Ala	0.00	0.00	0.00	0.00
Arg	-0.59	-0.32	0.08	0.22
Asn	-0.58	-0.13	0.49	0.32
Asp(COO <sup>-</sup> )	(0.9)	0.58	-0.30	-0.18
Asp(COOH)	(-0.9)	-0.12	0.69	(0.6)
Cys	-0.54	-0.46	0.62	0.55
Cys <sub>2</sub>	-0.74	-0.58	0.55	0.46
Gly	-0.22	0.22	0.27	0.17
Gln	-0.47	-0.27	0.06	0.20
Glu(COO <sup>-</sup> )	(-0.9)	0.31	-0.51	-0.15
Glu(COOH)	(-0.6)	-0.27	0.24	0.39
His			-0.10	0.14
His <sup>+</sup>	(-0.8)	-0.51	(0.8)	0.83
Ile	-0.91	-0.59	-0.73	-0.23
Leu	-0.57	-0.13	-0.58	-0.21
Lys	-0.56	-0.29	-0.04	0.12
Met	-0.64	-0.28	-0.01	0.11
Phe	-0.52	-0.43	-0.24	0.06
Pro( <i>trans</i> )		-0.19		-0.24
Pro( <i>cis</i> )		-0.85		0.60
Ser	-0.44	-0.39	0.37	0.30
Thr	-0.79	-0.47	-0.07	0.20
Trp	-0.40	-0.44	-0.41	-0.11
Tyr	-0.41	-0.37	-0.27	0.05
Val	-0.74	-0.30	-0.70	-0.14
N-term (NH <sub>3</sub> <sup>+</sup> )		-1.32		1.62
C-term (COO <sup>-</sup> )	0.96		(-1.8)	
C-term (COOH)	(0.05)			

Table A.1: Krc values for all Amino acid

	$\log k_A \text{ (M}^{-1} \text{ min}^{-1}\text{)}$	$\log k_B \text{ (M}^{-1} \text{ min}^{-1}\text{)}$	$\log k_w \text{ (min}^{-1}\text{)}$
N-Ac-A-A-A-N'MA	2.04	10.36	-1.5
PDLA	1.62	10.05	-1.5

Table A.2: K<sub>a</sub>, K<sub>b</sub>, and K<sub>w</sub> reference values

Table A.3: Protection Factor for Stable residues

Residues	P factor N235K	P Factor WT	P Factor N239Y
110 Arg	1.12E+06	0.00E+00	2.49E+06
112 Gly	3.72E+05	2.66E+05	4.66E+05
122 Val	2.15E+05	1.08E+05	1.08E+06
125 Thr	3.98E+06	0.00E+00	0.00E+00
127 Ser	4.27E+06	4.27E+05	4.27E+06
132 Lys	1.03E+06	5.15E+05	1.55E+06
133 Met	0.00E+00	0.00E+00	5.22E+06
134 Phe	1.20E+06	2.00E+05	1.34E+06
135 Cys	1.94E+06	1.55E+06	9.70E+06
139 Lys	1.85E+05	2.11E+05	0.00E+00
141 Cys	0.00E+00	1.07E+06	0.00E+00
145 Lue	3.38E+05	2.25E+05	1.35E+06
146 Trp	1.95E+05	3.89E+05	1.30E+06
156 Arg	4.42E+05	1.55E+06	7.73E+06
157 Val	2.69E+06	2.69E+05	1.79E+06
158 Arg	1.41E+06	3.53E+05	7.06E+06
159 Ala	6.73E+06	1.35E+06	3.37E+06
160 Met	1.59E+06	7.93E+05	5.28E+06
162 Ile	0.00E+00	1.51E+05	1.01E+06
178 His	no value	no value	no value
196 Arg	1.15E+06	3.40E+05	1.44E+06
204 Glu	6.81E+05	8.75E+05	0.00E+00
215 Ser	1.31E+06	5.86E+04	0.00E+00
216 Val	3.23E+05	0.00E+00	0.00E+00
217 Val	3.91E+05	2.94E+06	3.35E+05
218 Val	7.82E+05	2.94E+06	0.00E+00
220 Tyr	4.46E+05	5.26E+04	8.91E+05
232 Ile	4.79E+05	0.00E+00	9.57E+05
234 Tyr	0.00E+00	1.41E+06	1.47E+07
235 Asn	0.00E+00	3.64E+05	1.41E+07
236 Tyr	0.00E+00	2.90E+06	3.64E+06
238 Cys	1.45E+06	8.51E+04	2.90E+06
243 Met	7.03E+06	0.00E+00	2.81E+07
252 Leu	2.51E+05	0.00E+00	8.37E+05
253 Thr	4.26E+05	1.60E+05	4.26E+06
254 Ile	4.79E+05	8.89E+04	1.20E+06
255 Ile	5.93E+05	2.03E+05	5.93E+05
256 Thr	4.06E+06	1.95E+05	4.06E+06
258 Glu	2.48E+06	4.88E+06	5.79E+06
259 Asp	9.75E+06	4.46E+05	1.95E+07
265 Leu	0.00E+00	6.21E+05	5.26E+05
266 Gly	2.07E+05	1.66E+06	0.00E+00
268 Asn	1.66E+07	7.94E+05	2.77E+07
272 Val	7.94E+05	4.71E+05	2.65E+06
273 Arg	1.41E+06	8.16E+05	0.00E+00
275 Cyc	1.22E+06	4.62E+05	0.00E+00
283 Arg	0.00E+00	1.15E+06	1.62E+07
284 Thr	7.64E+05	2.31E+06	5.73E+06
287 Glu	0.00E+00	1.50E+04	8.65E+06
298 Glu	6.35E+06	0.00E+00	0.00E+00

Table A.4: Exchange rate for stable residues (experimental 'Kex' and random coil 'Krc')

Stable AA	Krc	Kex WT	Kex N235K	Kex N239Y
110 Arg	2.24E+02	0.00E+00	2.00E-04	9.00E-05
112 Gly	1.86E+02	7.00E-04	5.00E-04	4.00E-04
122 Val	6.46E+01	6.00E-04	3.00E-04	6.00E-05
125 Thr	3.98E+02	0.00E+00	1.00E-04	0.00E+00
127 Ser	4.27E+02	1.00E-03	1.00E-04	1.00E-04
132 Lys	3.09E+02	6.00E-04	3.00E-04	2.00E-04
133 Met	2.09E+02	0.00E+00	0.00E+00	4.00E-05
134 Phe	1.20E+02	6.00E-04	1.00E-04	9.00E-05
135 Cys	7.76E+02	5.00E-04	4.00E-04	8.00E-05
139 Lys	1.48E+02	7.00E-04	8.00E-04	0.00E+00
141 Cys	1.07E+03	1.00E-03	0.00E+00	0.00E+00
145 Lue	6.76E+01	0.00E+00	2.00E-04	5.00E-05
146 Trp	3.89E+01	1.00E-04	2.00E-04	3.00E-05
156 Arg	3.09E+02	2.00E-04	7.00E-04	4.00E-05
157 Val	5.37E+01	0.00E+00	2.00E-05	3.00E-05
158 Arg	1.41E+02	4.00E-04	1.00E-04	2.00E-05
159 Ala	2.69E+02	0.00E+00	4.00E-05	8.00E-05
160 Met	1.58E+02	2.00E-04	1.00E-04	3.00E-05
232 Ile	4.78E+01	0.00E+00	1.00E-04	4.79E+01
162 Ile	3.02E+01	2.00E-04	0.00E+00	3.00E-05
178 His	#value	6.00E-04	0.00E+00	8.00E-05
196 Arg	1.15E+02	6.00E-04	1.00E-04	8.00E-05
204 Glu	2.04E+02	6.00E-04	3.00E-04	0.00E+00
215 Ser	5.25E+02	0.00E+00	4.00E-04	0.00E+00
216 Val	6.46E+01	0.00E+00	2.00E-04	0.00E+00
217 Val	2.34E+01	4.00E-04	6.00E-05	7.00E-05
218 Val	2.34E+01	2.00E-04	3.00E-05	0.00E+00
220 Tyr	8.91E+01	5.00E-04	2.00E-04	1.00E-04
234 Tyr	5.89E+02	4.00E-04	0.00E+00	4.00E-05
235 Asn	5.62E+02	5.00E-04	0.00E+00	4.00E-05
236 Tyr	1.82E+02	3.00E-04	0.00E+00	5.00E-05
238 Cys	8.71E+02	1.00E-03	6.00E-04	3.00E-04
243 Met	5.62E+02	0.00E+00	8.00E-05	2.00E-05
252 Leu	2.51E+01	0.00E+00	1.00E-04	3.00E-05
253 Thr	8.51E+01	3.00E-04	2.00E-04	2.00E-05
254 Ile	4.79E+01	2.00E-04	1.00E-04	4.00E-05
255 Ile	1.78E+01	4.00E-04	3.00E-05	3.00E-05
256 Thr	8.13E+01	0.00E+00	2.00E-05	2.00E-05
258 Glu	1.74E+02	0.00E+00	7.00E-05	3.00E-05
259 Asp	1.95E+03	2.00E-04	2.00E-04	1.00E-04
265 Leu	2.64E+01	3.00E-04	0.00E+00	5.00E-05
266 Gly	1.86E+02	5.00E-04	9.00E-04	0.00E+00
268 Asn	8.32E+02	1.00E-04	5.00E-05	3.00E-05
272 Val	7.94E+01	3.00E-04	1.00E-04	3.00E-05
273 Arg	1.41E+02	6.00E-04	1.00E-04	0.00E+00
275 Cyc	4.90E+02	7.00E-04	4.00E-04	0.00E+00
283 Arg	3.24E+02	0.00E+00	0.00E+00	2.00E-05
284 Thr	2.29E+02	3.00E-04	3.00E-04	4.00E-05
287 Glu	6.92E+02	2.00E-04	0.00E+00	8.00E-05
298 Glu	1.91E+03	0.00E+00	3.00E-04	0.00E+00

Table A.5: Chemical shifts for WT Assignments residues

#	Assign F1	Assign F2	Height	Volume	Position F1	Position F2
1	110ArgH	110ArgN	1.89E+07	1.37E+08	9.14E+00	1.28E+02
2	112GlyH	112GlyN	1.55E+07	1.07E+08	8.54E+00	1.08E+02
3	122ValH	122ValN	2.00E+07	1.42E+08	8.05E+00	1.23E+02
4	125ThrH	125ThrN	1.22E+07	9.71E+07	9.64E+00	1.24E+02
5	127SerH	127SerN	1.30E+07	9.66E+07	8.39E+00	1.20E+02
6	131AsnH	131AsnN	1.38E+07	9.85E+07	8.01E+00	1.19E+02
7	132LysH	132LysN	2.83E+07	2.07E+08	6.87E+00	1.18E+02
8	134PheH	134PheN	1.22E+07	1.02E+08	9.28E+00	1.26E+02
9	135CysH	135CysN	2.41E+07	1.71E+08	9.33E+00	1.20E+02
10	136GlnH	136GlnN	1.31E+07	1.01E+08	7.87E+00	1.18E+02
11	138AlaH	138AlaN	1.20E+07	8.48E+07	9.04E+00	1.24E+02
12	139LysH	139LysN	5.32E+07	3.58E+08	7.50E+00	1.18E+02
13	141CysH	141CysN	1.52E+07	1.21E+08	9.29E+00	1.27E+02
14	143ValH	143ValN	2.10E+07	1.49E+08	9.12E+00	1.26E+02
15	145LeuH	145LeuN	1.89E+07	1.38E+08	9.43E+00	1.20E+02
16	146TrpH	146TrpN	1.57E+07	1.22E+08	9.10E+00	1.27E+02
17	156ArgH	156ArgN	1.98E+07	1.42E+08	9.73E+00	1.29E+02
18	157ValH	157ValN	2.58E+07	1.82E+08	9.12E+00	1.20E+02
19	158ArgH	158ArgN	1.99E+07	1.41E+08	9.59E+00	1.33E+02
20	159AlaH	159AlaN	2.09E+07	1.48E+08	8.78E+00	1.27E+02
21	160MetH	160MetN	22900000	166000000	8.17581	1.18E+02
22	162IleH	162IleN	1.88E+07	1.41E+08	8.50E+00	1.12E+02
23	163TyrH	163TyrN	1.09E+07	8.13E+07	9.23E+00	1.23E+02
24	178HisH	178HisN	1.29E+07	9.46E+07	7.80E+00	1.16E+02
25	193HisH	193HisN	7.19E+06	6.56E+07	7.29E+00	1.18E+02
26	196ArgH	196ArgN	1.12E+07	8.40E+07	8.84E+00	1.22E+02
27	198GluH	198GluN	6.03E+06	4.29E+07	8.66E+00	1.29E+02
28	203ValH	203ValN	7.48E+06	5.37E+07	6.88E+00	1.19E+02
29	204GluH	204GluN	2.52E+07	1.83E+08	8.74E+00	1.26E+02
30	206LeuH	206LeuN	1.34E+07	1.08E+08	9.36E+00	1.26E+02
31	215SerH	215SerN	1.29E+07	9.42E+07	9.43E+00	1.15E+02
32	216ValH	216ValN	7.16E+06	5.65E+07	8.62E+00	1.17E+02
33	217ValH	217ValN	1.70E+07	1.29E+08	9.27E+00	1.31E+02
34	218ValH	218ValN	2.64E+07	1.97E+08	8.40E+00	1.17E+02
49	220TyrH	220TyrN	1.76E+07	1.32E+08	8.64E+00	1.24E+02
35	224GluH	224GluN	7.55E+06	6.76E+07	8.43E+00	1.23E+02
36	232IleH	232IleN	1.90E+07	1.40E+08	9.12E+00	1.30E+02
37	234TyrH	234TyrN	1.98E+07	1.45E+08	8.40E+00	1.23E+02
38	235AsnH	235AsnN	2.17E+07	1.56E+08	9.06E+00	1.17E+02
39	236TyrH	236TyrN	1.67E+07	1.18E+08	1.01E+01	1.22E+02
40	238CysH	238CysN	2.68E+07	1.86E+08	7.34E+00	1.20E+02
41	251IleH	251IleN	8.29E+06	6.59E+07	7.13E+00	1.12E+02
42	252LeuH	252LeuN	1.26E+07	9.07E+07	9.27E+00	1.18E+02
43	253ThrH	253ThrN	1.82E+07	1.28E+08	8.92E+00	1.14E+02
44	254IleH	254IleN	1.65E+07	1.33E+08	9.39E+00	1.27E+02
45	255IleH	255IleN	1.92E+07	1.48E+08	9.23E+00	1.30E+02
46	256ThrH	256ThrN	2.46E+07	1.70E+08	9.62E+00	1.17E+02
47	258GluH	258GluN	2.44E+07	1.77E+08	9.24E+00	1.25E+02
48	259AspH	259AspN	3.62E+07	2.64E+08	8.46E+00	1.20E+02
50	265LeuH	265LeuN	7.61E+06	6.42E+07	9.66E+00	1.24E+02
51	266GluH	266GluN	1.93E+07	1.34E+08	7.96E+00	1.07E+02
52	268AsnH	268AsnN	1.52E+07	1.24E+08	9.65E+00	126.82476
53	270PheH	270PheN	2.36E+07	1.67E+08	8.16E+00	1.14E+02
54	271GluH	271GluN	1.21E+07	9.26E+07	8.64E+00	1.23E+02
55	272ValH	272ValN	1.72E+07	1.29E+08	8.16E+00	1.24E+02
56	273ArgH	273ArgN	1.43E+07	9.73E+07	8.56E+00	1.28E+02
57	274ValH	274ValN	4.69E+06	3.28E+07	8.59E+00	1.30E+02



58	275CysH	275CysN	1.96E+07	1.43E+08	1.00E+01	1.24E+02
59	281AspH	281AspN	5.83E+06	5.13E+07	8.25E+00	1.21E+02
60	282ArgH	282ArgN	9.42E+06	6.86E+07	7.76E+00	1.21E+02
61	283ArgH	283ArgN	3.15E+07	2.39E+08	7.31E+00	1.18E+02
62	284ThrH	284ThrN	1.94E+07	1.41E+08	8.49E+00	1.16E+02
63	285GluH	285GluN	1.54E+07	1.16E+08	8.18E+00	1.21E+02
64	286GluH	286GluN	2.37E+07	1.66E+08	8.65E+00	1.20E+02
65	298GluH	298GluN	1.36E+07	1.05E+08	8.46E+00	1.22E+02
66	311AsnH	311AsnN	7.81E+06	6.84E+07	8.40E+00	1.20E+02
67	312ThrH	312ThrN	9.41E+06	7.14E+07	7.75E+00	1.19E+02

Figure A.9: Wild Type HSQC

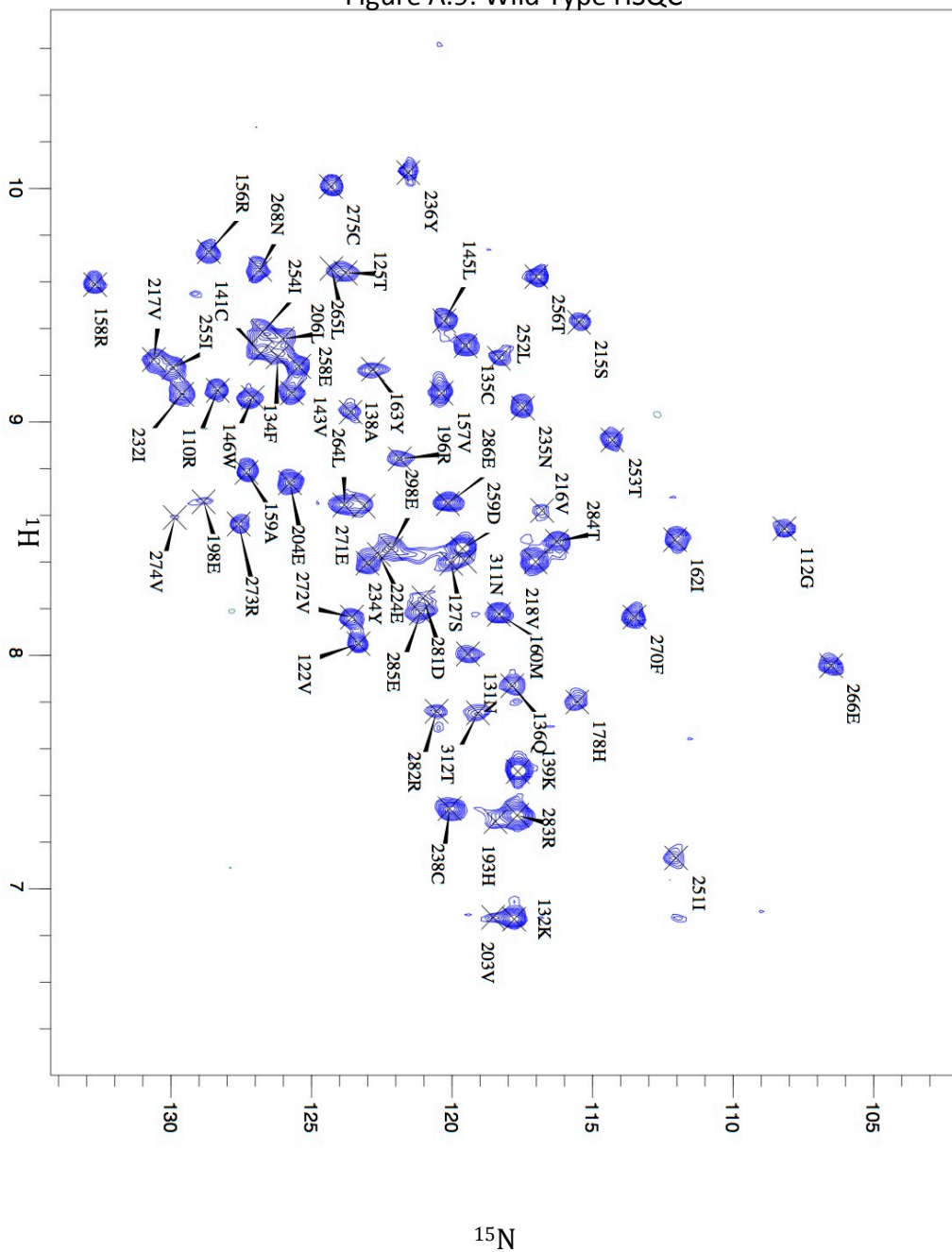
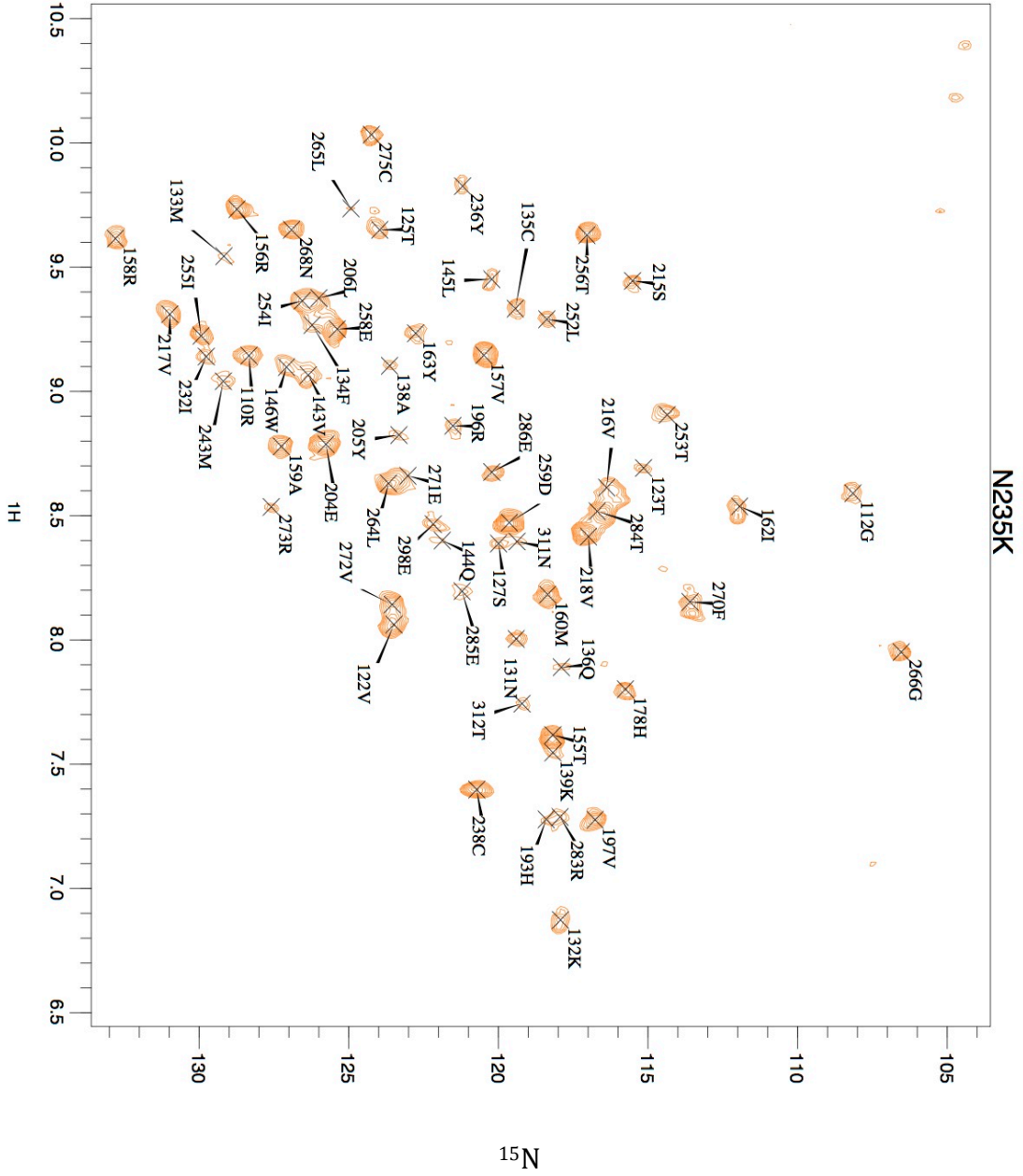


Figure A.10 : N235K HSQC





## Appendix B

## ***B.1: MT-JSRV sequence and parameters***

Sequence:

MGSSHHHHHSSGLVPRGSHMKTLIGVILVFIIIVVILIFPCLVRGMVRDFLKMRVEMLH  
MKYRNMLQHQLMELLKNKERGDAGDDP

Number of amino acids: 89

Molecular weight: 10242.2

Theoretical pI: 9.74

Amino acid composition:

Ala (A)	1	1.1%
Arg (R)	6	6.7%
Asn (N)	2	2.2%
Asp (D)	4	4.5%
Cys (C)	1	1.1%
Gln (Q)	2	2.2%
Glu (E)	3	3.4%
Gly (G)	8	9.0%
His (H)	10	11.2%
Ile (I)	7	7.9%
Leu (L)	11	12.4%
Lys (K)	5	5.6%
Met (M)	8	9.0%
Phe (F)	3	3.4%
Pro (P)	3	3.4%
Ser (S)	5	5.6%
Thr (T)	1	1.1%
Trp (W)	0	0.0%
Tyr (Y)	1	1.1%
Val (V)	8	9.0%
Pyl (O)	0	0.0%
Sec (U)	0	0.0%

(B) 0 0.0%

(Z) 0 0.0%

(X) 0 0.0%

Total number of negatively charged residues (Asp + Glu): 7

Total number of positively charged residues (Arg + Lys): 11

Atomic composition:

Carbon	C	455
Hydrogen	H	738
Nitrogen	N	136
Oxygen	O	115
Sulfur	S	9

Formula:  $C_{455}H_{738}N_{136}O_{115}S_9$   
Total number of atoms: 1453

Extinction coefficients:

This protein does not contain any Trp residues. Experience shows that this could result in more than 10% error in the computed extinction coefficient.

Extinction coefficients are in units of  $M^{-1} \text{ cm}^{-1}$ , at 280 nm measured in water.

Ext. coefficient 1490  
Abs 0.1% (=1 g/l) 0.145, assuming all pairs of Cys residues form cystines

Ext. coefficient 1490  
Abs 0.1% (=1 g/l) 0.145, assuming all Cys residues are reduced

Estimated half-life:

The N-terminal of the sequence considered is M (Met).

The estimated half-life is: 30 hours (mammalian reticulocytes, in vitro).  
>20 hours (yeast, in vivo).  
>10 hours (Escherichia coli, in vivo).

Instability index:

The instability index (II) is computed to be 23.49  
This classifies the protein as stable.

Aliphatic index: 106.07

Grand average of hydropathicity (GRAVY): 0.043  
sib\_body

## ***B.2: CT-JSRV sequence and parameters***

Sequence:

MGSSHHHHHSSGLVPRGSHMRGMVRDFLKMRVEMLHMKYRNMLQHQLMELLKNKERGDA  
GDDP

Number of amino acids: 65

Molecular weight: 7663.8

Theoretical pI: 9.81

Amino acid composition:

Ala (A)	1	1.5%
Arg (R)	6	9.2%
Asn (N)	2	3.1%
Asp (D)	4	6.2%
Cys (C)	0	0.0%
Gln (Q)	2	3.1%
Glu (E)	3	4.6%
Gly (G)	6	9.2%
His (H)	10	15.4%
Ile (I)	0	0.0%
Leu (L)	7	10.8%
Lys (K)	4	6.2%
Met (M)	8	12.3%
Phe (F)	1	1.5%
Pro (P)	2	3.1%
Ser (S)	5	7.7%
Thr (T)	0	0.0%
Trp (W)	0	0.0%
Tyr (Y)	1	1.5%
Val (V)	3	4.6%
Pyl (O)	0	0.0%
Sec (U)	0	0.0%

(B) 0 0.0%

(Z) 0 0.0%

(X) 0 0.0%



Total number of negatively charged residues (Asp + Glu): 7  
Total number of positively charged residues (Arg + Lys): 10

Atomic composition:

Carbon	C	324
Hydrogen	H	517
Nitrogen	N	111
Oxygen	O	90
Sulfur	S	8

Formula:  $C_{324}H_{517}N_{111}O_{90}S_8$   
Total number of atoms: 1050

Extinction coefficients:

This protein does not contain any Trp residues. Experience shows that this could result in more than 10% error in the computed extinction coefficient.

Extinction coefficients are in units of  $M^{-1} cm^{-1}$ , at 280 nm measured in water.

Ext. coefficient 1490  
Abs 0.1% (=1 g/l) 0.194

Estimated half-life:

The N-terminal of the sequence considered is M (Met).

The estimated half-life is: 30 hours (mammalian reticulocytes, in vitro).  
>20 hours (yeast, in vivo).  
>10 hours (Escherichia coli, in vivo).

Instability index:

The instability index (II) is computed to be 20.54  
This classifies the protein as stable.

Aliphatic index: 56.92

Grand average of hydropathicity (GRAVY): -1.000  
sib\_body

### ***B.3: Nogo-66 sequence and parameters***

#### **Sequence:**

MHHHHHHLVPRGMRIYKGVIAIQKSDEGHPFRAYLESEVAISEELVQKYSNSALGHVNCTIKELRR  
LFLVDDLVDLSLK

Number of amino acids: 79 Molecular weight: 9142.4 Theoretical pI: 7.10

#### Amino acid composition:

Ala (A)	4	5.1%
Arg (R)	5	6.3%
Asn (N)	2	2.5%
Asp (D)	4	5.1%
Cys (C)	1	1.3%
Gln (Q)	3	3.8%
Glu (E)	6	7.6%
Gly (G)	4	5.1%
His (H)	8	10.1%
Ile (I)	5	6.3%
Leu (L)	9	11.4%
Lys (K)	5	6.3%
Met (M)	2	2.5%
Phe (F)	2	2.5%
Pro (P)	2	2.5%
Ser (S)	6	7.6%
Thr (T)	1	1.3%
Trp (W)	0	0.0%
Tyr (Y)	3	3.8%
Val (V)	7	8.9%
Pyl (O)	0	0.0%
Sec (U)	0	0.0%
(B)	0	0.0%
(Z)	0	0.0%
(X)	0	0.0%

Total number of negatively charged residues (Asp + Glu): 10 Total number of positively charged residues (Arg + Lys): 10

#### Atomic composition:

Carbon	C	406
Hydrogen	H	644
Nitrogen	N	120
Oxygen	O	115
Sulfur	S	3

Formula: C406H644N120O115S3 Total number of atoms: 1288

Extinction coefficients:

This protein does not contain any Trp residues. Experience shows that this could result in more than 10% error in the computed extinction coefficient. Extinction coefficients are in units of  $M^{-1} \text{ cm}^{-1}$ , at 280 nm measured in water.

Ext. coefficient

Abs 0.1% (=1 g/l)

Ext. coefficient

Abs 0.1% (=1 g/l)

Estimated half-life:

4470

0.489, assuming all pairs of Cys residues form cystines

4470

0.489, assuming all Cys residues are reduced

The N-terminal of the sequence considered is M (Met).

The estimated half-life is: 30 hours (mammalian reticulocytes, in vitro).

>20 hours (yeast, in vivo).

>10 hours (Escherichia coli, in vivo).

Instability index:

The instability index (II) is computed to be 38.95

This classifies the protein as stable.

Aliphatic index: 99.87 Grand average of hydropathicity (GRAVY): -0.368

### ***B.3: Nogo- Δ20 sequence and parameters***

#### **Sequence:**

MGHHHHHHHHSSGHIEGRHMTGTKIAYETKVDLVQTSEATPSPVLPDIVMEAPLNSLLPSAGA  
SVVQPSVSPLEAPPPNVALKALGTKEGIKPEPESFNAAVQETEAPYISACDLIKEEKSVPEHAELVEDSS  
PESEPVDLFAIQESLYPTAQLCPSFEEAEVSYDSI KLEPENPPPYEEAMTKLSTEPSPDFSNYSEIAKF

Number of amino acids: 204

Molecular weight: 22231.7

Theoretical pI: 4.72

#### **Amino acid composition:**

Ala (A)	18	8.8%
Arg (R)	1	0.5%
Asn (N)	5	2.5%
Asp (D)	7	3.4%
Cys (C)	2	1.0%
Gln (Q)	5	2.5%
Glu (E)	27	13.2%
Gly (G)	7	3.4%
His (H)	13	6.4%
Ile (I)	10	4.9%
Leu (L)	15	7.4%
Lys (K)	10	4.9%
Met (M)	4	2.0%
Phe (F)	5	2.5%
Pro (P)	23	11.3%
Ser (S)	23	11.3%
Thr (T)	10	4.9%
Trp (W)	0	0.0%
Tyr (Y)	6	2.9%
Val (V)	13	6.4%
Pyl (O)	0	0.0%
Sec (U)	0	0.0%
(B)	0	0.0%
(Z)	0	0.0%
(X)	0	0.0%

Total number of negatively charged residues (Asp + Glu): 34

Total number of positively charged residues (Arg + Lys): 11

Atomic composition:

Carbon	C	984
Hydrogen	H	1513
Nitrogen	N	253
Oxygen	O	322
Sulfur	S	6

Formula: C<sub>984</sub>H<sub>1513</sub>N<sub>253</sub>O<sub>322</sub>S<sub>6</sub>

Total number of atoms: 3078

Extinction coefficients:

This protein does not contain any Trp residues. Experience shows that this could result in more than 10% error in the computed extinction coefficient.

Extinction coefficients are in units of M<sup>-1</sup> cm<sup>-1</sup>, at 280 nm measured in water.

Ext. coefficient 9065

Abs 0.1% (=1 g/l) 0.408, assuming all pairs of Cys residues form cystines

Ext. coefficient 8940

Abs 0.1% (=1 g/l) 0.402, assuming all Cys residues are reduced

Estimated half-life:

The N-terminal of the sequence considered is M (Met).

The estimated half-life is: 30 hours (mammalian reticulocytes, in vitro).

>20 hours (yeast, in vivo).

>10 hours (Escherichia coli, in vivo).

Instability index:

The instability index (II) is computed to be 63.76

This classifies the protein as unstable.

Aliphatic index: 75.10

Grand average of hydropathicity (GRAVY): -0.472

## ***B.5 : Nogo-66 Hydrogen bonds used in docking studies***

! make\_hbonds.nawk Table ! Date: Sat Dec 16 13:47:59 EST 1995

! Path: /spire3/dgarrett/E1/Structures

!

! 12/19/95 Commented beta G10 to A222 Constraint

! 2/20/96 Updated Entries Based on X-Ray Structure

! alpha helices H-BOND constraints

assign (resid 13 and name o )

(resid 16 and name hn ) 2.0 0.7 0.5

assign (resid 13 and name o )

(resid 16 and name n ) 3.0 0.7 0.5

assign (resid 14 and name o )

(resid 18 and name hn ) 2.0 0.7 0.5

assign (resid 14 and name o )

(resid 18 and name n ) 3.0 0.7 0.5

assign (resid 15 and name o )

(resid 19 and name hn ) 2.0 0.7 0.5

assign (resid 15 and name o )

(resid 19 and name n ) 3.0 0.7 0.5

assign (resid 16 and name o )

(resid 19 and name hn ) 2.0 0.7 0.5

assign (resid 16 and name o )

(resid 19 and name n ) 3.0 0.7 0.5

assign (resid 17 and name o )

(resid 20 and name hn ) 2.0 0.7 0.5

assign (resid 17 and name o )

(resid 20 and name n ) 3.0 0.7 0.5

assign (resid 18 and name o )

(resid 21 and name hn ) 2.0 0.7 0.5

assign (resid 18 and name o )

(resid 21 and name n ) 3.0 0.7 0.5

assign (resid 19 and name o )

(resid 22 and name hn ) 2.0 0.7 0.5

assign (resid 19 and name o )

(resid 22 and name n ) 3.0 0.7 0.5

assign (resid 20 and name o )

(resid 24 and name hn ) 2.0 0.7 0.5

assign (resid 20 and name o )

(resid 24 and name n ) 3.0 0.7 0.5

assign (resid 22 and name o )

(resid 25 and name hn ) 2.0 0.7 0.5

assign (resid 22 and name o )  
    (resid 25 and name n ) 3.0 0.7 0.5  
assign (resid 29 and name o )  
    (resid 32 and name hn ) 2.0 0.7 0.5  
assign (resid 29 and name o )  
    (resid 32 and name n ) 3.0 0.7 0.5  
assign (resid 31 and name o )  
    (resid 34 and name hn ) 2.0 0.7 0.5  
assign (resid 31 and name o )  
    (resid 34 and name n ) 3.0 0.7 0.5  
assign (resid 33 and name o )  
    (resid 36 and name hn ) 2.0 0.7 0.5  
assign (resid 33 and name o )  
    (resid 36 and name n ) 3.0 0.7 0.5  
assign (resid 34 and name o )  
    (resid 37 and name hn ) 2.0 0.7 0.5  
assign (resid 34 and name o )  
    (resid 37 and name n ) 3.0 0.7 0.5  
assign (resid 36 and name o )  
    (resid 39 and name hn ) 2.0 0.7 0.5  
assign (resid 36 and name o )  
    (resid 39 and name n ) 3.0 0.7 0.5  
assign (resid 37 and name o )  
    (resid 40 and name hn ) 2.0 0.7 0.5  
assign (resid 37 and name o )  
    (resid 40 and name n ) 3.0 0.7 0.5  
assign (resid 38 and name o )  
    (resid 42 and name hn ) 2.0 0.7 0.5  
assign (resid 38 and name o )  
    (resid 42 and name n ) 3.0 0.7 0.5  
assign (resid 39 and name o )  
    (resid 43 and name hn ) 2.0 0.7 0.5  
assign (resid 39 and name o )  
    (resid 43 and name n ) 3.0 0.7 0.5  
assign (resid 42 and name o )  
    (resid 45 and name hn ) 2.0 0.7 0.5  
assign (resid 42 and name o )  
    (resid 45 and name n ) 3.0 0.7 0.5  
assign (resid 45 and name o )  
    (resid 49 and name hn ) 2.0 0.7 0.5  
assign (resid 45 and name o )  
    (resid 49 and name n ) 3.0 0.7 0.5  
assign (resid 49 and name o )  
    (resid 53 and name hn ) 2.0 0.7 0.5

assign (resid 49 and name o )  
    (resid 53 and name n ) 3.0 0.7 0.5  
assign (resid 53 and name o )  
    (resid 59 and name hn ) 2.0 0.7 0.5  
assign (resid 53 and name o )  
    (resid 56 and name n ) 3.0 0.7 0.5  
assign (resid 56 and name o )  
    (resid 60 and name hn ) 2.0 0.7 0.5  
assign (resid 56 and name o )  
    (resid 60 and name n ) 3.0 0.7 0.5  
assign (resid 57 and name o )  
    (resid 61 and name hn ) 2.0 0.7 0.5  
assign (resid 57 and name o )  
    (resid 61 and name n ) 3.0 0.7 0.5  
assign (resid 59 and name o )  
    (resid 63 and name hn ) 2.0 0.7 0.5  
assign (resid 59 and name o )  
    (resid 63 and name n ) 3.0 0.7 0.5  
assign (resid 60 and name o )  
    (resid 64 and name hn ) 2.0 0.7 0.5  
assign (resid 60 and name o )  
    (resid 64 and name n ) 3.0 0.7 0.5  
assign (resid 61 and name o )  
    (resid 65 and name hn ) 2.0 0.7 0.5  
assign (resid 61 and name o )  
    (resid 65 and name n ) 3.0 0.7 0.5  
assign (resid 64 and name o )  
    (resid 68 and name hn ) 2.0 0.7 0.5  
assign (resid 64 and name o )  
    (resid 68 and name n ) 3.0 0.7 0.5  
assign (resid 67 and name o )  
    (resid 71 and name hn ) 2.0 0.7 0.5  
assign (resid 67 and name o )  
    (resid 71 and name n ) 3.0 0.7 0.5  
assign (resid 73 and name o )  
    (resid 76 and name hn ) 2.0 0.7 0.5  
assign (resid 73 and name o )  
    (resid 76 and name n ) 3.0 0.7 0.5  
assign (resid 74 and name o )  
    (resid 77 and name hn ) 2.0 0.7 0.5  
assign (resid 74 and name o )  
    (resid 77 and name n ) 3.0 0.7 0.5



## ***B.6: Transformation protocol***

- 1- Thaw ~30  $\mu$ l (one aliquot) BL21 pLysS cells on Ice (-80°C)
- 2- Thaw plasmid on ice (-20°C)
- 3- Add 1  $\mu$ l plasmid to cells and incubate on ice 10-30 min
- 4- Heat at 42°C for 30-60 sec
- 5- Add 250  $\mu$ l of SOC or LB and incubate/shake for 1 hour at 37°C and 225 rpm
- 6- Remove LB/Amp plate from Fridge and place in 37°C incubator
- 7- Plate 50  $\mu$ l of 1 hour culture on LB/Amp plate
- 8- Place plate in incubator at 37°C for over night (12-16 hours)

## B.7 : Nogo-66 , : Nogo- Δ20 Expression Vector



### pEF-16b Vector

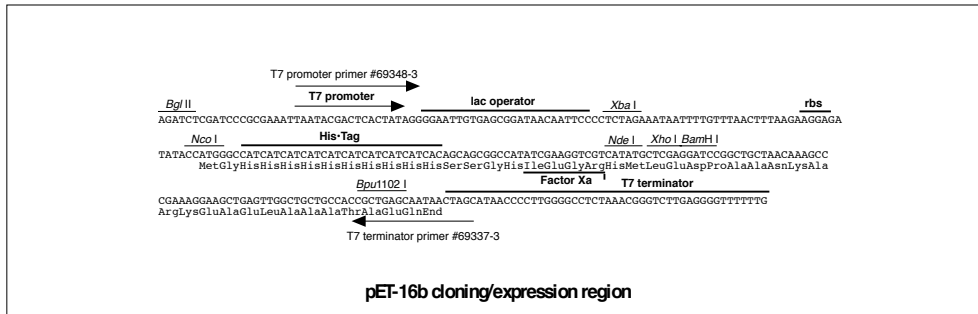
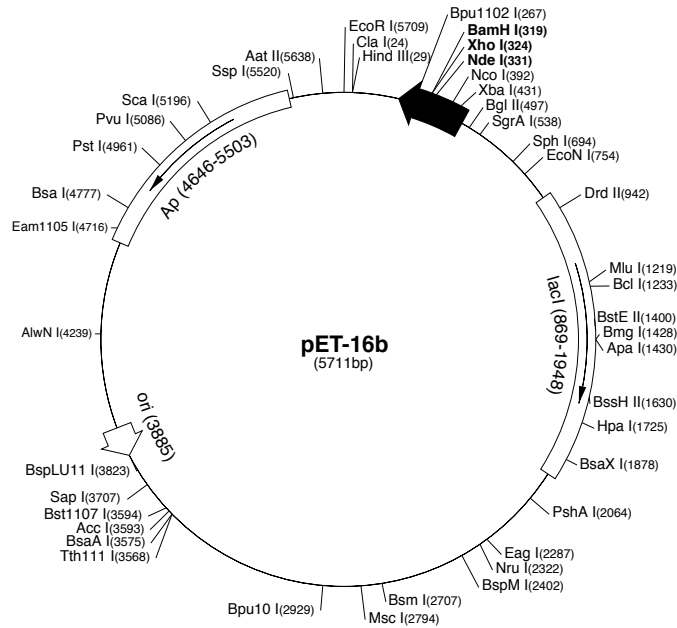


TB046 2/00

The pET-16b vector (Cat. No. 69662-3) carries an N-terminal His•Tag® sequence followed by a Factor Xa site and three cloning sites. Unique sites are shown on the circle map. Note that the sequence is numbered by the pBR322 convention, so the T7 expression region is reversed on the circular map. The cloning/expression region of the coding strand transcribed by T7 RNA polymerase is shown below.

#### pET-16b sequence landmarks

T7 promoter	466-482
T7 transcription start	465
His•Tag coding sequence	360-389
Multiple cloning sites ( <i>Nde</i> I - <i>Bam</i> H I)	319-335
T7 terminator	213-259
<i>lacI</i> coding sequence	869-1948
pBR322 origin	3885
<i>bla</i> coding sequence	4646-5503



Novagen · ORDERING 800-526-7319 · TECHNICAL SUPPORT 800-207-0144

